UNCLASSIFIED

AD NUMBER
ADB007291
LIMITATION CHANGES
TO: **Approved for public release; distribution is unlimited.**
FROM: **Distribution authorized to U.S. Gov't. agencies only; Test and Evaluation; JUL 1975. Other requests shall be referred to Air Force Avionics lab., Wright-Patterson AFB, OH 45433.**
AUTHORITY
AFAL ltr 10 Mar 1978

THIS PAGE IS UNCLASSIFIED

Copy No. 2

AFAL-TR-75-139

LINEAR DETECTOR ARRAY

Honeywell Radiation Center

July 1975

TECHNICAL REPORT AFAL-TR-75-139

Final Report for Period April 1972 - April 1975

Distribution Statement

Distribution limited to U.S. Government agencies only (test and evaluation). Other requests for this document will be referred to AFAL/RWI-4, Wright-Patterson AFB, Ohio

NOTICE

When Government drawings, specifications, or other data are used for any purpose other than in connection with a definitely related Government procurement operation, the United States Government thereby incurs no responsibility nor any obligation whatsoever; and the fact that the government may have formulated, furnished, or in any way supplied the said drawings, specifications, or other data, is not to be regarded by implication or otherwise as in any manner licensing the holder or any other person or corporation, or conveying any rights or permission to manufacture, use, or sell any patented invention that may in any way be related thereto.

This final report was submitted by Honeywell Radiation Center, 2 Forbes Road, Lexington, MA 02193, under contract F33615-72-C-1556, job order 20040229 with the Air Force Avionics Laboratory, AFAL/RWI, W-PAFB, OH 45433. Dr. William C. Eppers Jr. AFAL/CC was the Laboratory Director and Mr. William C. Schoonover was the Project Engineer-in-Charge.

This Technical Report has been reviewed and is approved for publication.

William C Schoonover

WILLIAM C. SCHOONOVER
Project Engineer

FOR THE COMMANDER

MERLE G. CARR
Asst Chief, Reconnaissance
and Weapon Delivery Division

ACCESSION for		
NTIS	White Section ☐	
DDC	Buff Section ☑	
UNANNOUNCED ☐		
JUSTIFICATION		
BY		
DISTRIBUTION/AVAILABILITY CODES		
Dist.	AVAIL. and/or SPECIAL	
B		

Copies of this report should not be returned unless return is required by security considerations, contractual obligations, or notice on a specific document.

UNCLASSIFIED

SECURITY CLASSIFICATION OF THIS PAGE (When Data Entered)

REPORT DOCUMENTATION PAGE

READ INSTRUCTIONS BEFORE COMPLETING FORM

1. REPORT NUMBER AFAL TR-75-139	2. GOVT ACCESSION NO.	3. RECIPIENT'S CATALOG NUMBER
4. TITLE (and Subtitle) LINEAR DETECTOR ARRAY		5. TYPE OF REPORT & PERIOD COVERED FINAL April 72 to April 75
		6. PERFORMING ORG. REPORT NUMBER
7. AUTHOR(s) D.A. Macdonald		8. CONTRACT OR GRANT NUMBER(s) F33615-72-C-1556
9. PERFORMING ORGANIZATION NAME AND ADDRESS Honeywell Radiation Center 2 Forbes Road, Lexington, Mass. 02173		10. PROGRAM ELEMENT, PROJECT, TASK AREA & WORK UNIT NUMBERS 6102 2004 2001
11. CONTROLLING OFFICE NAME AND ADDRESS U.S. Air Force Systems Command Hq. 4950th Test Wing, WPAFB 45433 4950/PMEA		12. REPORT DATE August 1975
		13. NUMBER OF PAGES 101
14. MONITORING AGENCY NAME & ADDRESS (if different from Controlling Office) DCASR BOSTON 666 Summer St, Boston, Mass		15. SECURITY CLASS. (of this report) UNCLASSIFIED
		15a. DECLASSIFICATION/DOWNGRADING SCHEDULE

16. DISTRIBUTION STATEMENT (of this Report) 30 OCT 1975 Distribution limited to U.S. Government agencies only (test and evaluation). Other requests for this document will be referred to AFAL/RWI-4, Wright-Patterson AFB, Ohio.

17. DISTRIBUTION STATEMENT (of the abstract entered in Block 20, if different from Report)

18. SUPPLEMENTARY NOTES

19. KEY WORDS (Continue on reverse side if necessary and identify by block number)

IR Linear Detector Arrays CO_2 laser beam expander
IR Receivers heterodyne and nonheterodyne

20. ABSTRACT (Continue on reverse side if necessary and identify by block number)

Design, fabrication and test of a beam expander for a 250-watt CO_2 laser is described. A laser beam of circular cross section is expanded into a fan-shaped beam 5 milliradians by 1 milliradian. The design, fabrication and test of two five-channel receivers for use at 10.6 micrometers is described. A non-heterodyne five-channel receiver uses a linear array of five

DD FORM 1 JAN 73 1473 EDITION OF 1 NOV 65 IS OBSOLETE

UNCLASSIFIED

SECURITY CLASSIFICATION OF THIS PAGE (When Data Entered)

20)

photoconductive (Hg,Cd)Te detectors with D^*_λ of 2×10^{10} cm $Hz^{1/2}/W$. The preamplifier video bandwidths are 10 Hz to 1 MHz. A linear array of five photovoltaic (Hg,Cd)Te detectors is used in the heterodyne five-channel receiver. The preamplifiers have i-f bandwidths of 7 MHz to 13 MHz and video bandwidths after the second detector of dc to 1 MHz.

PREFACE

This report summarizes the technical activities conducted at the Honeywell Radiation Center, 2 Forbes Road, Lexington, MA 02173 under Contract No. F33615-72-C-1556, from April 1972 through April 1975. This program was conducted under Project 2004, Task 200402.

The technical monitor for the government was Mr. William C. Schoonover of the Air Force Avionics Laboratory/RWI at Wright-Patterson AFB, Ohio. The five-channel nonheterodyne optical receiver using a linear array of photoconductor detectors at 10.6 micrometers was evaluated at the Air Force Avionics Laboratory by Mr. C. Stevens, AFAL/TEA. This receiver has been extensively and successfully used in an Air Force sensor flight test program at the Environmental Research Institute of Michigan. The contractor's measurement of the detector quantum efficiency for the five-channel heterodyne optical receiver has been confirmed at the Air Force Avionics Laboratory by Mr. P. Schriber, AFAL/TEA. A single (Hg,Cd)Te photovoltaic detector, with similar characteristics to those described in this report, has been successfully flight tested by Raytheon Company under a separate Air Force Contract.

The prime Honeywell Radiation Center personnel which technically contributed to the program were D. MacDonald, R. Pellar, J.B. McCullough, T. Koehler, D. Shafer, R. Wespiser, M.C. Terrell, and J. Wiley.

TABLE OF CONTENTS

LIST OF ILLUSTRATIONS

LIST OF ILLUSTRATIONS (CONT.)

LIST OF ILLUSTRATIONS (CONT.)

LIST OF TABLES

SUMMARY

The objectives of the program were:

- The design and fabrication of a beam expander for a 250-watt cw laser.
- The design and fabrication of a five-channel nonheterodyne optical receiver using a linear array of photoconductive (Hg,Cd)Te detectors at 10.6 micrometers.
- The design and fabrication of a five-channel heterodyne optical receiver using a linear array of photovoltaic (Hg,Cd)Te detectors at 10.6 micrometers.

SECTION 1

INTRODUCTION

This report describes the design, fabrication and test of a beam expander for a 10.6-micrometer laser, a nonheterodyne 10.6-micrometer five-channel receiver, and a heterodyne 10.6-micrometer five-channel receiver.

The objective of the procurement was to evaluate the use of linear arrays of closely spaced detectors with a mechanically scanned fan-shaped 10.6-micrometer laser beam in both the heterodyne and nonheterodyne modes for use in airborne vehicles. The fan-shaped illuminator beam used in conjunction with a matched detector array permits lower cross-track scanning rates to be used with less doppler spread from the scanning mirror. This is an advantage in moving target indication of slowly moving target vehicles. The beam expander converts a 0.25-inch diameter, CO_2 laser beam into a fan-shaped beam with an FOV of 5 milliradians by 1 milliradian, and is capable of handling 250 watts cw.

The receiver channels of the nonheterodyne array have a video bandwidth of 10 Hz to 1 MHz with dc restoration, while the heterodyne array receiver channels have two outputs, an i-f output which can vary from 7 MHz to 13 MHz and a video output with an upper limit of 1 MHz.

SECTION 2

ANAMORPHIC LASER BEAM SHAPER WITH A PHASE STEP

Some active infrared optical systems irradiate a scene with a laser beam and image this onto a linear array of detectors. The contractor has designed and built an active system which optically modifies the output of the laser in order to irradiate the scene in a more favorable fashion.

OPTICAL DESIGN

The optical system described here shapes the far field intensity pattern of a CO_2 10.6-μm laser beam, but the same principles can be used at any wavelength. The normal Gaussian pattern is altered so that the energy falling within the field of view of a row of 5 square detectors is nearly equal on each detector, and yet the energy which falls outside their total field of view is minimized.

The first step in the design of such a laser beam shaper is to consider the effects of simple modifications to a laser beam upon its far field intensity distribution. Let us consider five detectors in a row, each corresponding to a 1.0 x 1.0 milliradian square field of view when used in conjunction with some imaging optics. Spacing between the detectors is 10% of their width, and the array is shown in Figure 1.

Now the simplest possible approach would be to irradiate this field of view with a Gaussian laser beam with a far field divergence of, for example, 5 to 10 milliradians at the $1/e^2$ intensity points. This is shown in Figure 2. In both cases it is clear that most of the laser beam energy falls off the detectors and is wasted. In the case of the 5.0-milliradian beam divergence, more energy falls on the detector but less uniformly, with the end detectors positioned in the weak tail of the Gaussian distribution.

The next step up in sophistication is to squeeze the Gaussian beam in one direction by using an anamorphic optical system following the laser. By this means, a 5.0-milliradian divergence beam can be made to match more closely the detector array, as shown in Figure 3. Most of the energy falls on the detectors, but the end detectors are still very poorly irradiated compared to the center detector.

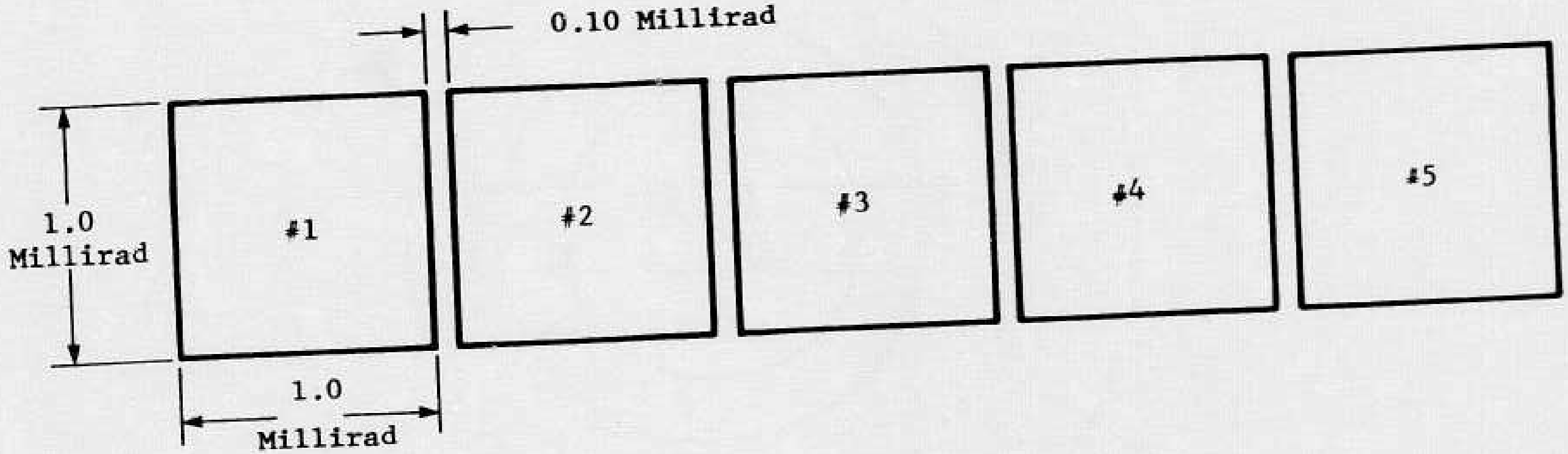

Figure 1 Detector field of view

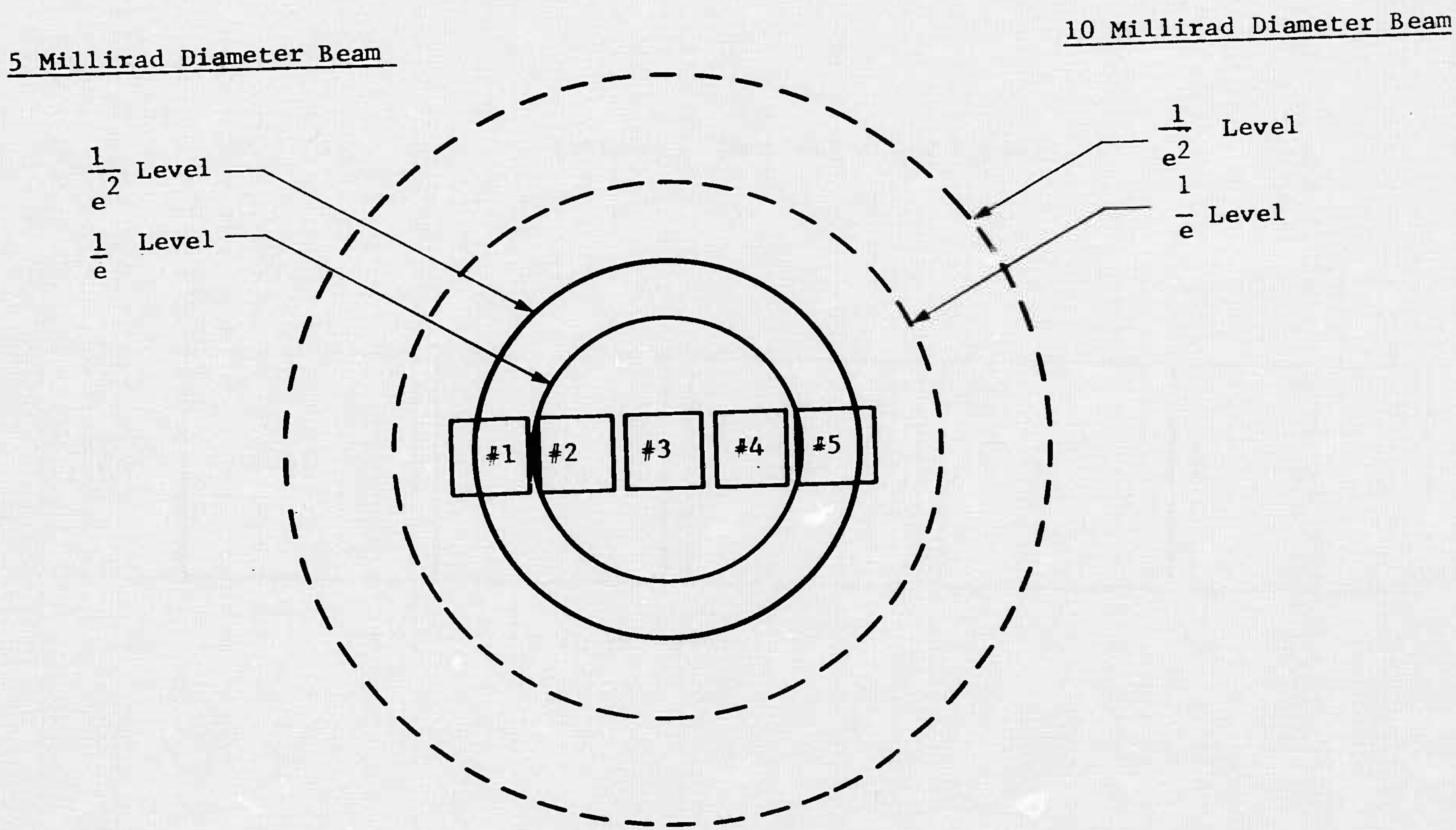

Figure 2 Gaussian beam match to detector fields of view

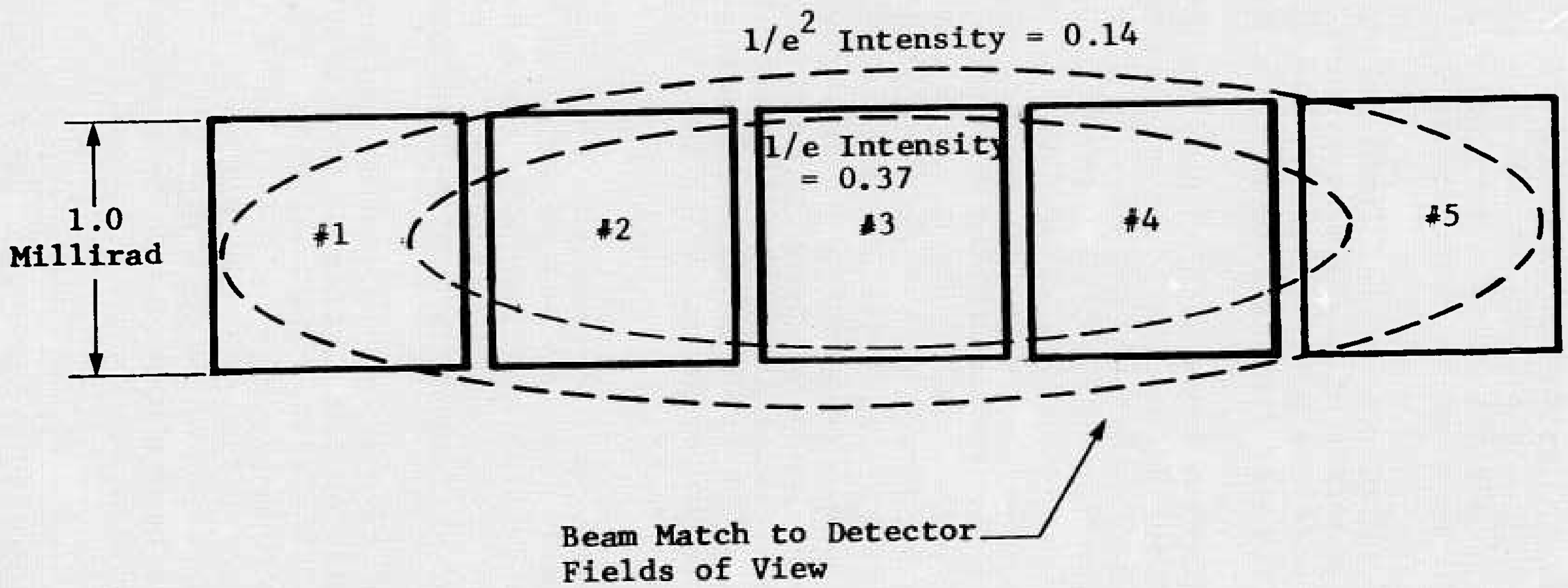

Figure 3 Anamorphically compressed gaussian beam

Nothing more can be done as long as the Gaussian distribution is retained. However, by introducing a phase step into the beam, the far field distribution can be made to assume a variety of different forms.* One type of distribution in particular gives good uniformity of energy from detector to detector as will now be shown.

Figure 4 shows the effect on the far field intensity distribution of increasing the diameter of a phase step which introduces a $\lambda/2$ phase retardation into the central part of the laser beam. The transmission of the phase step is assumed to be 100%.

In case D, the pattern appears as a ring of radiation with a dark center and a faint set of concentric side-lobes which are very weak and will be ignored for the moment. If this ring of radiation is compressed in one direction by an anamorphic optical system, it can be matched with the detector array field of view in the manner shown in Figure 5. The $1/e^2$ width of the radiation ring is indicated. This case clearly shows a more uniform distribution of energy from detector to detector than the simple Gaussian case shown in Figure 3. Because of the curvature of the ring's elliptical shape, more length of the radiation ring falls on detectors No. 2 and No. 4 than on the center one. By choosing the beam divergence properly, the end detectors, No. 1 and No. 5, can be made to receive energy equal to that on the center detector. Although this is only a qualitative analysis, it is clear that the amount of energy each detector receives is proportional to the length of the ring of radiation that falls on it.

It turns out, however, that the optimum far-field pattern is that of case C of Figure 4. It consists of a ring of radiation with a central spot. The central spot increases the energy on the central detector and by adjusting the divergency of the pattern in the far field, the detector uniformity is better than that in case D.

A beam shaper based on a $\lambda/2$ phase step and an anamorphic optical system has been built by the contractor for use with a high power CO_2 laser (250 watts). The design goal was that at least 75% of the energy leaving the beam shaper should fall on the 5 detector fields of view shown in Figure 1 and that the energy variation from detector to detector be no more than 25%. Furthermore, the transmission of the beam shaper was to be maximized.

---

*Haskel H. "Thermomagnetic Writing with Non-Gaussian Laser Beam Intensity Distributions" IEEE Vol. 58, No. 5, P. 802, 1970.

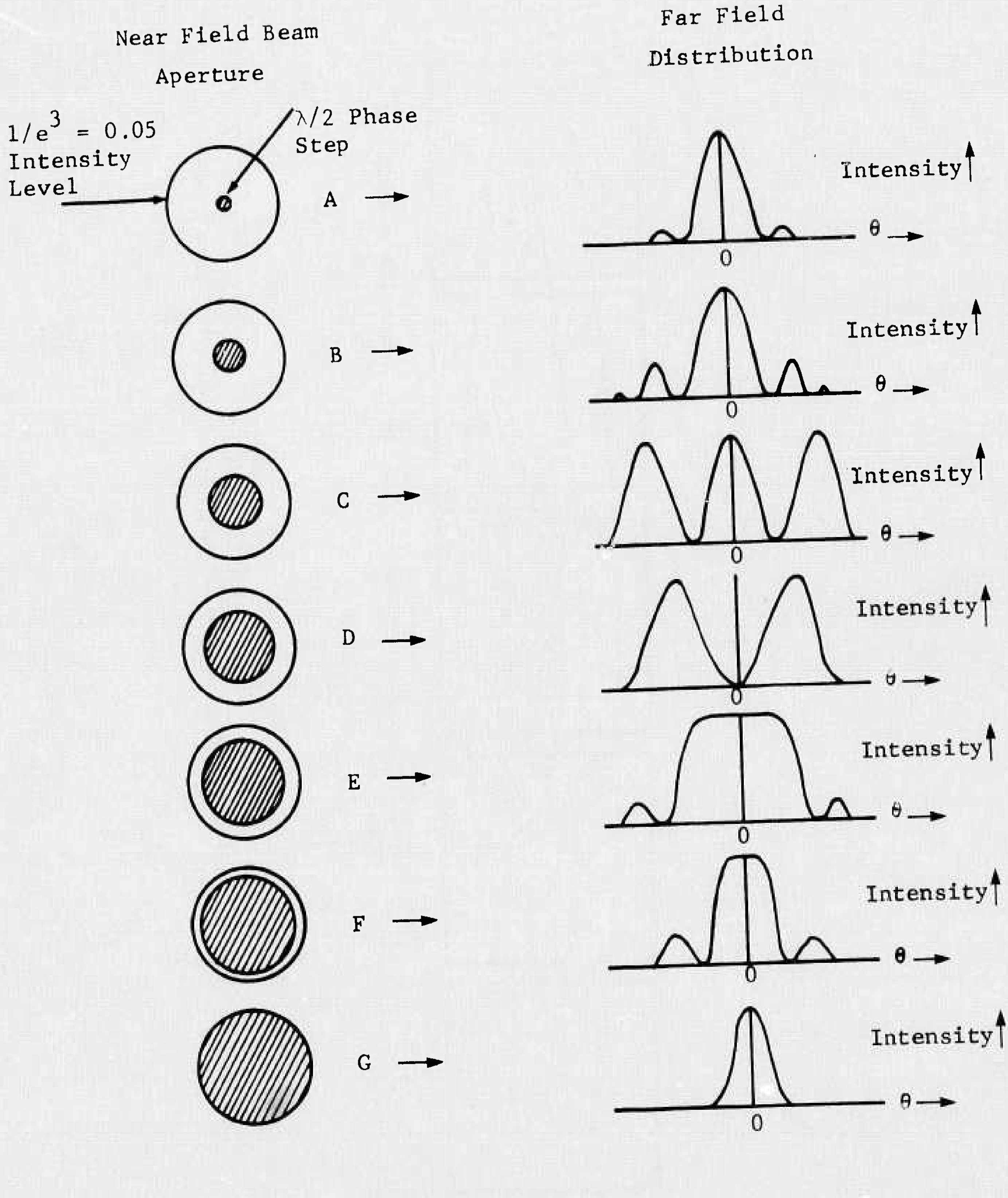

Figure 4 Phase step in gaussian beam

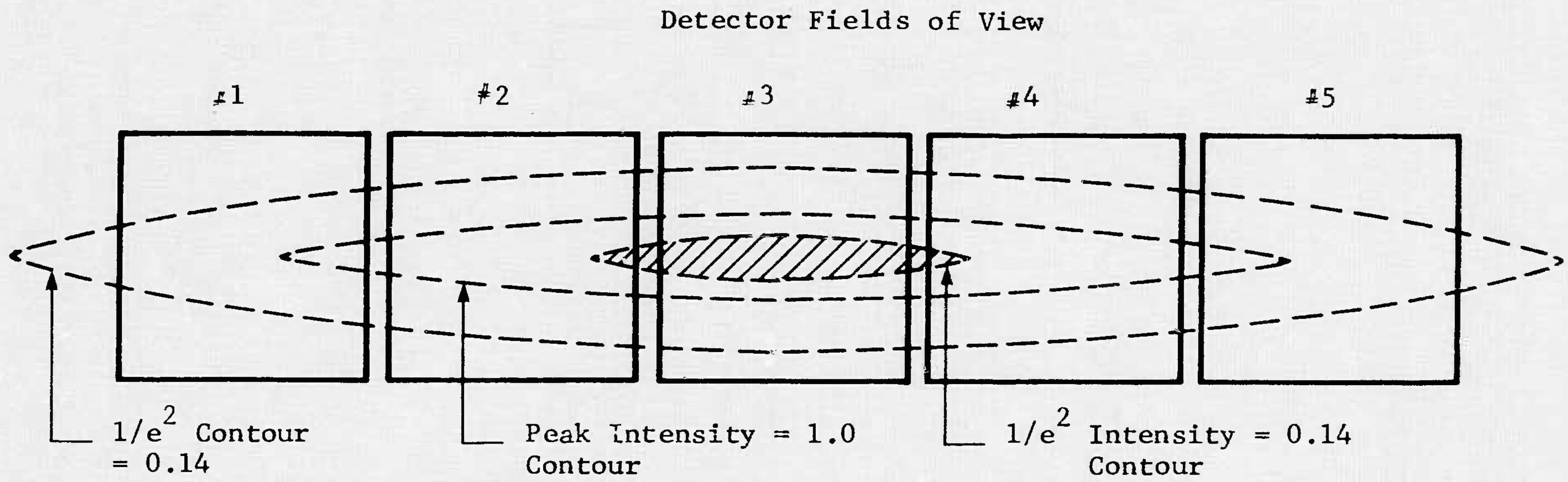

Figure 5 Phase step altered gaussian beam - anamorphically compressed

The first part of the design consists of an all-reflective beam expander; this is shown in Figure 6. Because of the high power levels, refractive optics were not considered. The beam expander, which is an 8-power telescope, consists of two spherical mirrors. They are used with the input laser beam displaced from the optical axis of the telescope so that there is no obscuration introduced into the beam. By using long radii on the two mirrors, it was easy to obtain a diffraction-limited (at 10.6 μm) design, that was reasonably compact. The contractor's design converts a 0.63-cm diameter beam (measured at the $1/e^2$ points) from the CO_2 laser into a 5.1-cm diameter output beam within a length of 75 cm. The mirrors are sized so as to truncate the Gaussian laser beam at the $1/e^3$ points. This results in a 5% energy loss.

A $\lambda/2$ reflective phase step is located on the surface of the second mirror of the beam expander. It was deposited onto the mirror before the final gold coating and has a diameter which is 45% of the mirror diamater. An analysis indicated that if the Gaussian beam is truncated at the $1/e^3$ intensity points, a $\lambda/2$ phase step, which is 45% of the diameter of the truncated beam,would give the optimum performance (as defined earlier). Since the wavefront is to have a $\lambda/2$ step introduced, the reflecting phase step on the mirror must be $\lambda/4$ thick.

The second part of the beam shaper is an anamorphic system which squeezes the output of the 2-mirror beam expander in one direction. This consists of a pair of cylindrical mirrors which make up an 8-power reducing telescope, as shown in Figure 7, where it is combined with the preceding beam expander.

Now the beam size leaving the two-mirror beam expander, if allowed to travel out to the far field, would have a $1/e^2$ intensity level diameter of 0.78 milliradian as compared to 0.34 milliradian for the same beam diameter without the phase step, as shown in Figure 8. Therefore, the 1.0-milliradian square fields of view of Figure 1 are matched in one direction. The beam spread in the other direction depends on the diameter compression ratio introduced by the anamorphic telescope following the beam expander. Since this is an 8-power telescope in one direction and has no effect at all in the orthogonal direction, it follows that the far field pattern will also be stretched by that ratio and will have a $1/e^2$ intensity level contour that is 0.78 milliradian in the short direction and 6.24 milliradians in the long direction.

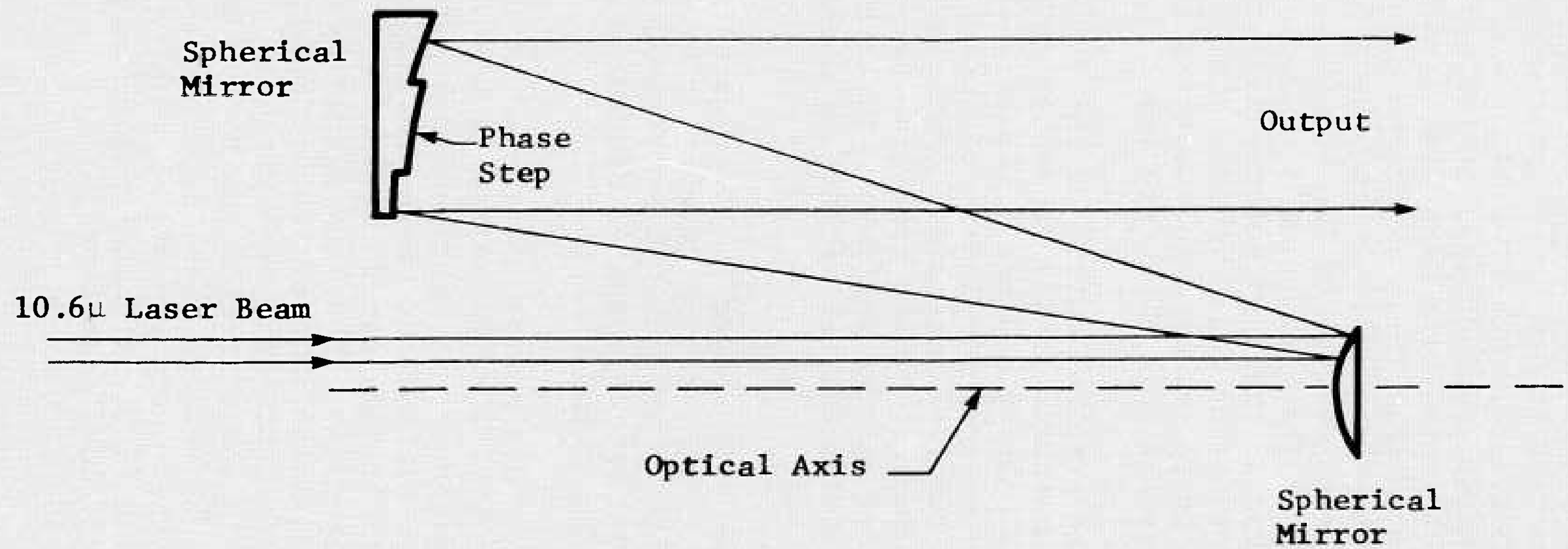

Figure 6 Beam expander (not to scale)

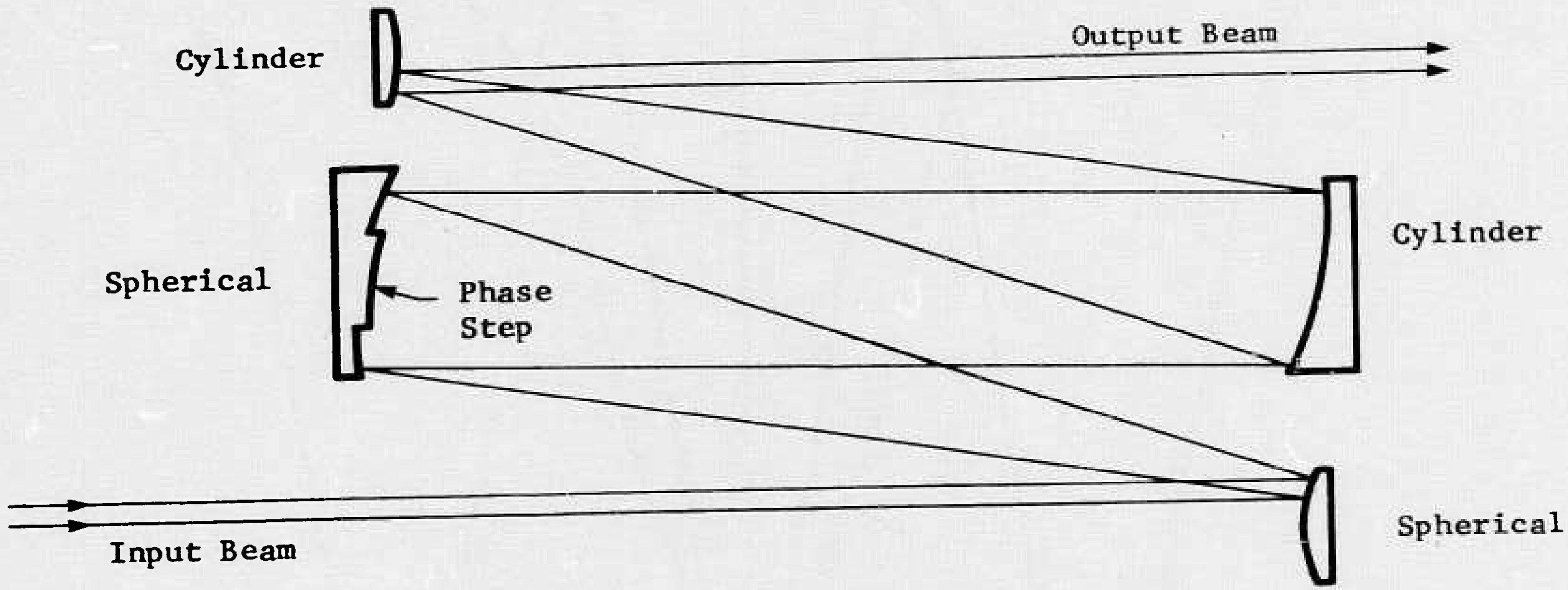

Figure 7 Laser beam shaper (not to scale)

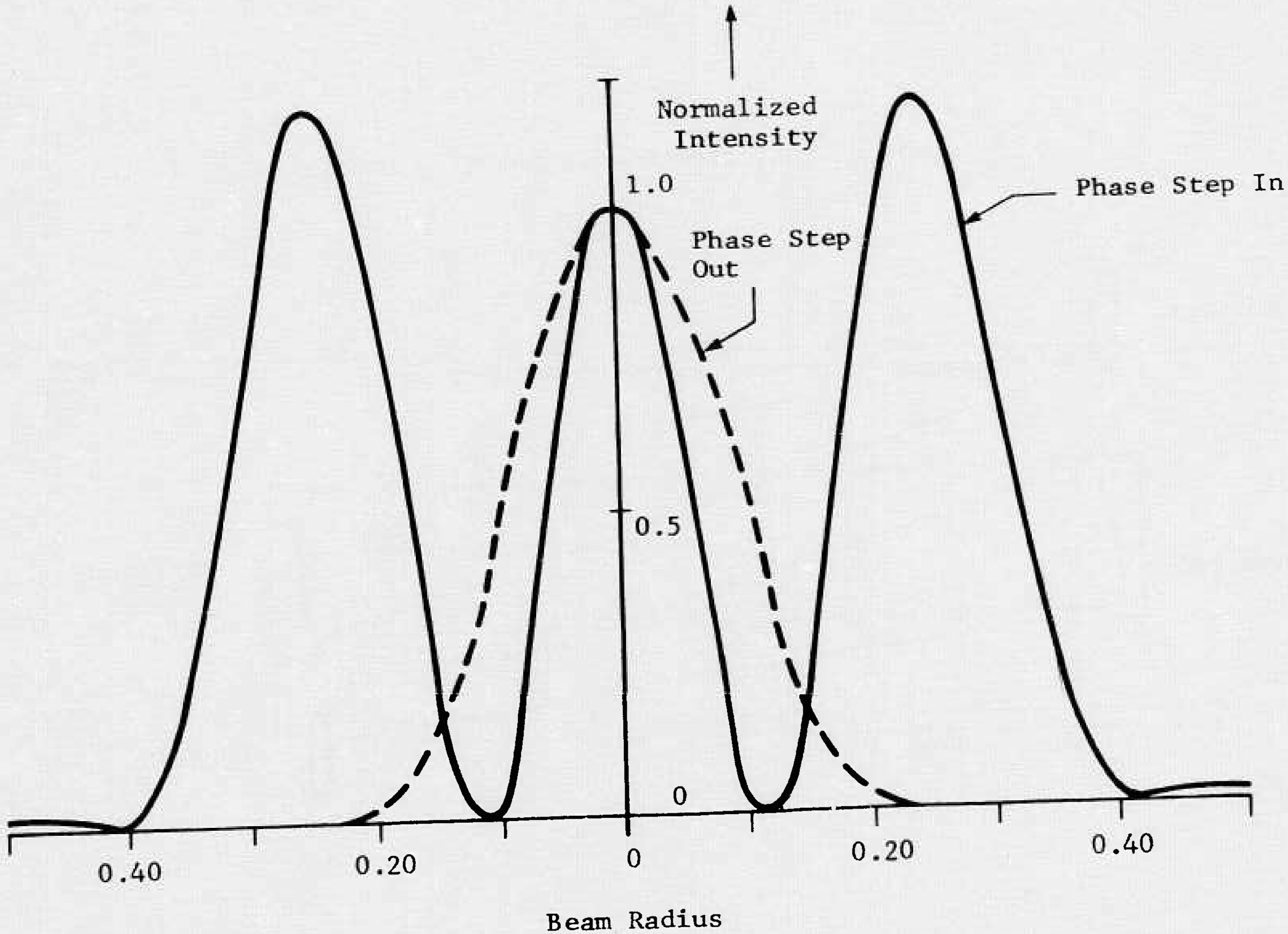

Figure 8 Far field beam profile

For the particular parameters of this system, it turned out that the magnification required for the two-mirror beam expander (8X) is the same as the reduction ratio (8X) of the two-mirror anamorphic beam compressor. The magnification and the anamorphic minification would not generally be the same, but since they are for this design, it means that the first two mirrors are actually superfluous - the two cylindrical mirrors alone would suffice if used in reverse order and with the phase step placed on one of the mirrors. This simpler one-stage system was not built because a long thin elliptical shaped phase step would be required on the large cylindrical mirror which would be difficult to deposit accurately. On the small mirror, the phase step could be circular but would have to withstand the high power density of the 250-watt laser beam, which was thought to be risky. In actual tests, the small mirrors easily withstood the high power densities with no apparent damage, so the phase step probably could have safely been placed on a small mirror and the simpler one-stage design used. Of course with different system parameters, the more general two-stage design would usually be required.

A computer program was written to integrate the energy in the pattern which falls within the 5 detector fields of view of 1.0 x 1.0 milliradian. The predicted results are shown in Figure 9. There is a tradeoff involved in the optimum magnification choice for the anamorphic telescope. The results of Figure 9 are for a design where the energy uniformity and the energy efficiency have been made equal. A slightly different value for the anamorphic magnification can result in an energy uniformity of 95% from detector to detector with only 21% of the energy falling outside the envelope of the 5 detectors. It is quite remarkable that such a small change in the amount of energy received can make a difference in the energy uniformity. The reason is that the tail of the pattern shown in Figure 8 has very little energy in it. Yet if the system is designed to bring that tail onto the detectors, than the uniformity will obviously suffer, with very little energy gain to compensate for the energy nonuniformity penalty.

To actually measure the true far field performance directly is impractical, because the far field does not begin until ranges of 500 meters or more. The presence of the phase step in the output wavefront causes the beginning of the far field region to be pushed much further away from the normal far field range, or "Rayleigh distance." For this reason, the intensity distribution at the focus of a parabolic mirror was measured with a mask having 5 slots

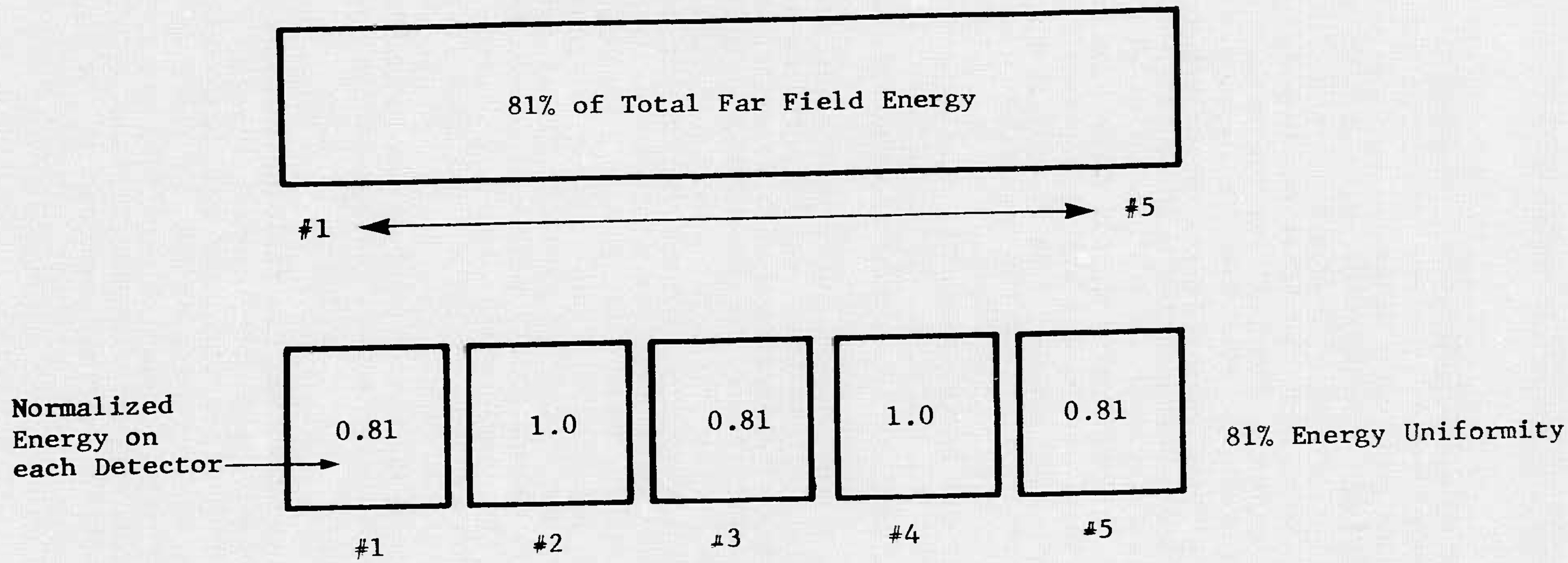

Figure 9 Energy efficiency and uniformity

of appropriate size to simulate the detectors, and a power meter. This arrangement simulates the far field behavior of the beam shaper. A 3-watt CO_2 laser was used for these measurements.

The diffraction pattern at the focus of the parabolic mirror, and hence the far field pattern of the laser beam shaper, is shown in Figure 10. The image is falling on an IR image plate which makes the pattern visible. Because of the large aspect ratio of the pattern, due to the anamorphic telescope, not much detail can be seen when the radiation is focused perpendicularly onto the IR image plate. For this reason, the IR plate was tilted by a large angle so that the very elongated diffraction pattern was projected onto the plate at nearly grazing incidence, thereby broadening out the pattern to the nearly circular shape of Figure 10, so that the detail can be seen. The ring of radiation with the central bright spot (Figure 8) is clearly visible (the IR plate gives a negative image). No sidelobes are visible.

The measured performance for uniformity, detector to detector, and energy loss outside the envelope of the 5 detectors is:

Measured Results

Energy in envelope of field of view	77%
Energy uniformity from detector to detector	82%

The design goals were met, and in a high power test with a 250-watt laser, none of the mirrors rose in temperature by more than a few degrees, while the gold coatings were unaffected. An interesting feature of the optical system is its lack of sensitivity to many parameters. The mirrors can be misaligned by a considerable amount, the input laser beam be somewhat off from the correct beam diameter, the beam off-center on the mirror having the phase step, and the laser have an output which is not very Gaussian in profile, andyet the system still retains its good performance numbers.

A simple optical system has been described which shapes the far field diffraction pattern of a 10.6-micrometer high power laser into a particular desired shape. The measured performance numbers agree closely with the predicted design performance, and the system is not very sensitive to misalignment or defects with the input laser beam. The basic idea of using a phase step in a laser beam

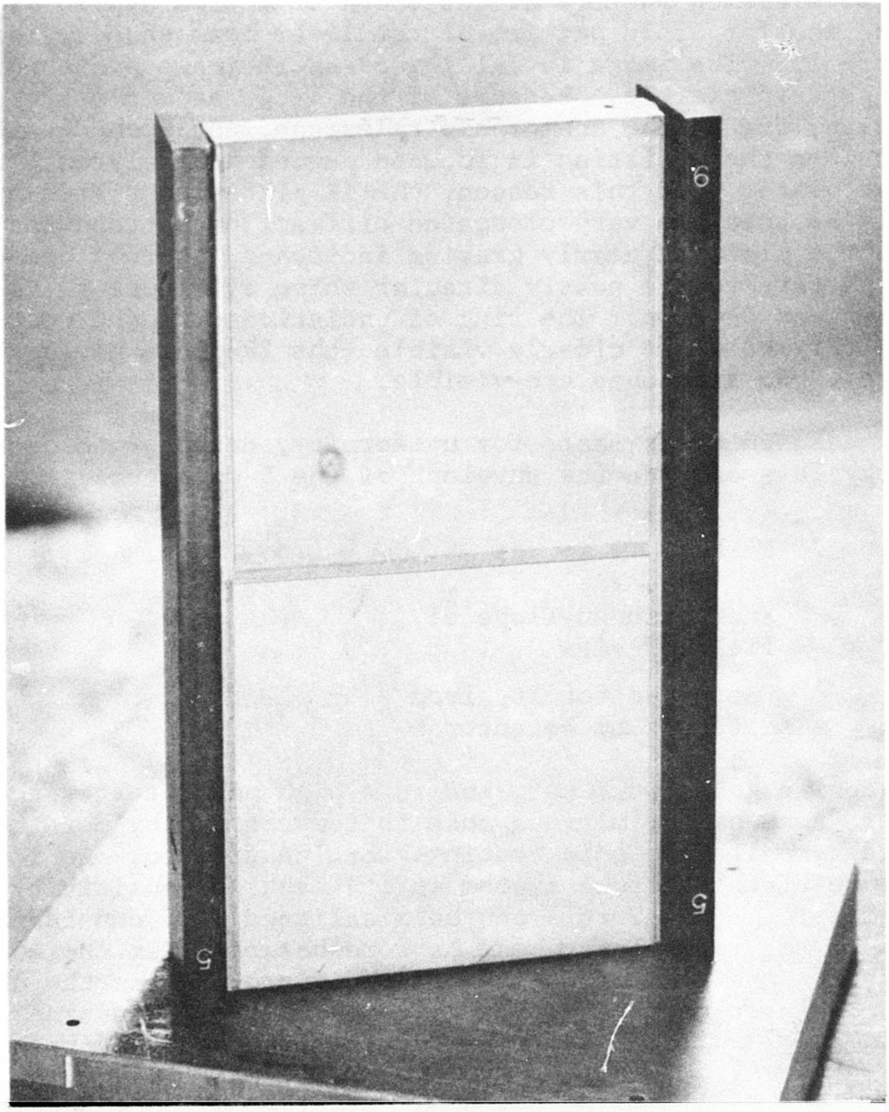

00706

Figure 10 Far field pattern of the laser beam shaper to change the far field pattern in a desired fashion has, therefore, been proven both theoretically and experimentally to be a valid, practical, and useful solution to efficient and uniform laser beam illumination.

MECHANICAL DESCRIPTION

The beam shaper optics comprise four first surface reflector mirrors. (See Optical Schematic 21010072, Figure 11.) These mirrors, M1 through M4 are supported in end plates which are separated by a tube. Mirrors M1 and M3 are mounted in the Output Endplate, M2 and M4 in the Input Endplate.

Mirror M1 is mounted directly to the Endplate which serves as a heat sink. This design successfully passed laboratory tests with 250-watt cw CO_2 laser power impinging upon it. The remaining mirrors are supported by spring mounts and positioned with adjusting screws. These adjusting screws should not be tampered with unless optical characteristics of beam are to be altered.

The two internal thermal shields shown on Assembly Drawing 21010062 (Figure 12) are furnished but not assembled since their use is considered unnecessary. The input shield, however, is considered necessary until the input beam is properly aligned with the input apertures.

All parts which could contribute to thermal instability are made of aluminum. This will allow the assembly to expand and contract uniformly and remain in focus.

The Assembly can be monitored in any attitude through the use of the three mounting clamps. See Installation Drawing BK13A (Figure 13) for hole patterns.

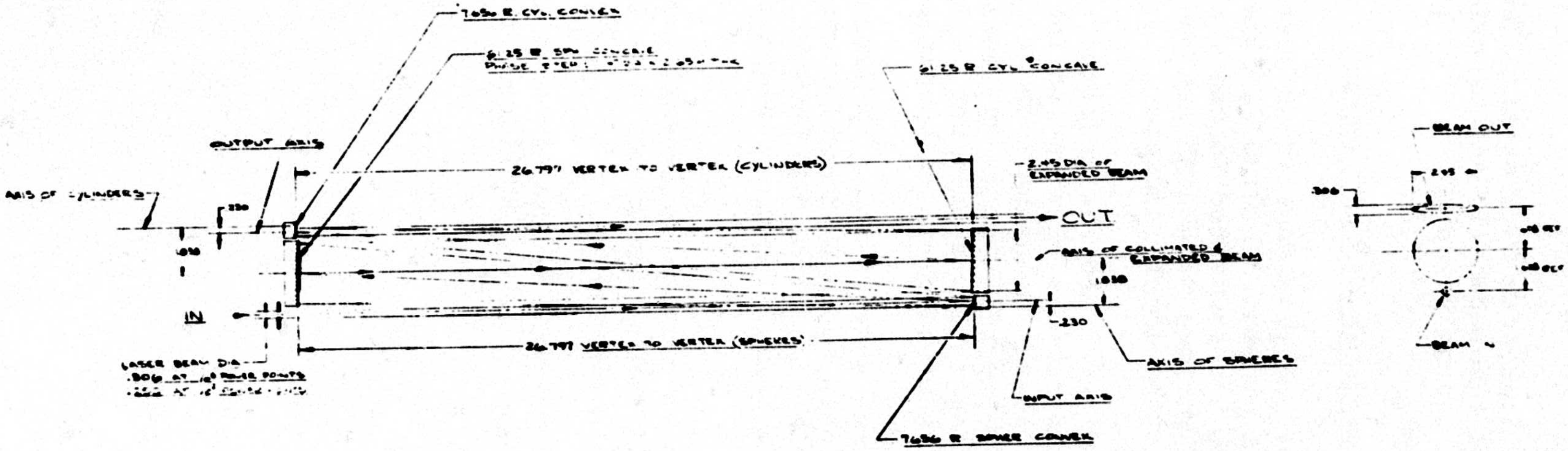

Figure 11 Optical schematic 21010072

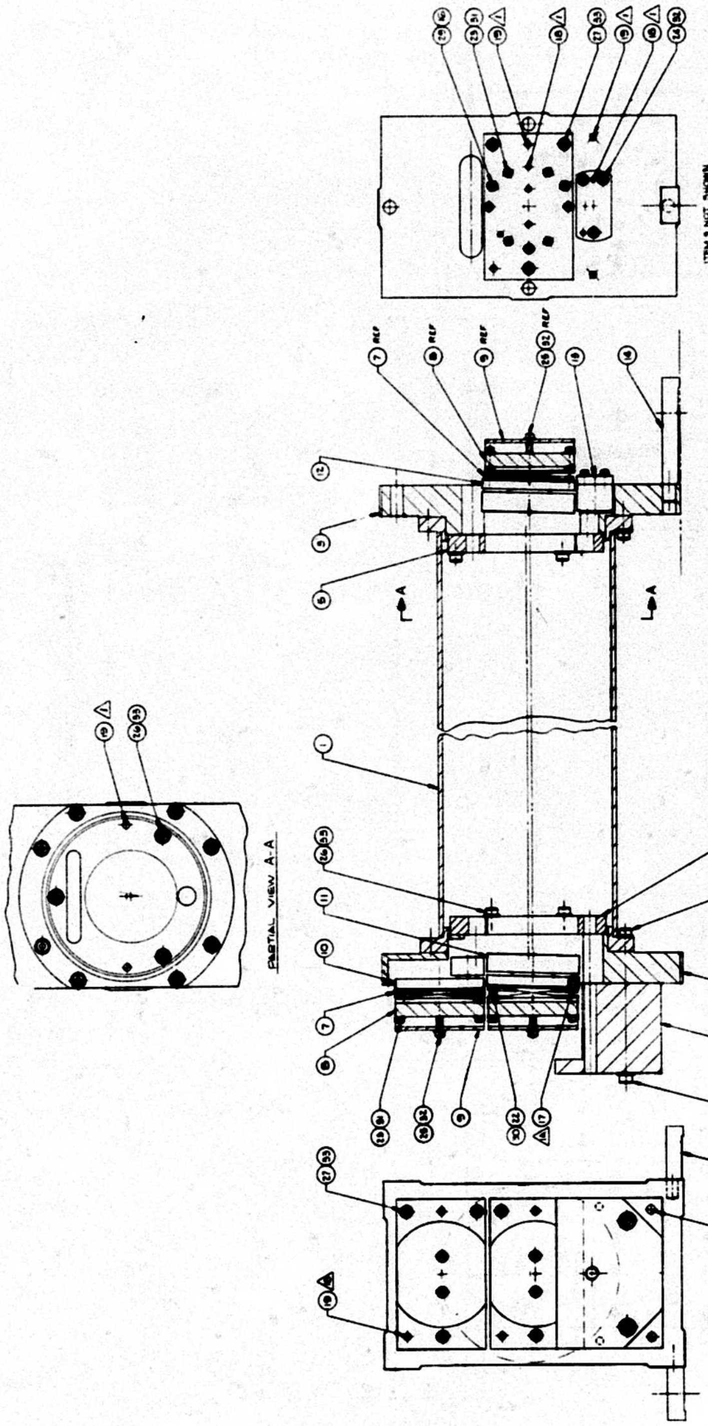

Figure 12 Assembly drawing 21010062

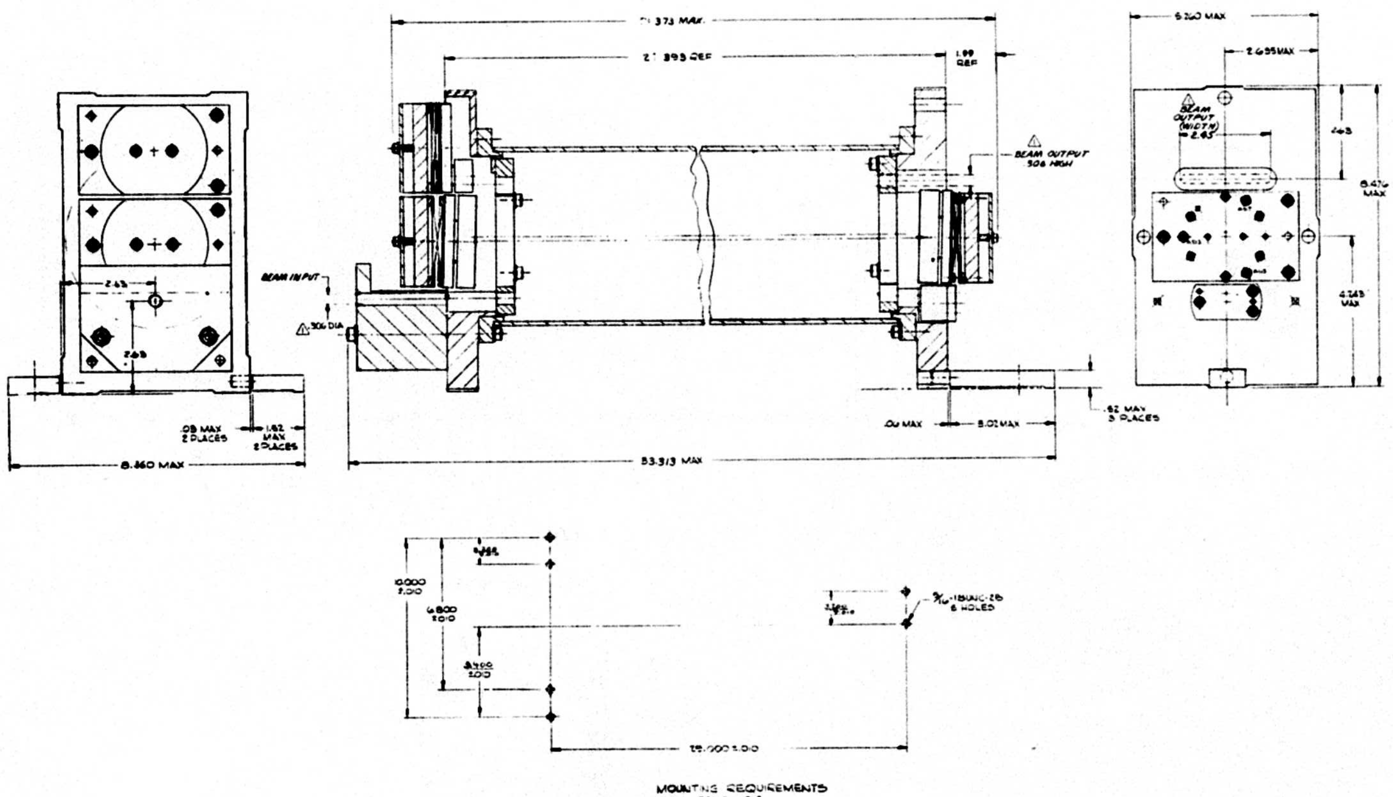

Figure 13 Installation drawing BK13A

SECTION 3

NON-COHERENT FIVE-CHANNEL RECEIVER

This section summarizes the technical effort expended in manufacturing a 5-element linear PC 10.6-micrometer (Hg,Cd)Te array for non-coherent operation. The specifications are delineated in Table 1.

Table 1

SPECIFICATIONS

Type detectors - Photoconductive (Hg,Cd)Te
Size detectors - 0.25 mm x 0.25 mm ± 10%
Detector spacing $\leq$ 0.025 mm
Cross talk $\leq$ 5% (Design goal $\leq$ 1%)
$D^*_\lambda \geq 2 \times 10^{10}$ cm Hz$^{1/2}$/watt (Receiver - See note)
Video bandwidth - 10 Hz to 1 MHz with dc restoration
Amplifier gain $\geq$ 40 dB
Filter width - 0.2 micrometer
Peak transmission of filter $\geq$ 65%
F number - 1
Coolant - LN_2
Coolant hold time with receiver operating $\geq$ 1 h

Note: This includes cold stop filter, window detector, amplifier, etc, which are used in video channel of receiver.

MANUFACTURING

The manufacturing relied on the mature PC array technology capability of the contractor which is well documented in engineering specifications, fabrication inspection orders, inspection procedures, and standard testing methods. Because the fabrication process is defined in detail in other documents, this section will only reference the documents used and will dwell on modifications, discrepancies or problems encountered in the manufacturing process.

The extraordinary items to be discussed include:

1. Documentation Reference List
2. Material selection procedure
3. Special cold 10.6-μm narrow band filter
4. Canting of cold filter to shift center frequency to 10.59 μm
5. Evaporation mask problems
6. G-factor calculation
7. Inadequacy of PE-112 to resolve detector/filter response
8. Test results on final array

Documentation Reference List

Part Number Final Array	21009213-102
EPA	23638-06
FIO (array fab)	A40172-141
Engineering specification	23158-ES05
FIO (final assy)	B40172-141
FIO (array rework)	RB40172-141
Engineering specification	23943-ES-2

Material Selection Procedure

Slab 40172-S141 was selected on the basis of data compiled and maintained by Toivo Juvonen in a regular program of ingot evaluation. The criteria for selection included:

1. Wavelength peak 10.6 μm
2. High percentage of BLIP
3. BLIP improvement with reduced background
4. Mercury pit density
5. Resistivity
6. Ingot Hall data

Cold Filter

The filter was purchased from OCLI and exceeded specifications. The actual figures were:

$$\lambda_o = 10.6057\ \mu m$$

$$\Delta\lambda = 0.0982\ \mu m$$

$$T = 75\%$$

Cold Filter Canting

Because the filter center wavelength was 0.0157 micrometer greater than the desired wavelength of 10.59 micrometers, the filter was canted with respect to the dewar axis by 3 degrees. The tilting was accomplished by inserting a FOV aperture which was machined with a 3 degree bevel.

Evaporation Mask Problems

The design goal for element spacing in the array was 0.001 inch. Extra material is usually allowed in the photomask to allow for etch undercutting. This gives the element a bowed cross section. The contact mask separations were exactly 0.001 inch. Problems occurred when the mask failed to cover the entire area to be evaporated, thus causing indium metallization to short adjacent elements. The problem can be solved by lapping elements thinner in order to minimize etch time, or by making contact mask pads undersize. A cleaning procedure which removed excess indium from the array spacing was used to fabricate the final array.

G-factor Calculation

The g-factor is calculated on the basis of OCLI test data because inhouse spectrometer could not resolve the filter spectrum. This calculation is shown in detail in the final acceptance test report. The factor was:

$$g = 182.17$$

where

$$D^*_{\lambda} = g\, D^*_{BB}$$

PE-112 Test Station Spectral Results

The spectral response measured at HRC indicates a half width of 0.46 micrometer (see Figures 14 and 15). Since the filter half width is 0.0982 micrometer, the detector with cold filter has resolved the slit width of the spectrometer. The slit width could not be reduced further because the sensitivity of the spectral test station is limited by the 6-Hz bandwidth of the HP 302 wave analyzer.

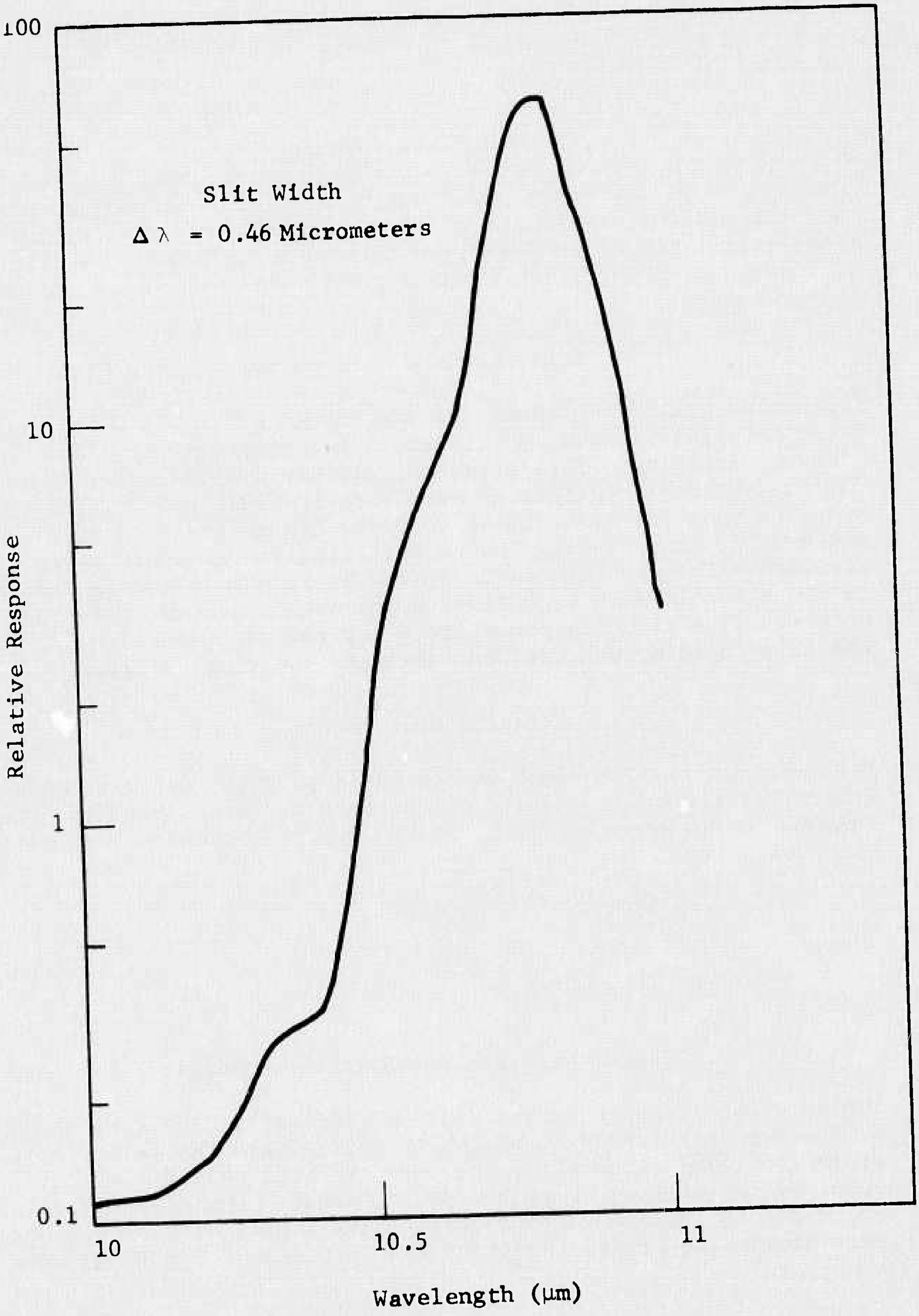

Figure 14 Relative response

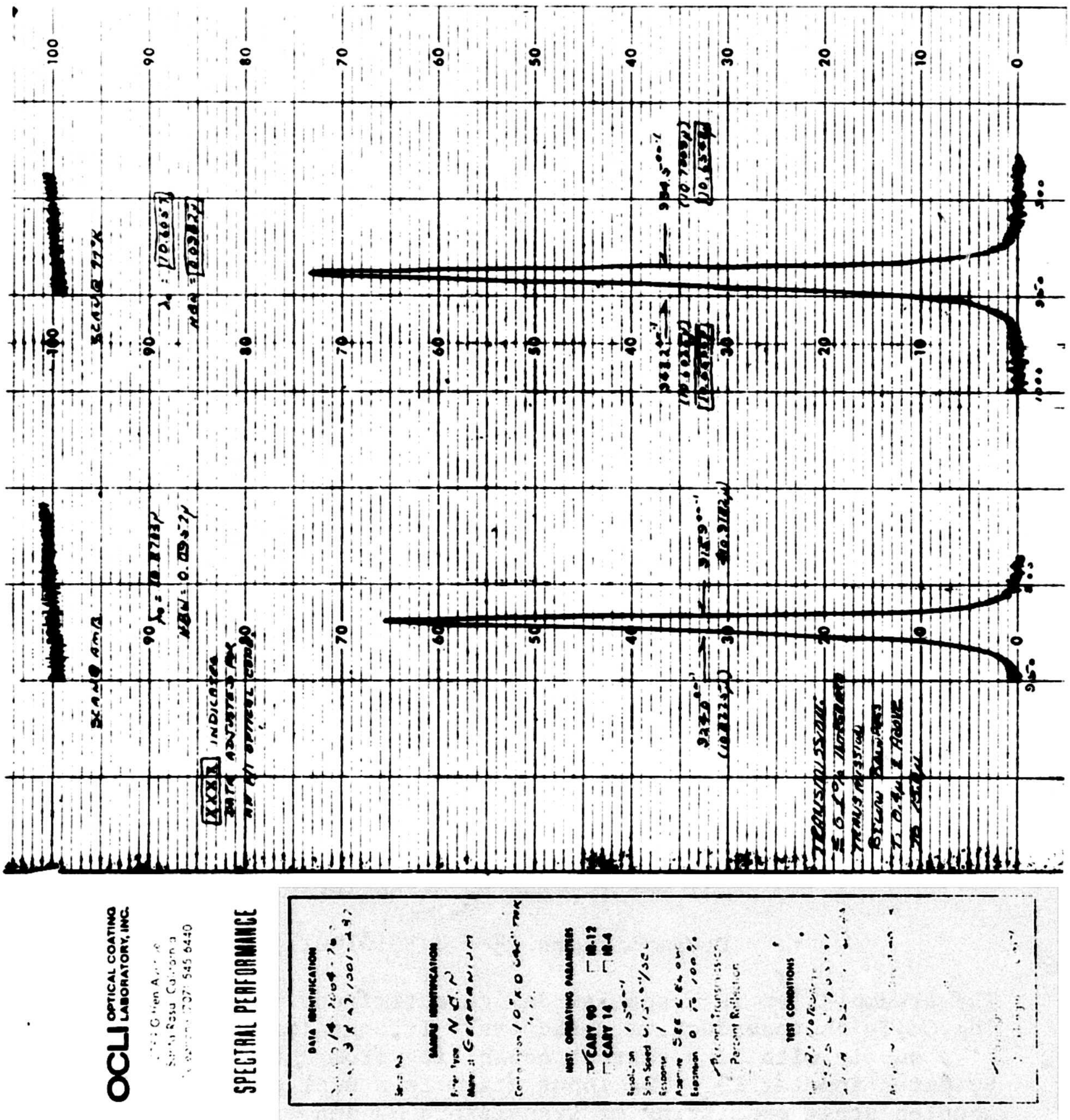

Figure 15 Spectral performance

Test Results

All the elements of the 5-element array met the design specification D^*_λ (10.6 μm, 10 kHz, 60°, 1) of 2×10^{10} cm $Hz^{1/2}$/watt. The results are shown in Table 2.

Table 2

D^*(10.6 μm, 10 kHz, 60°, 1)

Element	R_d(77°K) ohms	D^*_{BB} cm $Hz^{1/2}$/W	D^*_λ cm $Hz^{1/2}$/W	R_λ V/W
1	57.5	1.68×10^8	3.06×10^{10}	25,120
2	31.1	2.14×10^8	3.9×10^{10}	21,980
3	26.9	1.9×10^8	3.46×10^{10}	17,590
4	36.8	3.33×10^8	6.07×10^{10}	30,150
5	41.8	7.14×10^8	1.3×10^{11}	21,360
Acceptance Criterion: $D^*_\lambda = 2 \times 10^{10}$ cm $Hz^{1/2}$/watt minimum				

SIGNAL PROCESSING CIRCUITRY

Preamplifiers (Ref. F21010013)

The preamplifier is a special design optimized for high speed (Hg,Cd)Te photoconductive detectors. It contains a well regulated bias supply with bias current capability from 0 to -6 mA determined by potentiometer R3. The input stage is a dual common emitter, ac coupled stage consisting of transistors Q2 and Q3 and capacitors

C4, C5 and C6. Transistor Q1 provides a low impedance load for the input stage thus minimizing the Miller capacitance effects, L1 & R5 determine the peaking provided in the frequency response with C10 controlling the major part of the upper -3 dB point. The frequency response is set at -3 dB at 20 Hz and 2 MHz with +3 dB of peaking at 1.2 MHz to compensate for optical spatial MTF and detector temporal responses. Transistor Q4 provides level shifting to transistor Q5 which is the output emitter follower stage. Overall preamplifier gain is controlled by R6 and can be varied from 0 to 2000 to account for detector responsivity and dynamic range capability. The output signal range is approximately ±6 volts, ac coupled to the load by capacitor 69. Due to large gr noise of the detector, the preamplifier noise figure is negligible.

Clamp and Buffer Stage (Ref F21010011)

For channel number 1, R4 provides impedance buffering from the preamplifier during clamping and sets the clamp frequency response. Resistor R5 determines low frequency cutoff of this stage with C9 of the preamplifier when the clamp is open. The operational amplifier HA-2602, AR3 provides output signal buffering, with R6 providing impedance matching for long cable loads.

FINAL ACCEPTANCE TEST

This section covers the acceptance test data on the Non-coherent Receiver, LK128A1, provided as item 0001AC of contract F33615-72-C-1556.

APPLICABLE DOCUMENTS

21009110 - Detector Assembly (Non-coherent), Figure 16
21009212 - Dewar and Detector Assembly, Figure 17
21009213 - Housing, Dewar and Detector Assembly, Figure 18
21009215 - Preamplifier Assembly, Figures 19 and 20
21010011 - Clamp and Buffer, Figure 21
21010012 - Power Distribution, Figures 22 and 23
21010013 - Preamplifier, Figures 24 through 27
LK128A - Installation - Non-coherent Receiver, Figure 28

TEST RESULTS

Mechanical Inspection

All dimensions and electrical wiring were verified to be in accordance with the drawings specified above.

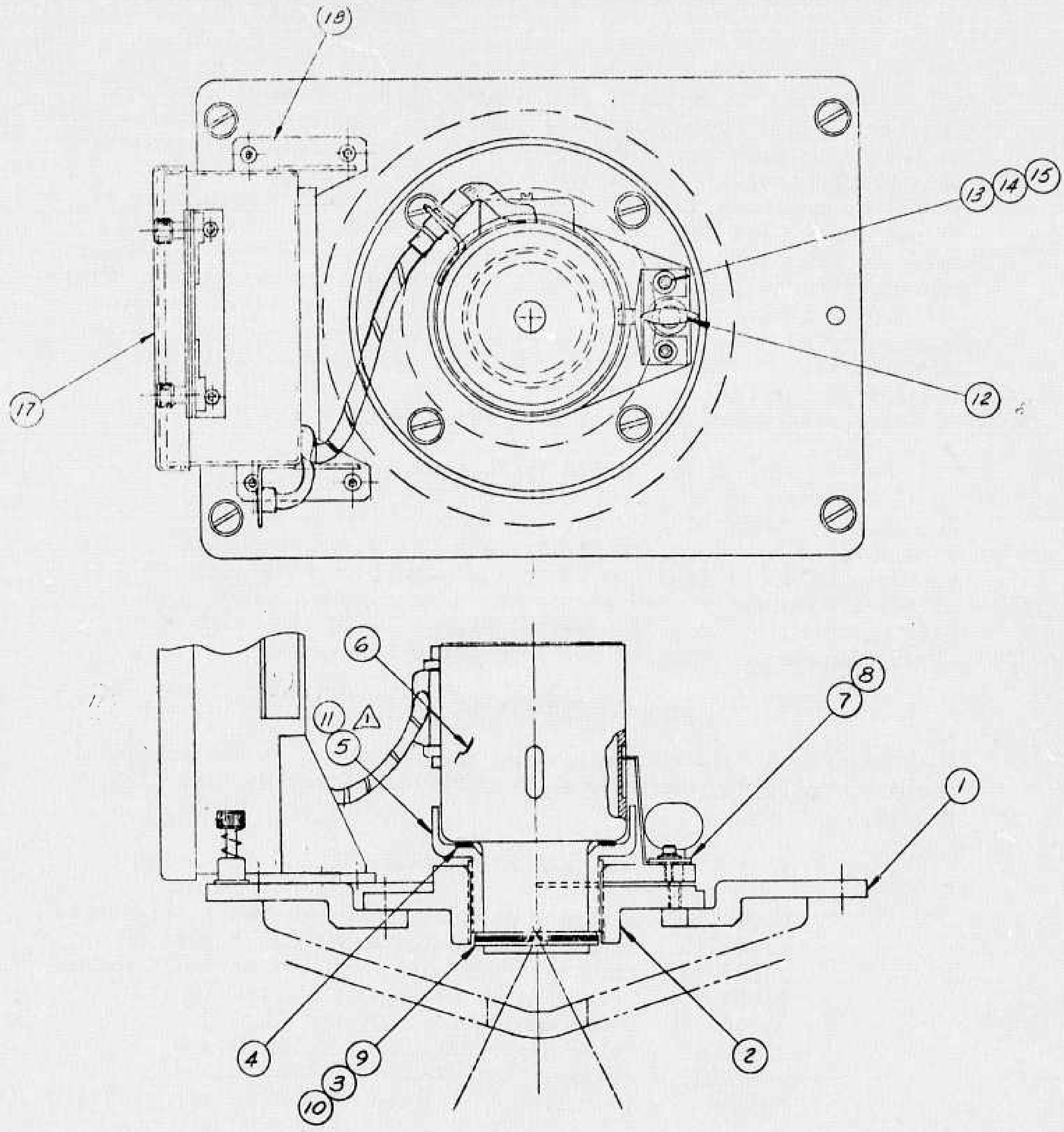

Figure 16 Detector assembly (non-coherent) 21009110

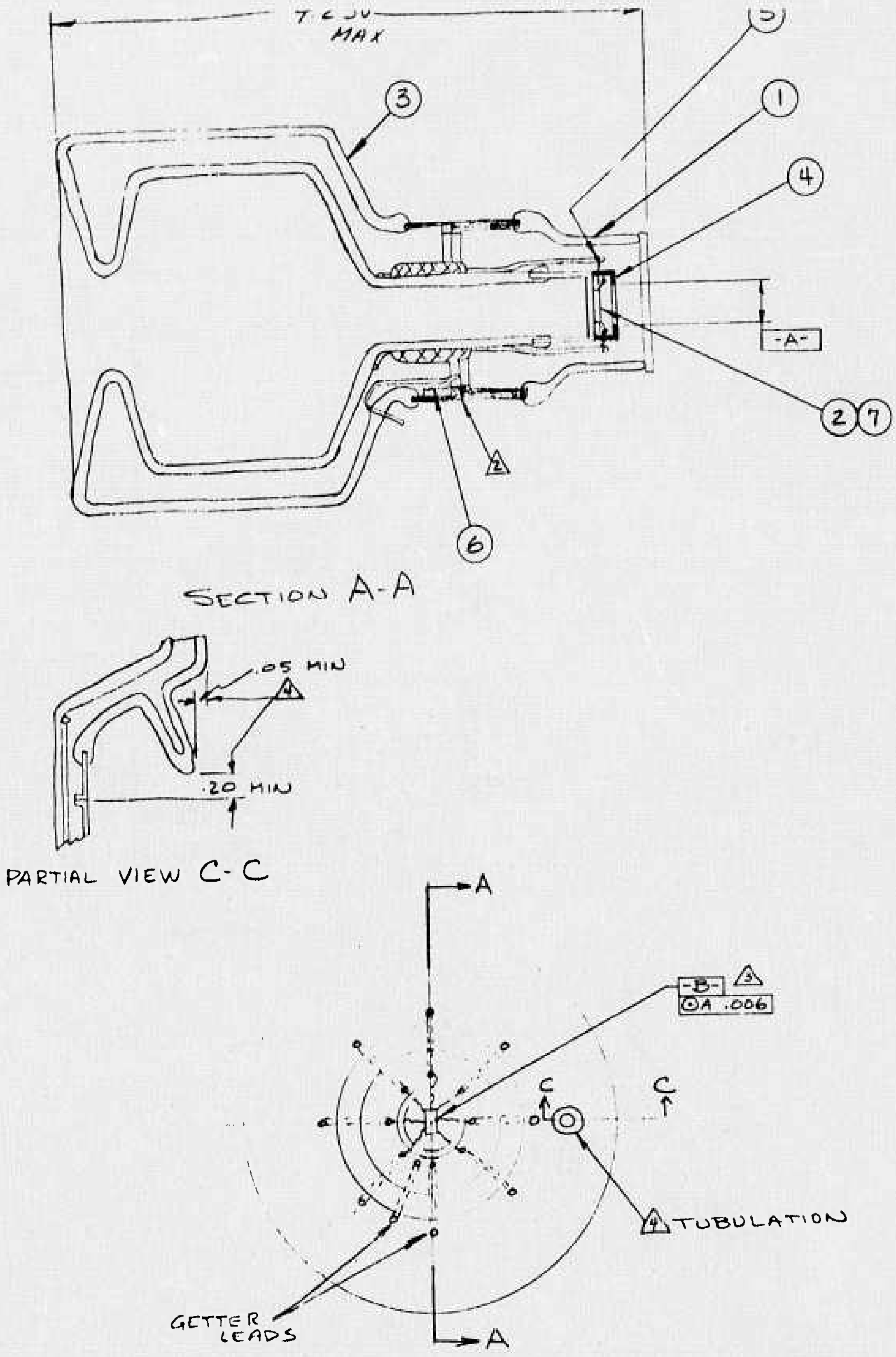

Figure 17 Dewar and detector assembly (21009212)

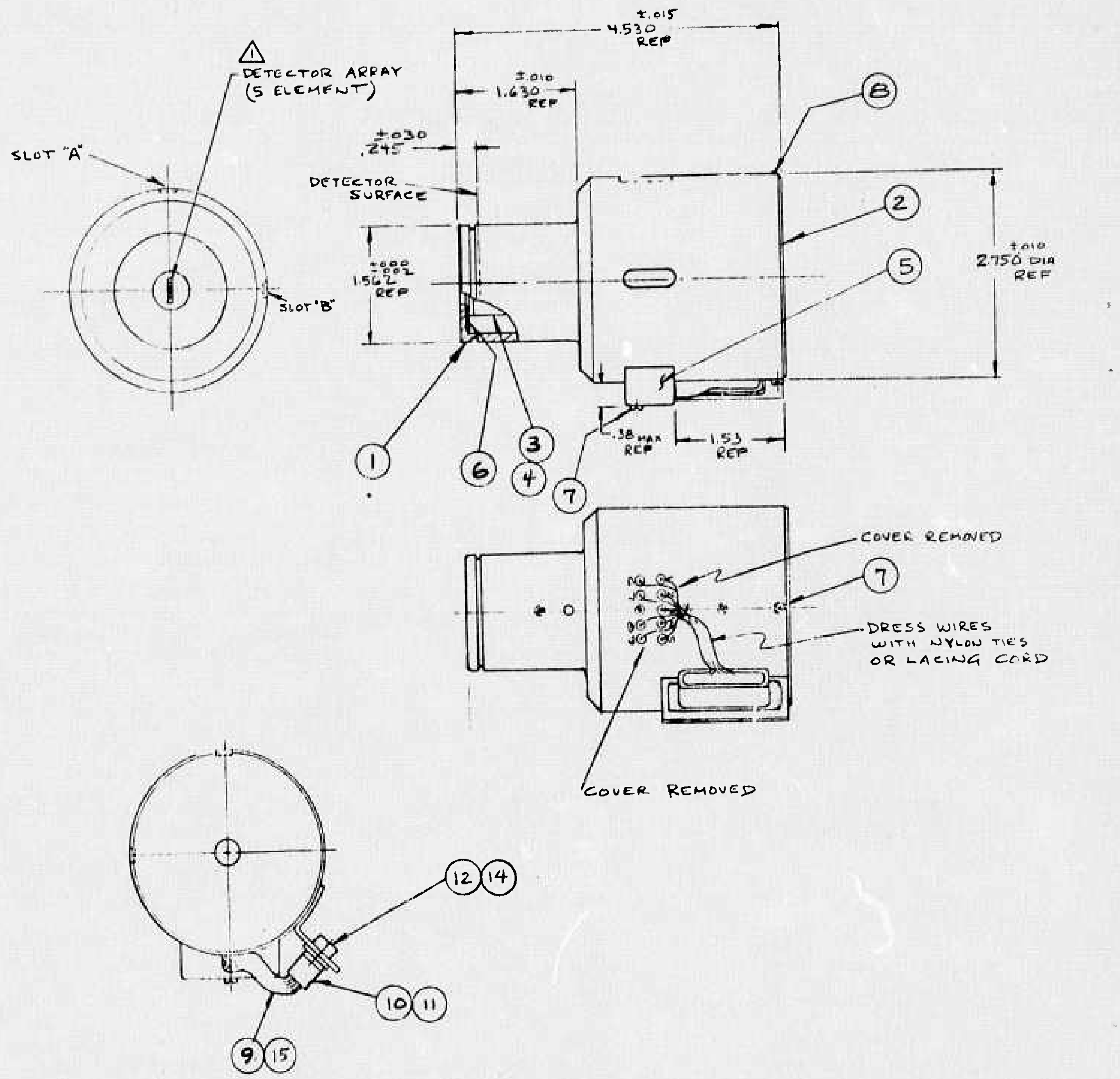

Figure 18 Housing, dewar and detector assembly (21009213)

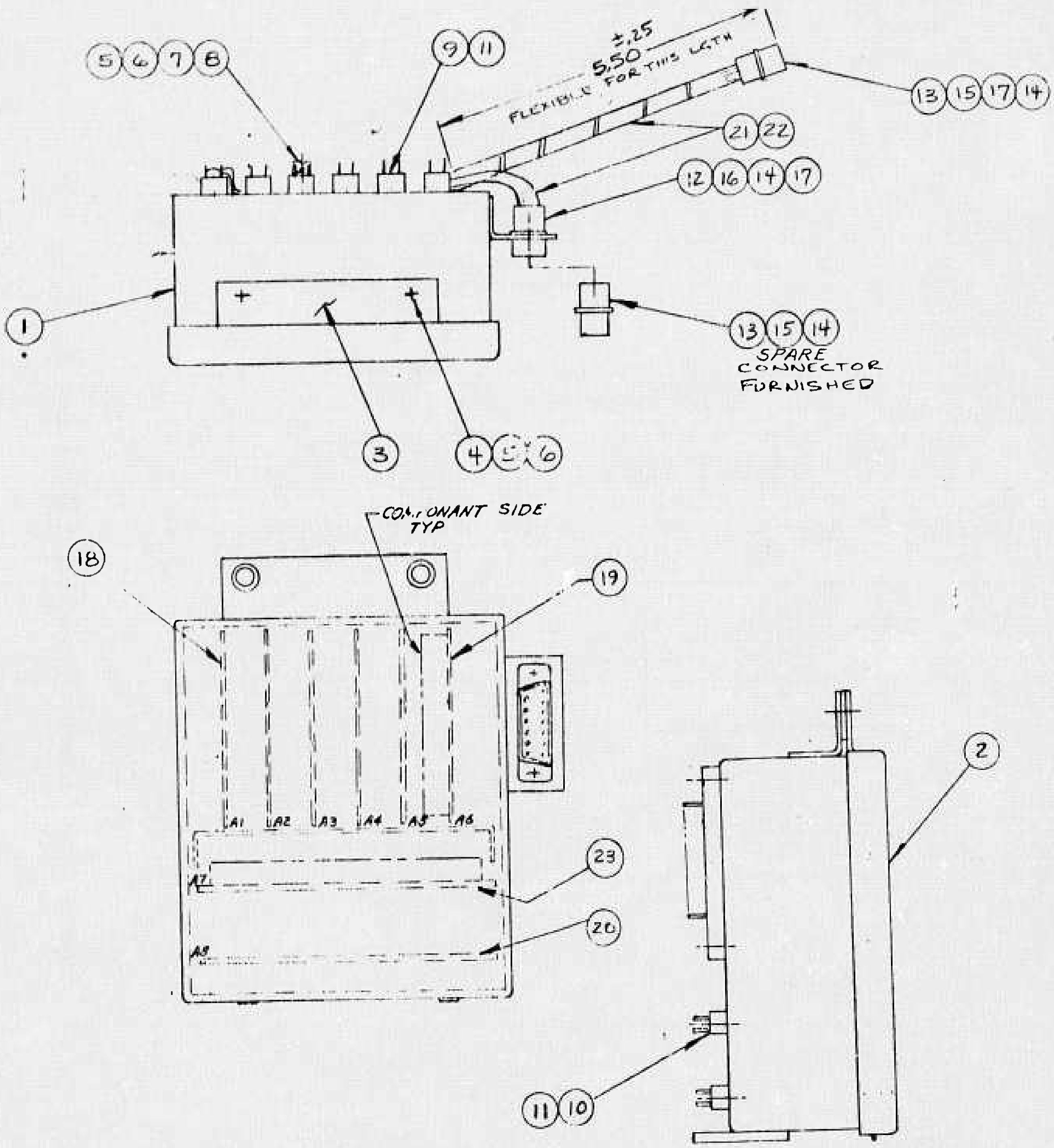

Figure 19 Preamplifier Assembly (21009215) Sheet 1

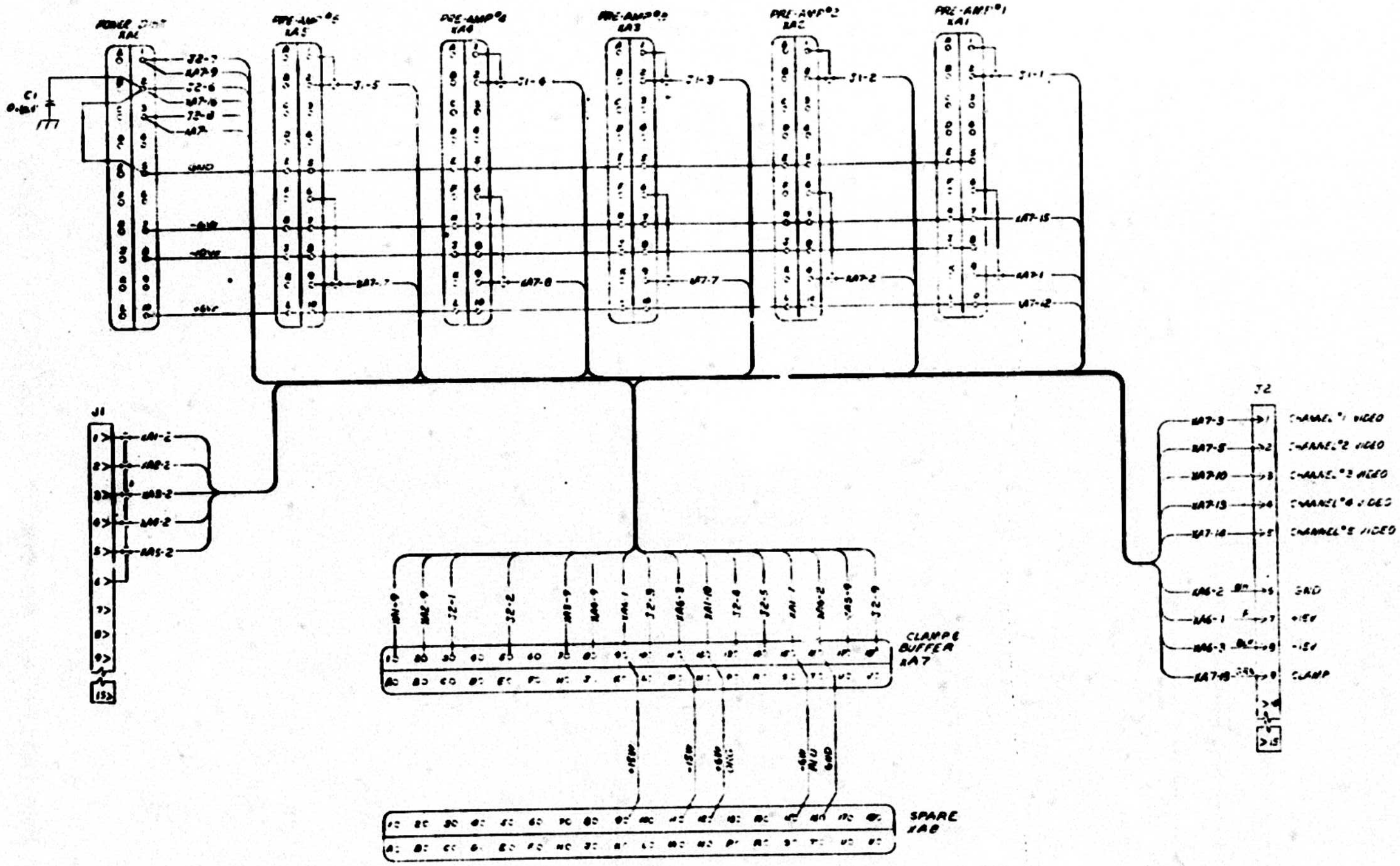

Figure 20 Preamplifier assembly (21009215) Sheet 2

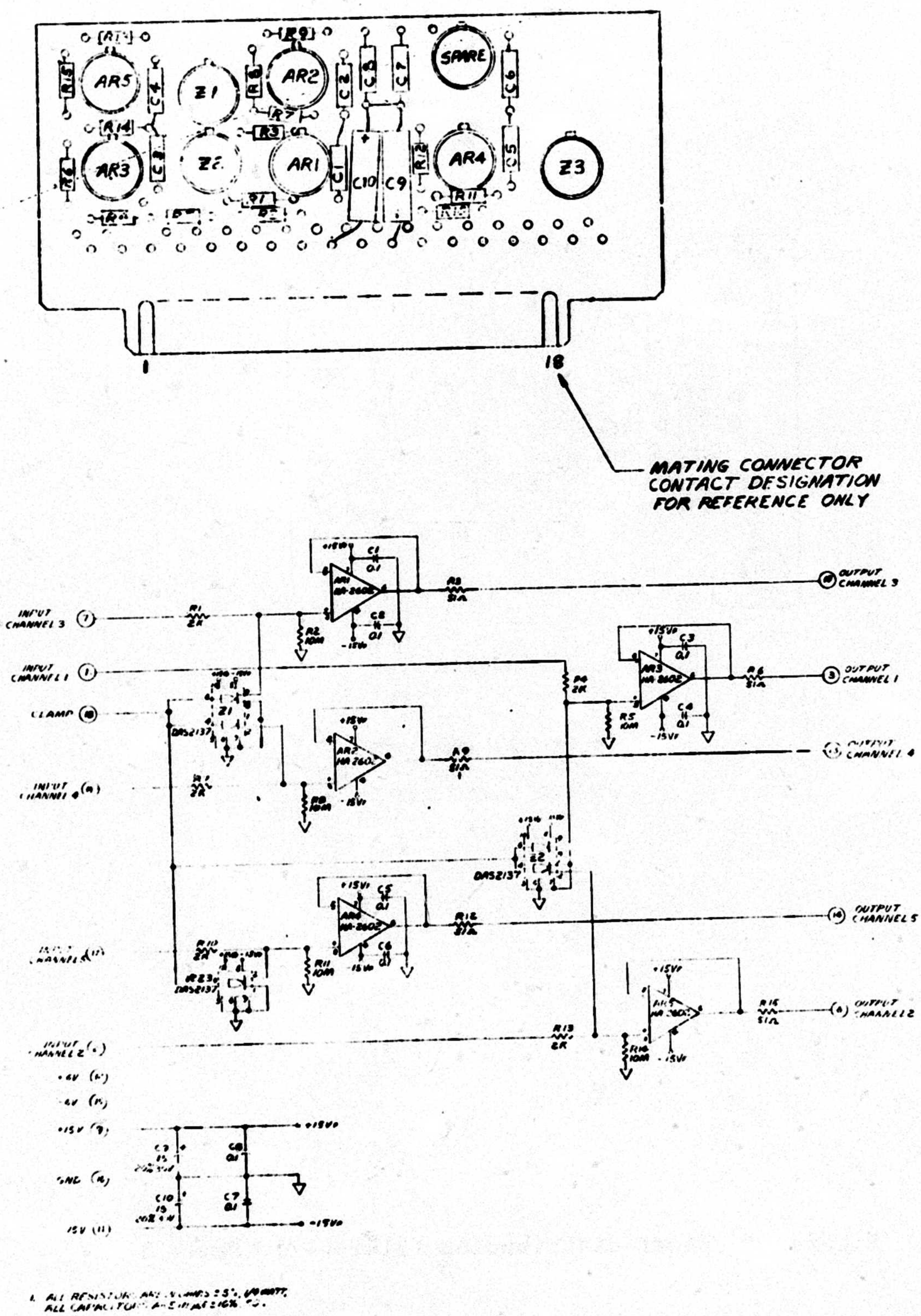

Figure 21 Clamp and buffer (21010011)

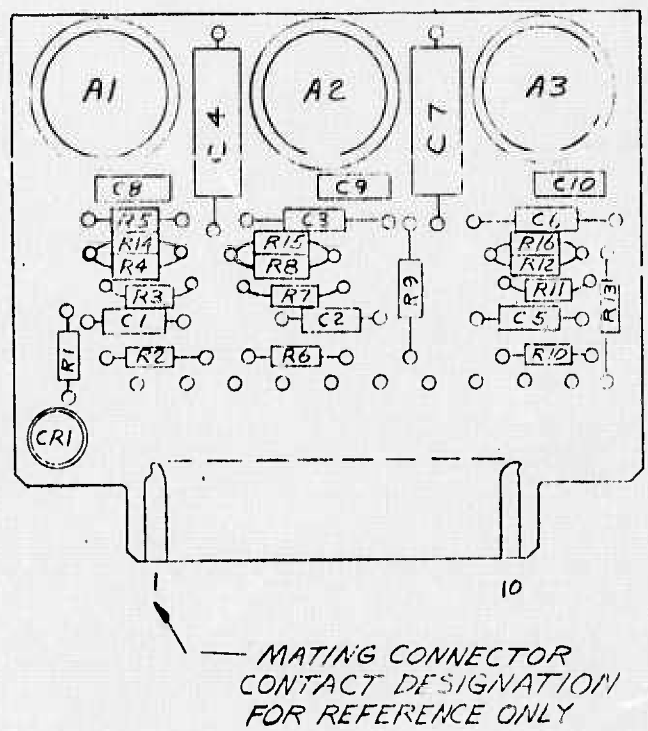

Figure 22 Power distribution (21010012) Sheet 1

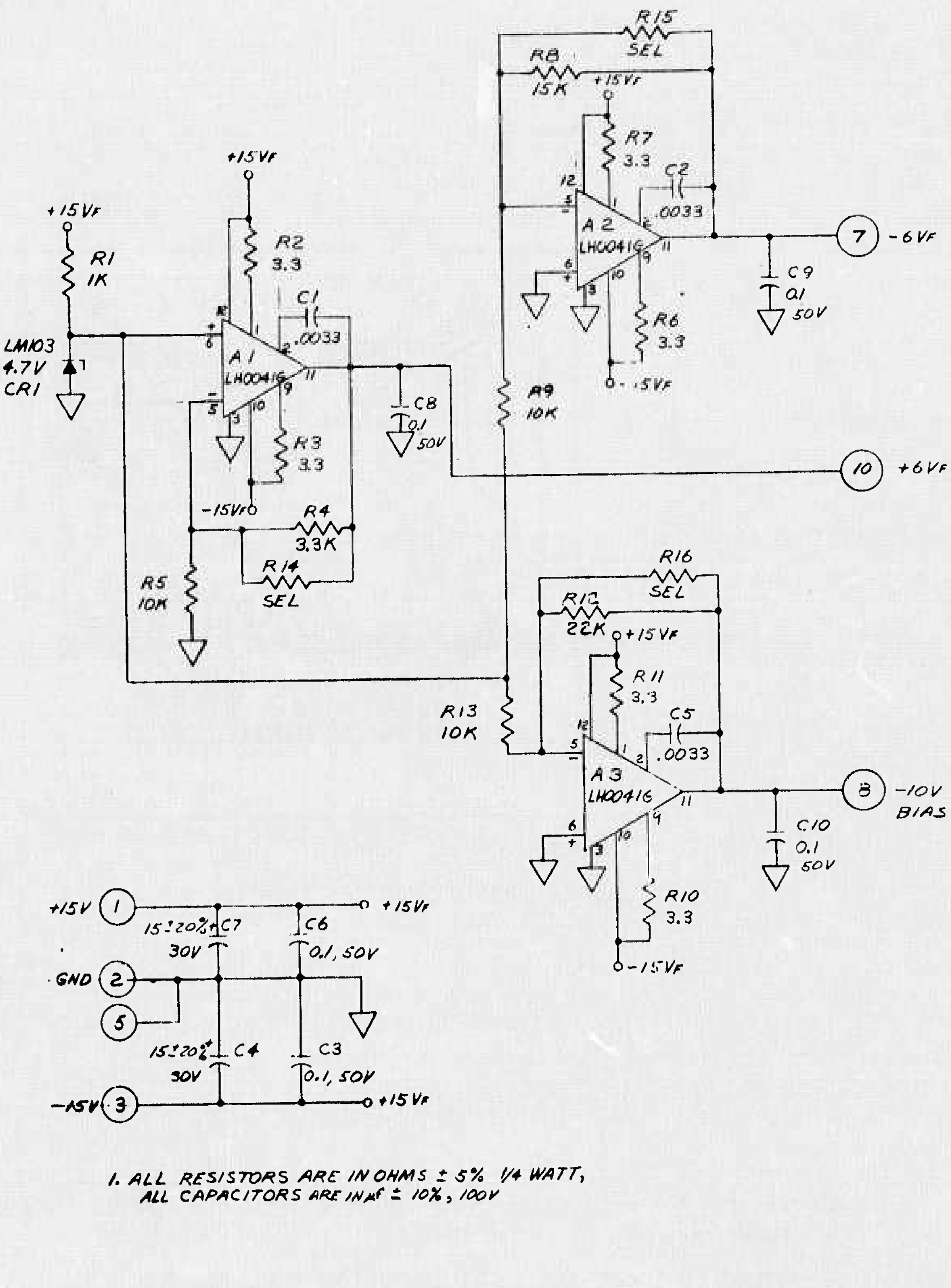

Figure 23 Power distribution (21010012) Sheet 2

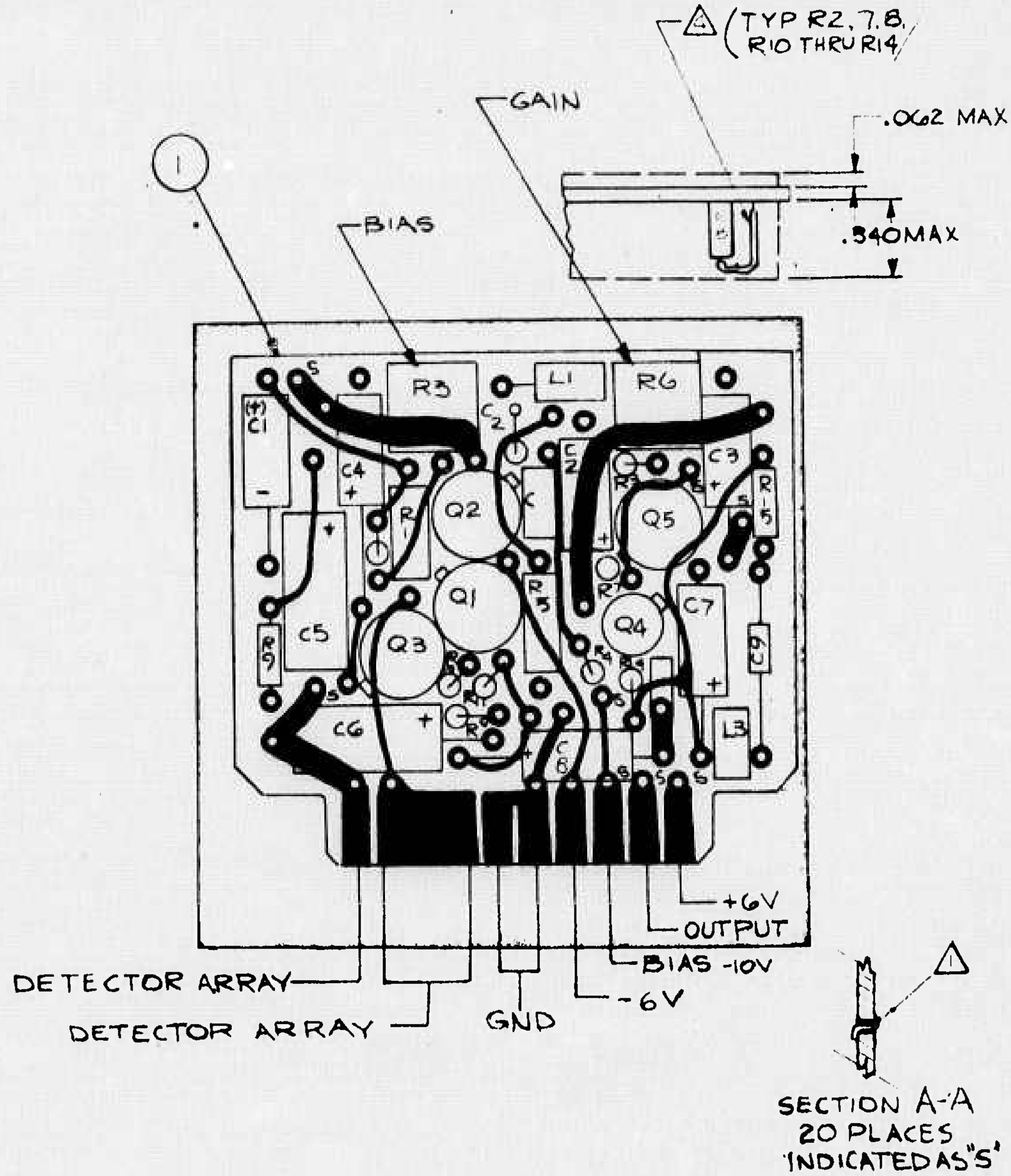

4 NO. 26 AWG TEFLON TUBING PER MATERIAL SPEC 7004

3 FOR SCHEMATIC SEE SHT 2

2 SOLDER PER PC 4824-01 USING FIND NO. 28

1 INSTALL NO. 22 SOLID BUS WIRE IN ALL PLACES MARKED "S"

Figure 24 Preamplifier (21010013) Sheet 1

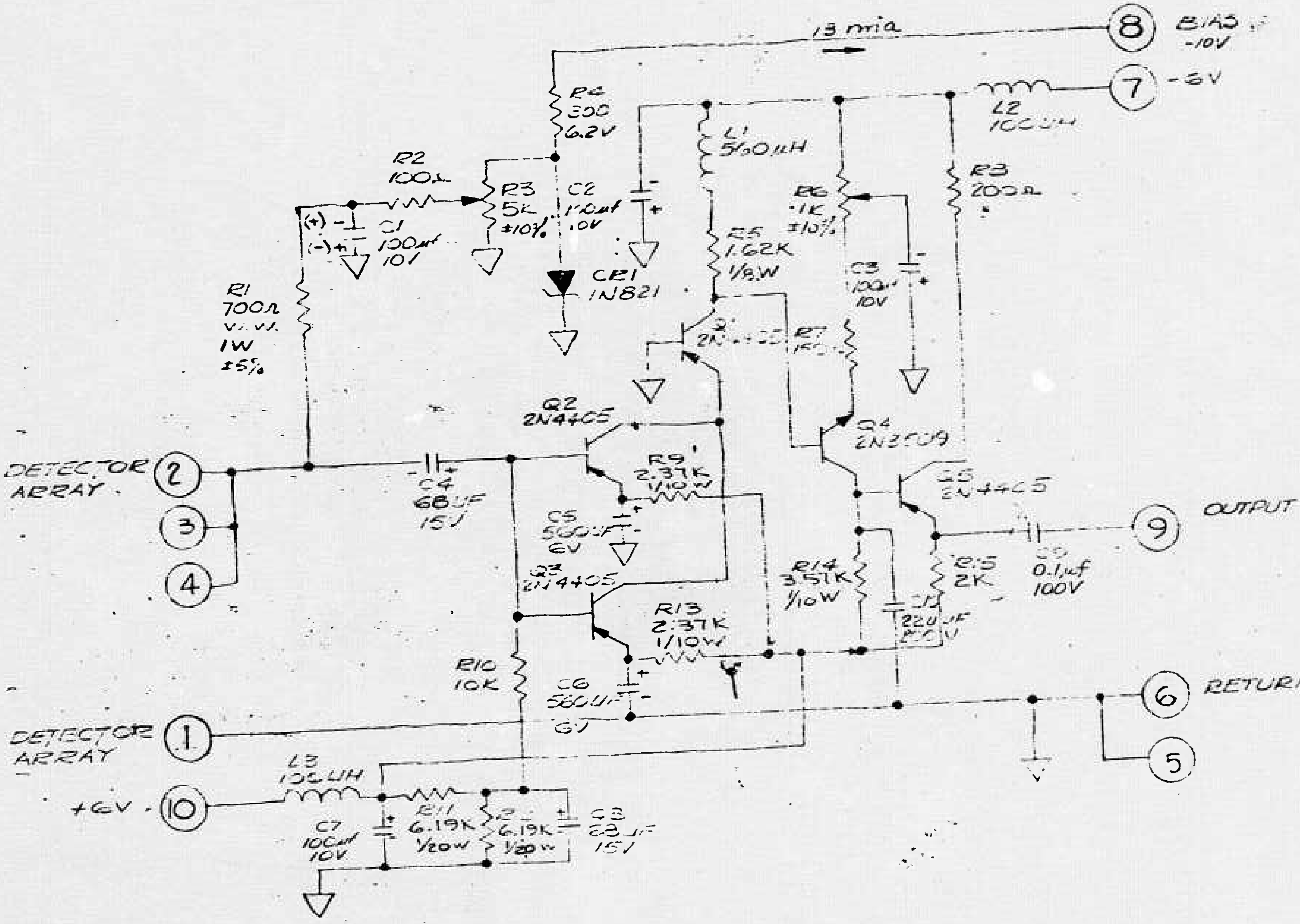

Figure 25 Preamplifier (21010013) Sheet 2

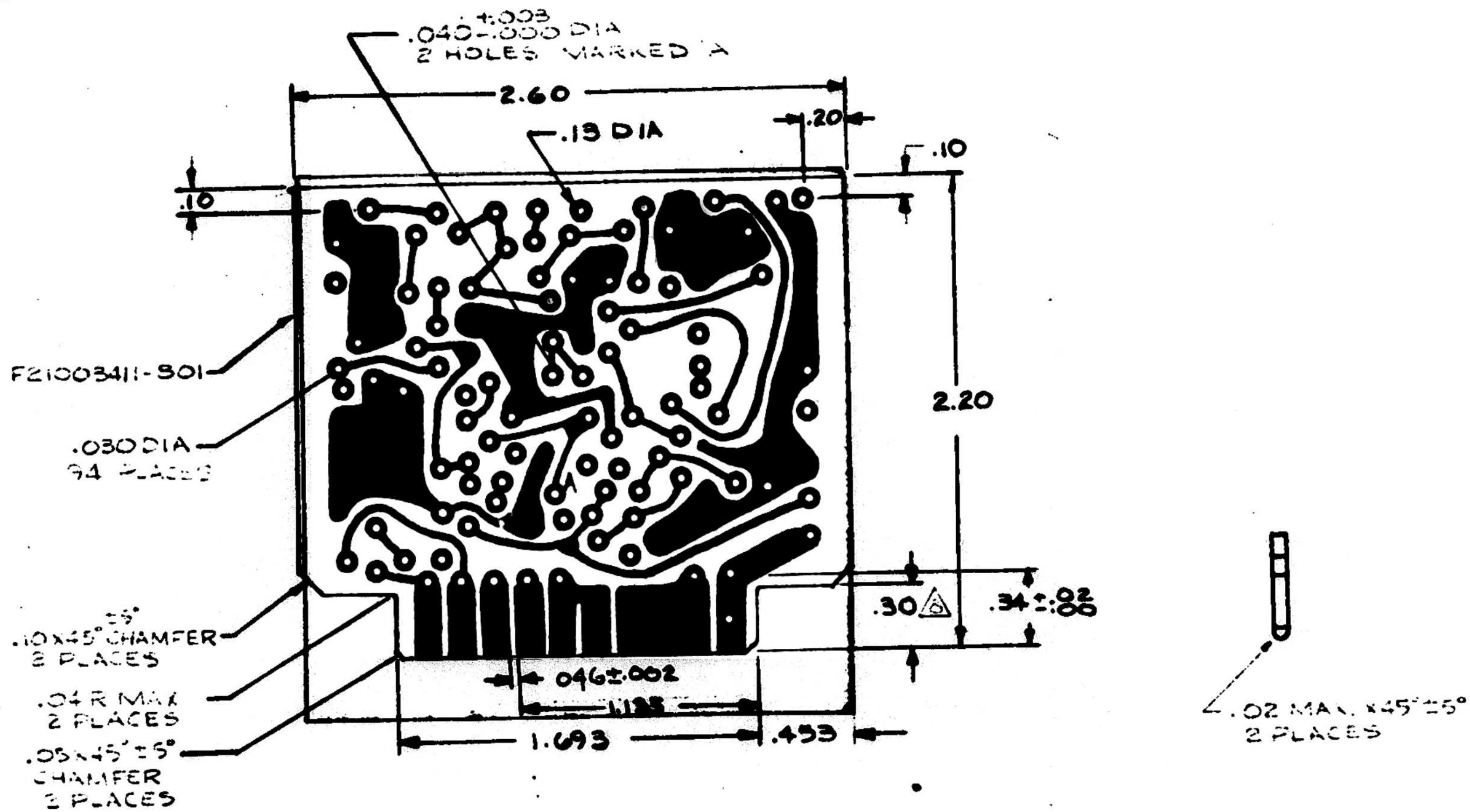

Figure 26 Preamplifier (21010013) Sheet 3

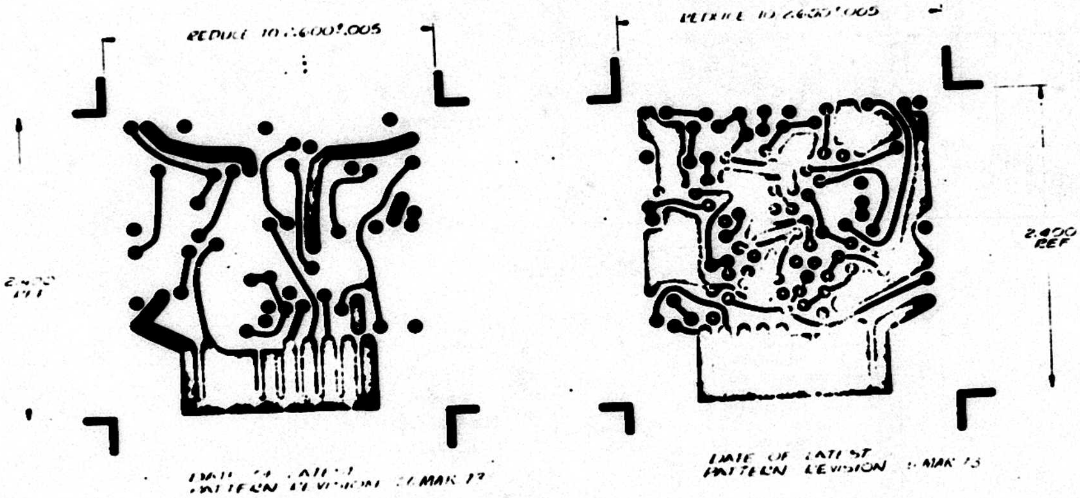

Figure 27 Preamplifier (21010013) Sheet 4

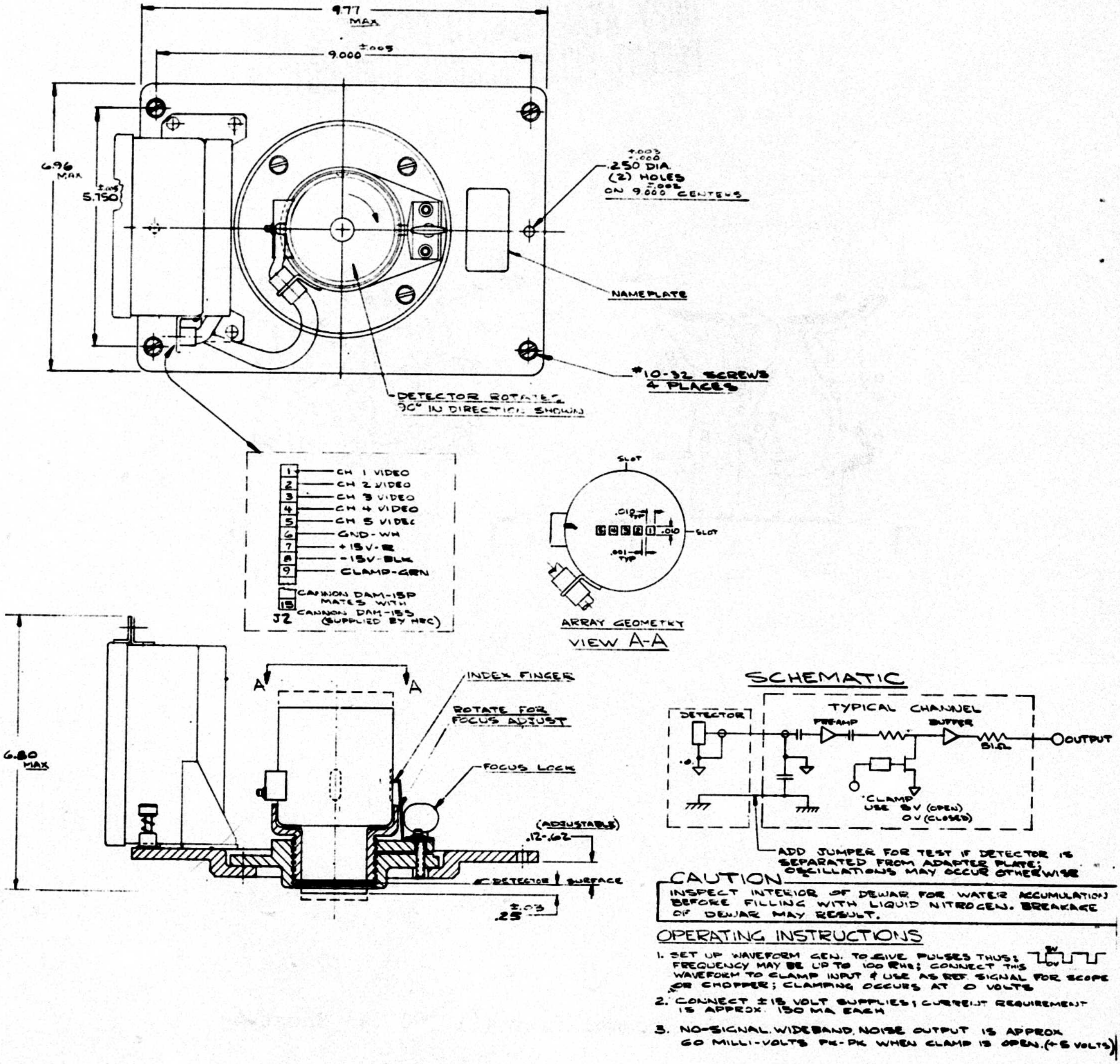

Figure 28 Installation - non-coherent receiver (LK128A)

Coolant Hold Time

The coolant hold time was measured to be in excess of 2 hours and 45 minutes with the detectors biased.

Acceptance Criterion: 1 hour minimum

Maximum Bias

The maximum bias applied to any detector element is 10 milliamperes. The current is limited by the preamplifier bias circuit (21010013).

Acceptance Criterion: 20 milliamperes maximum per element

Spectral Response

The spectral response of the receiver was checked on a Perkin-Elmer Spectrometer using an f/4.0 cone of radiation. The response of elements 1 and 3 were checked and found to be as shown in Figure 14. The slit width of 0.46 micrometer was the smallest slit possible to maintain good signal to noise ratio on the spectrometer. This test showed the relative response of the receiver and that no spectral leaks were present between 4 and 12 micrometers. However, the actual response of the receiver is determined by the cold filter and proper adjustment of the cold filter angle. The cold filter was built and tested by OCLI and the data are shown in Figure 12. The data are shown for room ambient and 77°K.

D^*_{BB} to D^*_{λ} Conversion Factor

The conditions of measurement were:

Detector Temperature	77°K
Chopping Frequency	1,000 Hz
Detector Area (A_D)	0.0625 mm^2
Orifice Diameter (d_B)	0.050 inch
Blackbody Temperature (T_B)	500°K
Background Temperature (T_c)	300°K
Emissivity	
Blackbody (ϵ_B)	1.0
Chopper (ϵ_C)	1.0
Noise Bandwidth (Δf)	6 Hz
Chopper rms Factor (K_1)	0.35
Detector to Orifice Distance (D)	15 cm

Stefan-Boltzmann Constant (K_2)	5.67×10^{-12} watt cm^{-2} $(°K)^{-4}$
Rms Noise Correction (K_3)	1.12
Amplifier Gain (same for signal & noise)	≈2,000

D* Formula:

$$D^*_{BB} = \frac{4D^2 \; (\Delta f)^{1/2}}{K_1 \; K_2 \; K_3 \; d^2_B \sqrt{A_D} \; (\epsilon_B \; T^4_B - \epsilon_C \; T_C^4)} \times \frac{S}{N}$$

Detector Readout Circuitry

The detector setup was as shown in Figure 29.

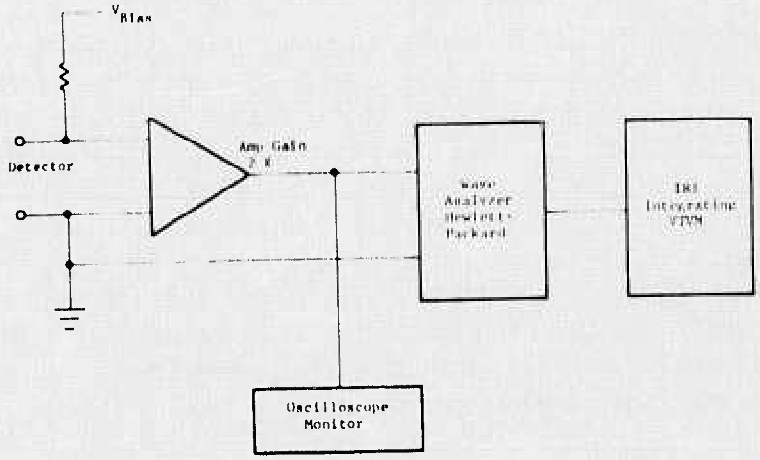

Figure 29. Detector test setup

Conversion Factor

$$D^*_\lambda = g \; D^*_{BB}$$

$$g = \frac{H_{BB}}{T\int_{\lambda_1}^{\lambda 2} \frac{R(\lambda)}{R(\lambda_{max})} H_\lambda(\lambda) \; d\lambda}$$

$$H_\lambda(\lambda) = Q(\lambda) \; \frac{h_c}{\lambda}$$

$$\frac{R_\lambda}{R_{\lambda\ max}} = \frac{\lambda}{\lambda_{max}}$$

$$g = \frac{H_{BB}}{T \int_{\lambda_1}^{\lambda 2} \frac{\lambda}{\lambda_{max}} \frac{h_c}{\lambda} Q(\lambda)\ d\lambda}$$

$$g = \frac{\lambda_{max} H_{BB}}{h_c T \int_{\lambda 1}^{\lambda 2} Q(\lambda)\ d\lambda}$$

assume transmission (T) = 1.

For a narrow spectral range:

$$g = \frac{H_{BB}}{H_{\lambda m} \frac{(H_\lambda)}{H_{\lambda\mu}} \Delta\lambda}$$

$\Delta\lambda = 0.982\ \mu m$

$H_{BB} = 0.355\ W/cm^2$

$H_{\lambda m} = 4.05 \times 10^{-2} W/cm^2\text{-}\mu m$

$H_\lambda = 10.6/H_{\lambda\mu} = 0.49$

$g = 182.17$

$T_{BB} = 500°K$

$\lambda_p = 10.6057\ \mu m$

Test Results

The test results of the 5 elements are given in Table 3

Table 3

$D^*(10.6\ \mu m, 10\ kHz, 60°, 1)$

Element	$R_d(77°K)$ ohms	D^*_{BB} cm $Hz^{1/2}/W$	D^*_λ cm $Hz^{1/2}/W$	R_λ V/W
1	57.5	1.68×10^8	3.06×10^{10}	25,120
2	31.1	2.14×10^8	3.9×10^{10}	21,980
3	26.9	1.9×10^8	3.46×10^{10}	17,590
4	36.8	3.33×10^8	6.07×10^{10}	30,150
5	41.8	7.14×10^8	1.3×10^{11}	21,360
Acceptance Criterion: $D^*_\lambda = 2 \times 10^{10}$ cm $Hz^{1/2}$/watt minimum				

Frequency Response

The noise bandwidth of each detector element was measured from 1 kHz to 5 MHz and is shown in Table 4. Table 5 depicts the signal response of each element from 125 Hz to 10 kHz.

ELECTRONIC RESPONSE

Preamplifier Low Frequency Response

The preamplifier low frequency response was verified by a pulse input and noting the low frequency response of one half cycle. The results are shown in Figure 30. As can be seen from Figure 30, $\tau = 0.01$ second

$$f_c = \frac{1}{2\pi\tau} = 15.9 \text{ Hz}$$

Dc Restoration Check

The dc restoration circuit was checked as shown in Figures 31 and 32. Figure 31 shows the sinusoidal output of the preamplifier clamped to ground at the negative peak. Figure 32 shows the same signal with and without dc restoration.

Table 4

NOISE BANDWIDTH

Frequency (kHz)	Element Number (noise mV)				
	1	2	3	4	5
1	150	64	50	20	80
2	150	64	50	19	80
3	150	64	50	19	70
4	150	64	50	19	70
5	140	64	46	18	66
10	140	58	44	17	60
20	140	56	44	17	58
40	130	52	44	17	56
60	130	52	42	17	56
80	120	52	40	17	56
100	110	50	39	17	56
200	110	50	36	17	52
400	110	60	46	20	61
600	110	62	46	20	62
800	140	66	46	16	72
1000	145	70	48	14	64
1200	130	64	44	11	64
1400	110	52	38	8	52
1600	90	46	32	5.2	46
1800	78	36	26	3.9	36
2000	65	32	23	3.3	30
2500	50	23	18	3.3	23
3000	38	18	16	3.3	18
3500	30	15	12	3.3	13
4000	15	8.0	8	3.3	2.6
4500	7.4	5.0	4.4	3.3	4.8
5000	3.6	2.6	2.2	3.3	1.8

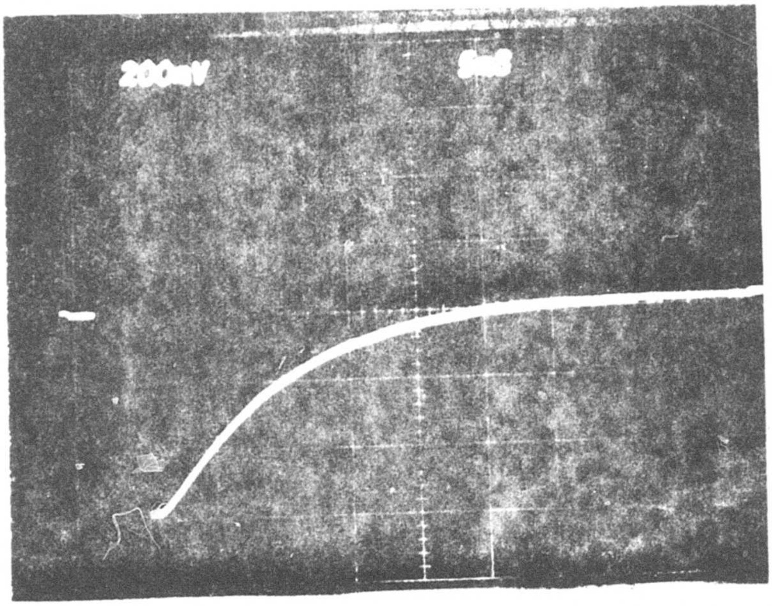

Figure 30 Preamplifier low frequency response

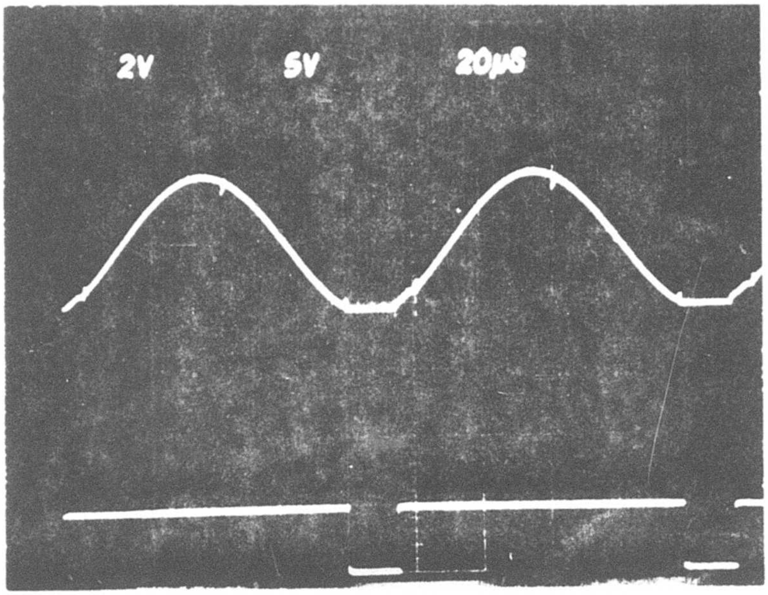

output

-clamp

Figure 31 Dc restoration

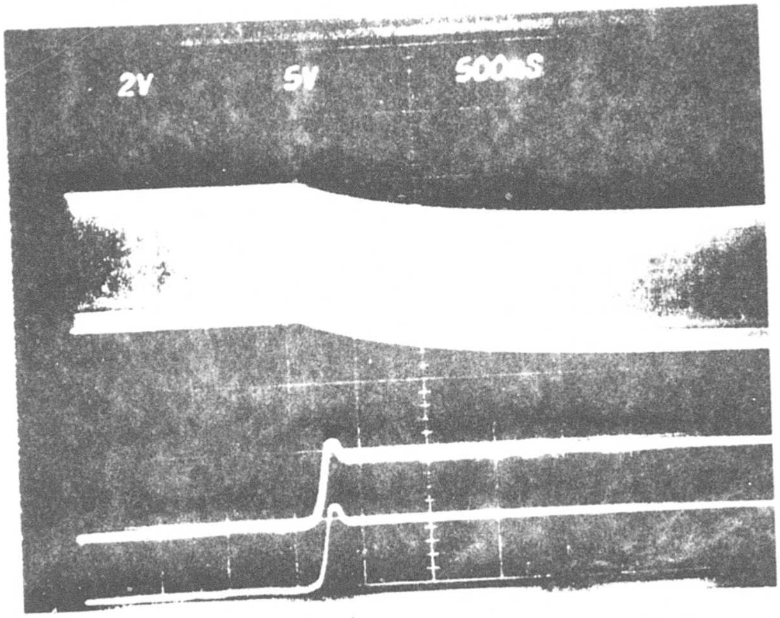

dc Restored

Not dc Restored

Figure 32 Dc restoration

Table 5

SIGNAL RESPONSE

Frequency (Hz)	Element Number (output mV)				
	1	2	3	4	5
125	0.4	0.34	0.28	0.48	0.34
600	0.4	0.34	0.28	0.48	0.34
1000	0.4	0.34	0.28	0.48	0.34
2000	0.4	0.34	0.28	0.48	0.34
3000	0.4	0.34	0.28	0.48	0.34
5000	0.4	0.34	0.28	0.48	0.32
9000	0.4	0.34	0.28	0.47	0.32
10000	0.4	0.34	0.28	0.46	0.32

Cross Talk

The cross talk between detector was measured to be significantly less than the design goal of 1%.

Acceptance Criterion: 5% maximum

LASER RESPONSE

The receiver was excited with a Sylvania model 941E CO_2 laser operating in the TEM_{oo} mode on the P20 line. The test setup is shown in Figure 33. The test showed that the receiver cold filter was correctly adjusted to give response to the laser. The detector was then flooded with energy using a black aluminum plate as a diffuser. A reference detector of known D* was compared to the non-coherent receiver elements. The reference detector D^*_λ at 10.6 micrometers was measured using standard blackbody techniques. The data is listed below:

$$D^*_\lambda \; 10.6 \; \mu m = 1.1 \times 10^{10}$$

Area = 5.04×10^{-4} cm^2 which is essentially the same as the non-coherent elements.

The detector noise bandwidth was measured and the data is shown in Table 6. The detector noise -3 dB point is at 20 kHz.

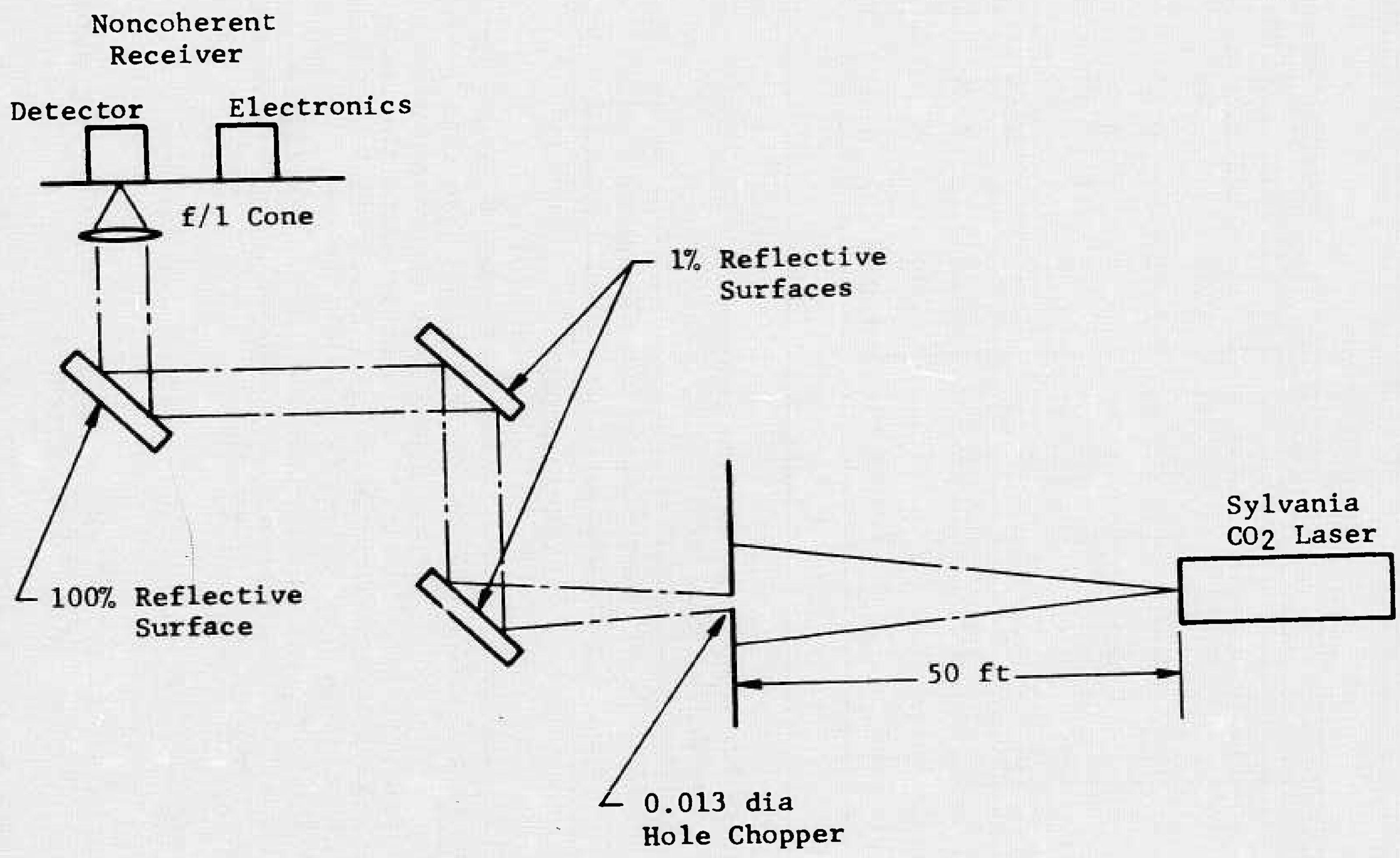

Figure 33 Laser response test setup

Table 6

REFERENCE DETECTOR NOISE BANDWIDTH

Frequency (kHz)	Output (mV)
1	60
10	25
30	15
100	3.6
300	0.44
500	0.16
700	0.10
1000	0.08

The signal output of reference detector when excited by the diffused laser beam was 3 volts peak-to-peak. The wideband noise was 100 mV rms. This yields a signal to noise ratio of 30.

Each element of the non-coherent receiver was then excited by the diffused laser beam. All of the signals and rms noise were measured to be approximately the same and as shown below:

rms noise = 8 mV

Signal = 150 mV pk-pk

The bandwidth of the reference detector must be considered and corrected for a bandwidth of 1.2 MHz.

S/N at 20 kHz = 30

$$S/N \text{ at } 1.2 \text{ MHz} = \frac{30}{\sqrt{\frac{1.2 \text{ MHz}}{20 \text{ kHz}}}} = 3.9$$

The signal to noise ratio of the non-coherent array is approximately 18.5. Then the comparative D^*_λ of the non-coherent receiver elements may be calculated.

$$D^*_\lambda = \frac{18.5}{3.9} \times 1.1 \times 10^{10} \approx 5.5 \times 10^{10}$$

This compares with the data shown in the section entitled Test Results.

The laser tests were witnessed by the Air Force Avionics Laboratory representative, Mr. William Schoonover.

DETECTOR GEOMETRY

The detector geometry is shown on outline drawing LK128A and in Figure 34.

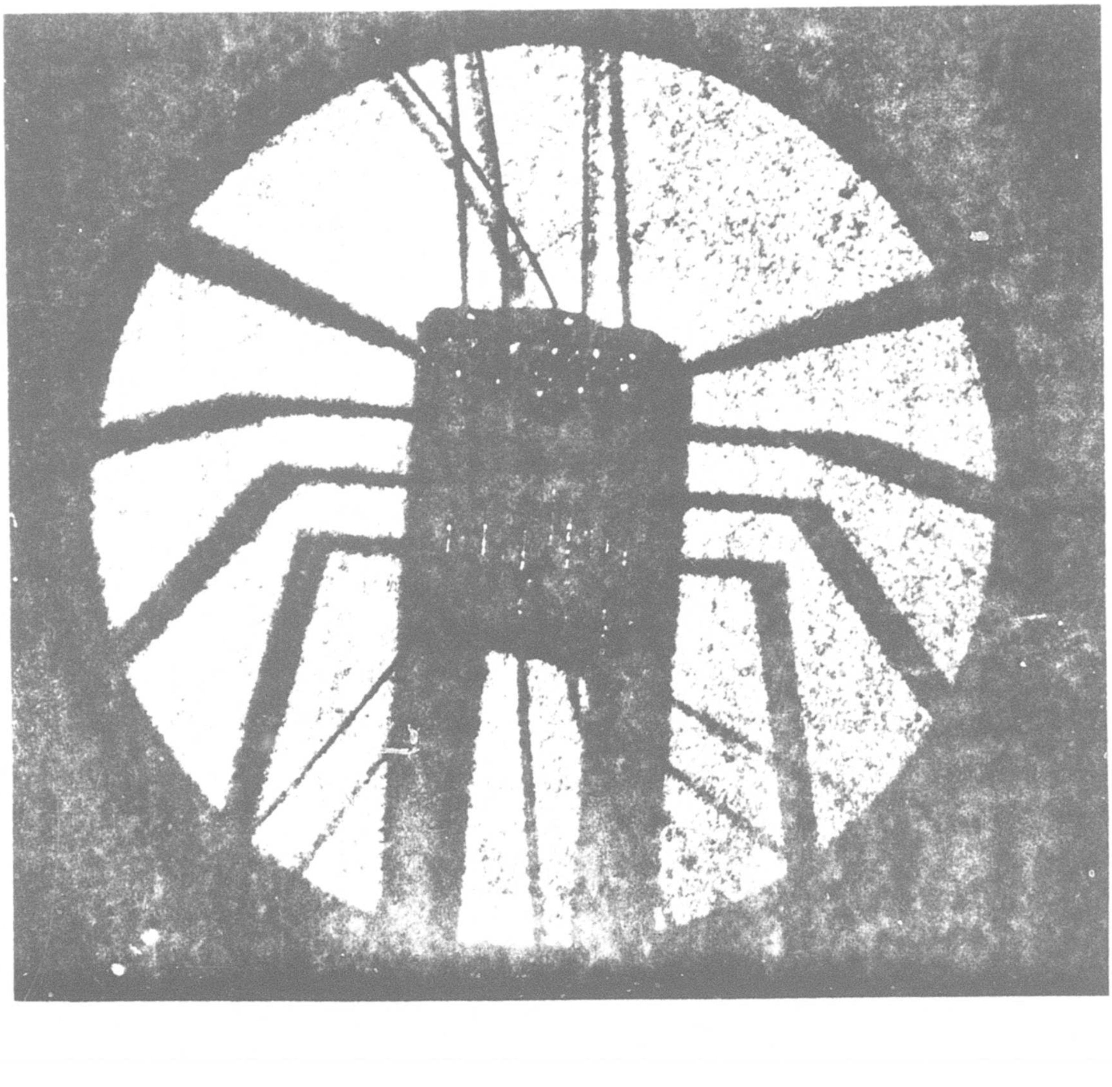

Figure 34 Photoconductive array

SECTION 4

COHERENT FIVE-CHANNEL RECEIVER

This section discusses the coherent five-channel Receiver. The receiver specifications are presented in Table 7.

Table 7

SPECIFICATIONS

Type	5 El (Hg,Cd)Te PV array
Size	0.25 mm x 0.25 mm ± 20%
Spacing	< 0.070 mm
Cross talk	< 10% (design goal ≤ 5%)
Quantum Efficiency	≥ 25% at 10.6 μm
Video Bandwidth (after second detector)	Dc to 1 MHz
FOV	f/1 (53°) min
Receiver Amplifier Gain	≥ 40 dB
Receiver Sensitivity (NEP)	≤ 6 dB ± 3 dB above theoretical limit
Coolant	LN_2
Coolant hold time with receiver operating	≥ 1 hour

DETECTOR RESULTS

Figure 35 shows the five-element linear array of photovoltaic (Hg,Cd)Te detectors showing the gold wire leads. Figure 36 shows the test results for the array. Listed are the series and shunt resistances, the peak and cut-off wavelengths, quantum efficiencies, responsivities and cross talk. The I-V curves are shown in Figure 37 and the spectral response of two elements in Figure38. Figure 39 shows spot scan results for three elements of a different array taken from the same slab. The conditions of measurement are shown in Table 8, and the detector readout circuitry in Figure 40.

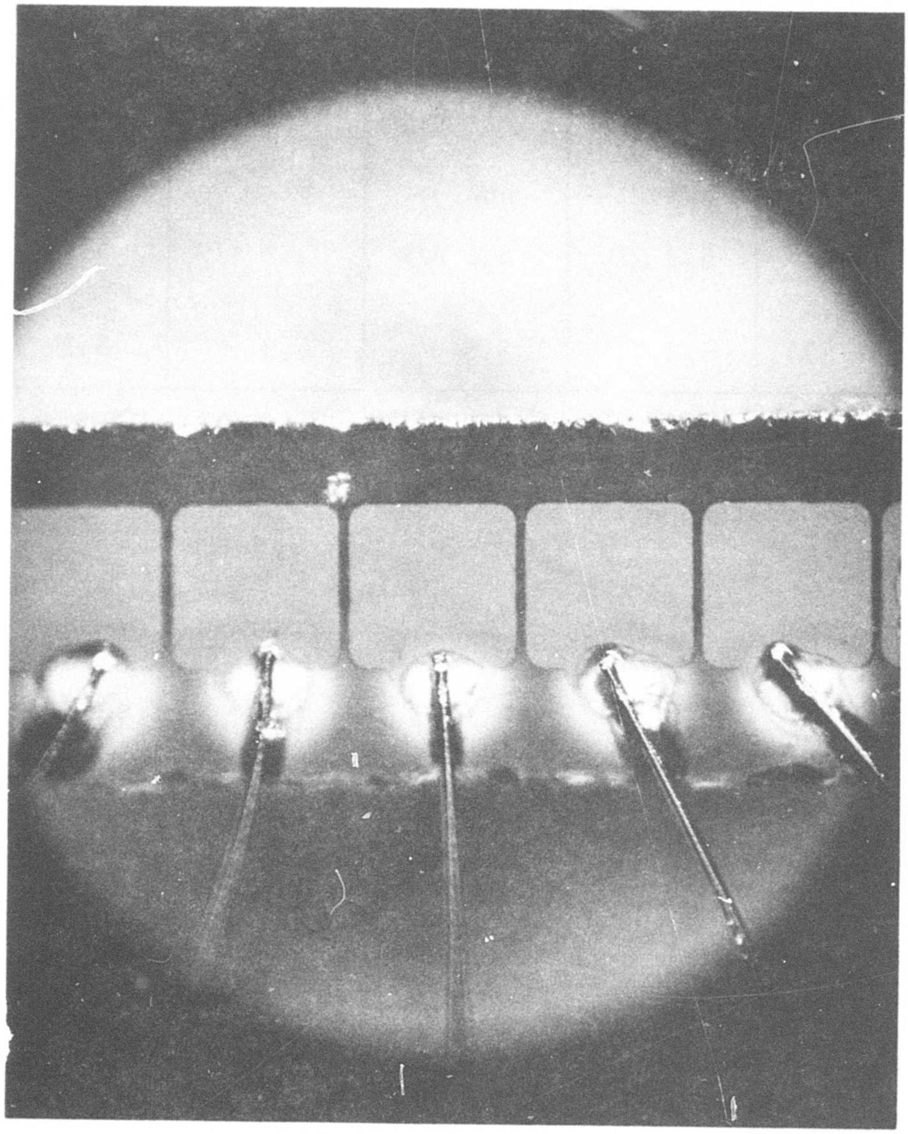

00705

Figure 35 Photo of 5-element array

	ELEMENTS				
	1	2	3	4	5
R_S	16 Ω	13 Ω	13 Ω	14 Ω	14 Ω
R_{sh}	255 Ω	245 Ω	190 Ω	205 Ω	400 Ω
λ_{peak}	*	11 μm	*	10.5 μm	*
λ_{co}	*	11.78 μm	*	11.83 μm	*
η**	62%	68%	61%	58%	34%
R_λ**	5.3 A/W	5.8 A/W	5.2 A/W	4.95 A/W	2.9 A/W
Cross talk (%)	6.3	5.3	6.9	6.8	3.5

* Two spectrals show uniformity; data for elements 1, 3 and 5 calculated with this data.

**Bias voltage = 100 mV.

Figure 36 Test results

Table 8

CONDITIONS OF MEASUREMENTS

Detector Temperature	77°K
Chopping Frequency	1,000 Hz
Detector Area (A_D)	See Figure 17
Orifice Diameter (d_B)	0.088 inch
Blackbody Temperature (T_B)	500°K
Background Temperature (T_c)	300°K
Emissivity Blackbody (ϵ_B)	1.0
Chopper (ϵ_C)	1.0
Noise Bandwidth (f)	6 Hz
Chopper rms Factor (K_1)	0.35
Detector to Orifice Distance(D)	26.4 cm
Stefan-Boltzmann Constant (K_2)	5.67×10^{-12} watt cm^{-2} $(°K)^{-4}$
Rms Noise Correction (K_3)	1.12
Amplifier Gain (same for signal & noise)	≈ 4,000

D* Formula:

$$D^*_{BB} = \frac{4D^2 \ (\Delta f)^{1/2}}{K_1 \ K_2 \ K_3 \ d_B^2 \sqrt{A_D} \ (\epsilon_B \ T_B^4 - \epsilon_C \ T_C^4)} \times \frac{S}{N}$$

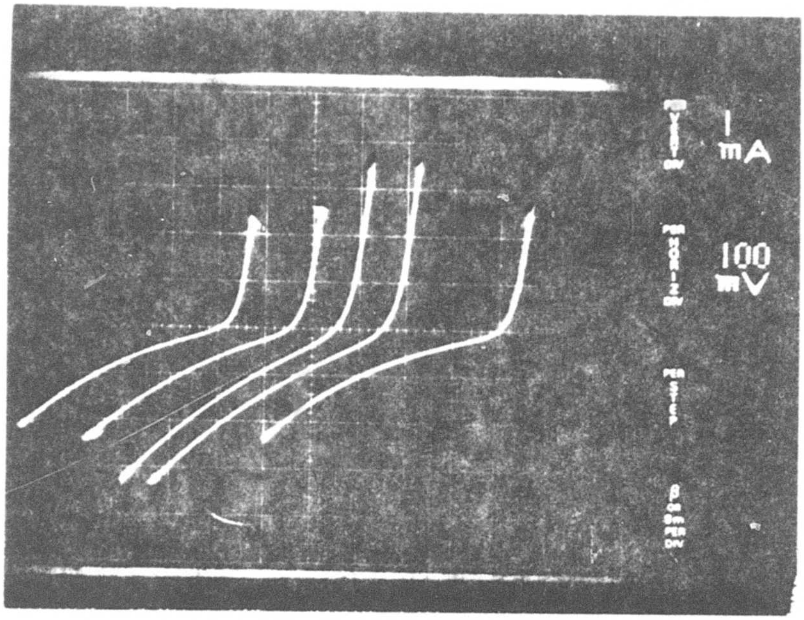

Elements # 1-5

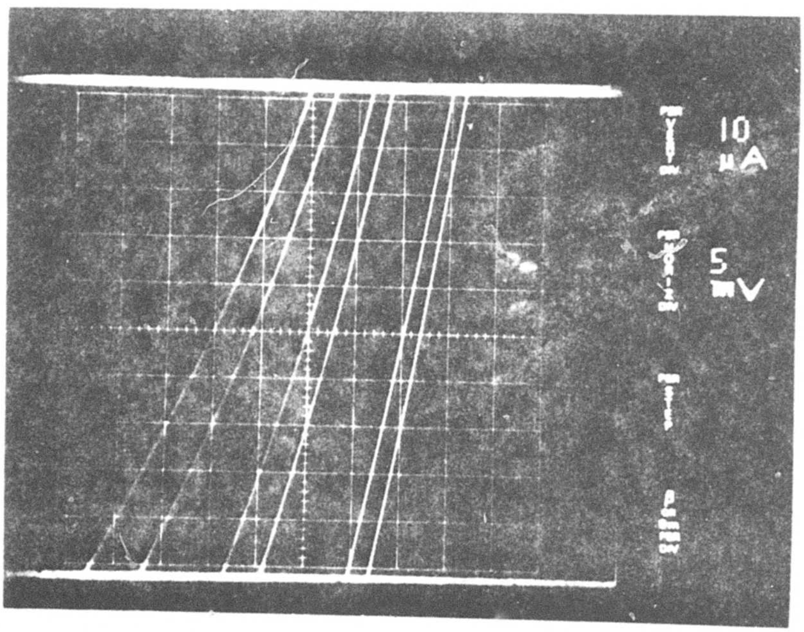

Elements # 1-3

Figure 37 I-V curves showing the change in dc current as the background is changed from 300°K to 77°K

I-V Curves

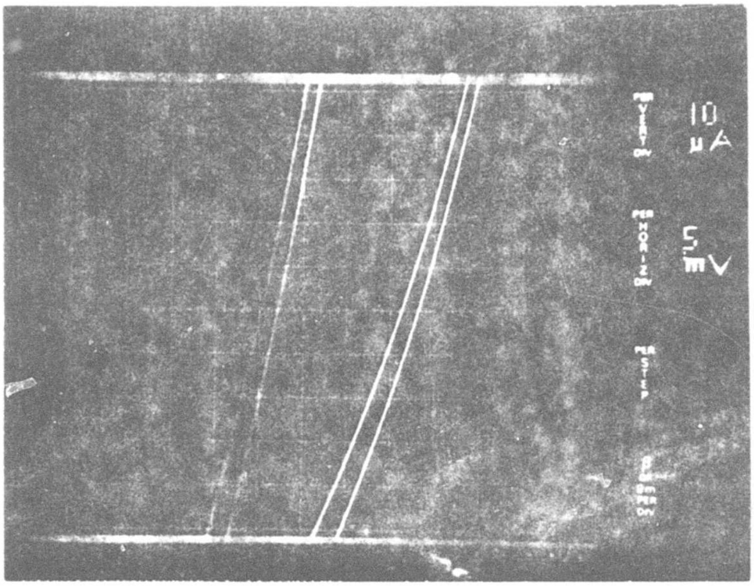

Elements # 4,5

Figure 37 I-V curves showing the change in dc current as the background is changed from 300°K to 77°K

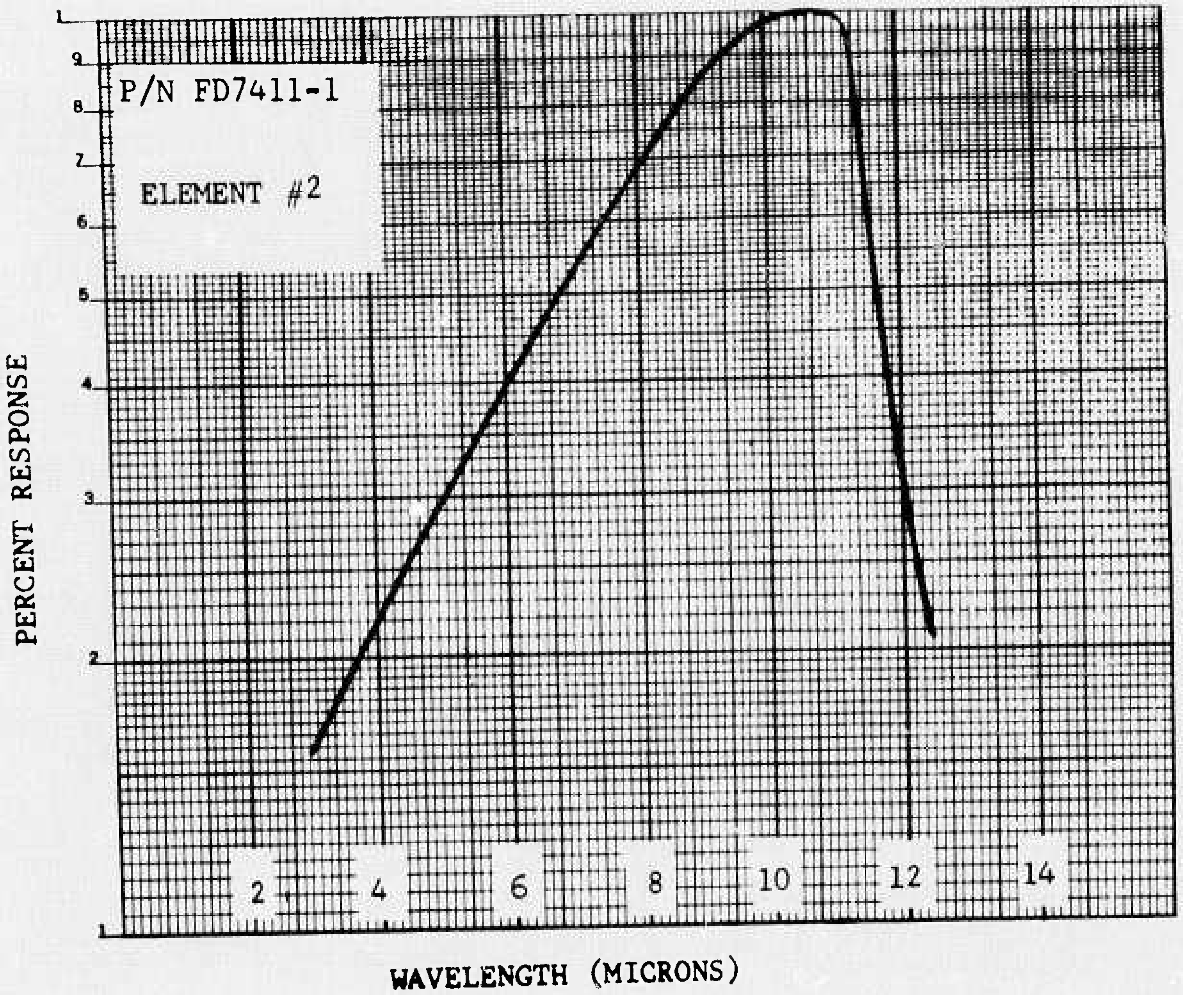

Figure 38 Relative spectral response

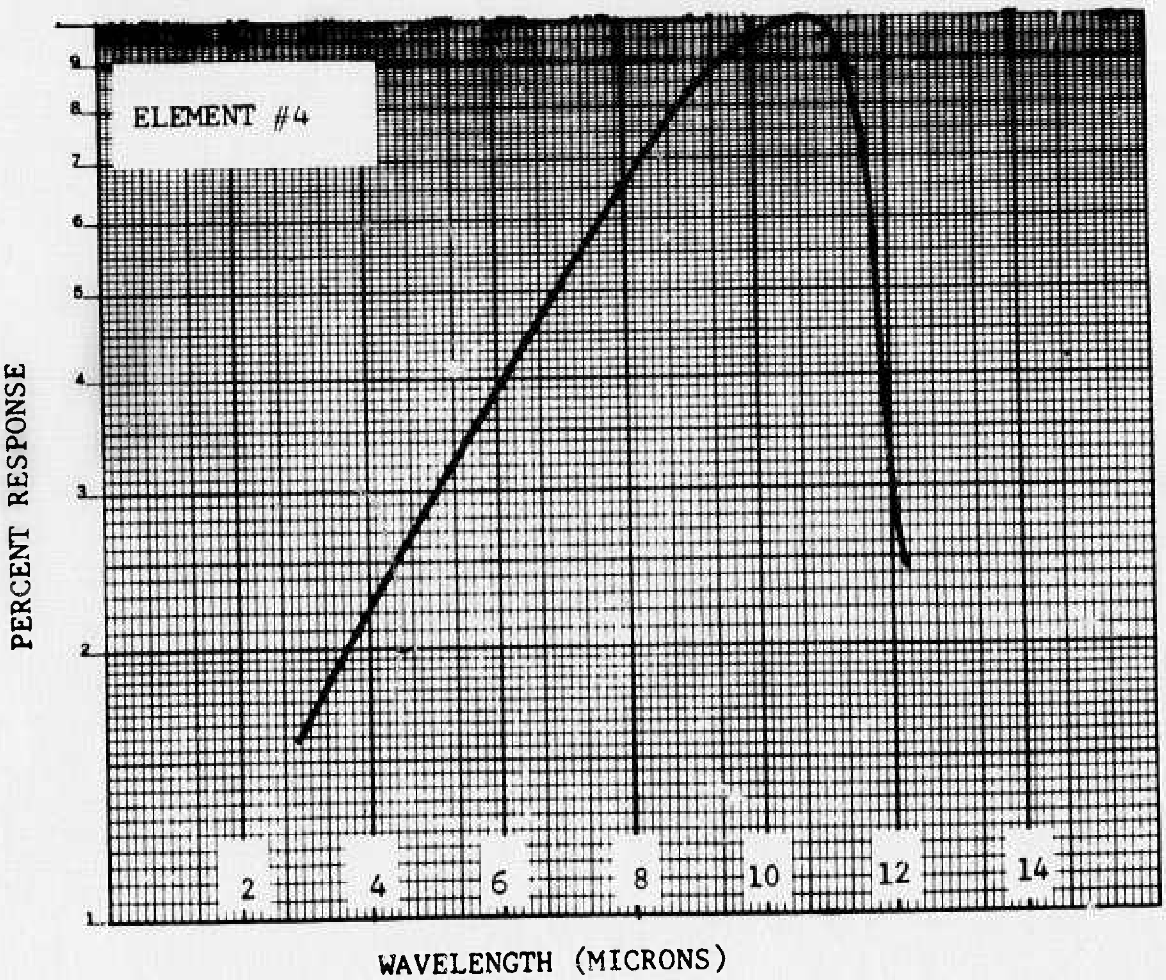

Figure 38 Relative spectral response (con't)

NOTE: Spot scan not done on final array, but this one is from the same slab.

Schoonover 10574 S3

Array B1

Spot B2

Scan B3

11/26/74 (B4 & B5 not done)

Spot Size = 1 mil

Spot scan shows about a 10.5 mil active area and 0.5 mil spacing.

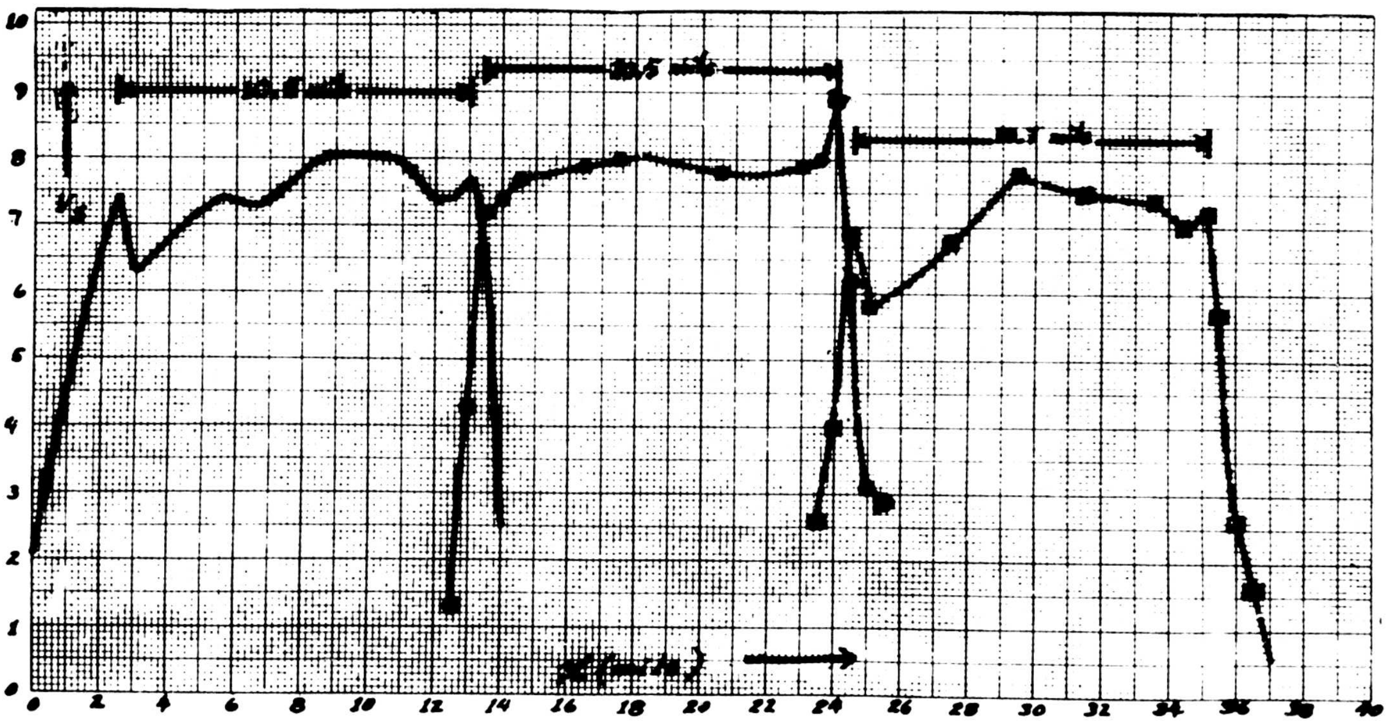

Figure 39 Spot scan results

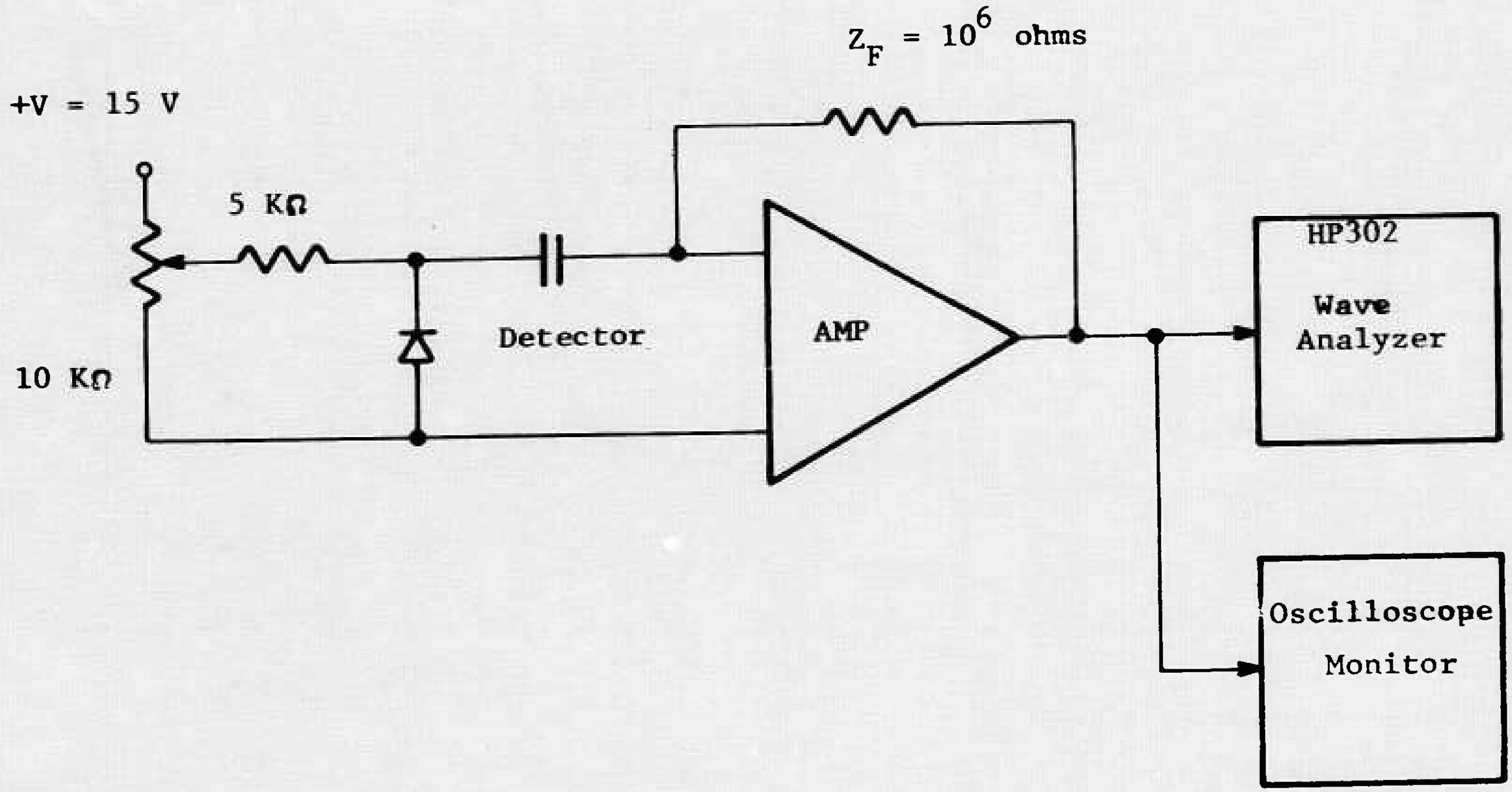

Figure 40 Detector readout circuitry

PREAMPLIFIER DESIGN

A block diagram of the preamplifier is shown in Figure 41 and the schematic in 42.

Each detector is coupled to its preamplifier by an impedance matching transformer T1. The use of transformer coupling provides both ground loop isolation and optimization of receiver noise figure by matching the detector impedance to RS opt of Q1.

The Standard Cascode Pair configuration (Figure 43) is dc stabilized and transformed to an inverted cascode pair as in Figure 44.

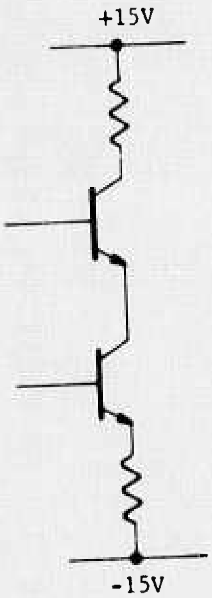

Figure 43 Standard cascade pair

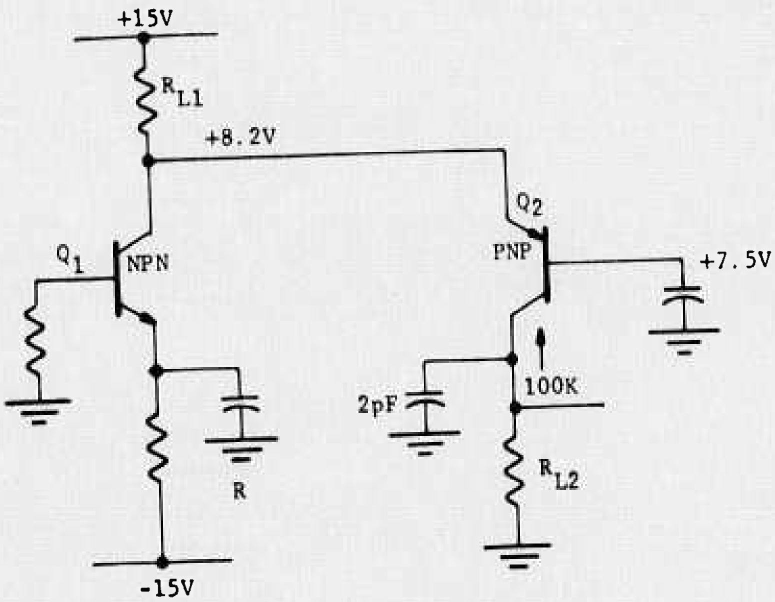

Figure 44 Inverted cascade pair

In the second stage the input impedance to the Bandpass Filter is 1000 Ω, the output impedance is 866 Ω. An emitter follower acts as a unity voltage gain buffer to transform to a low impedance.

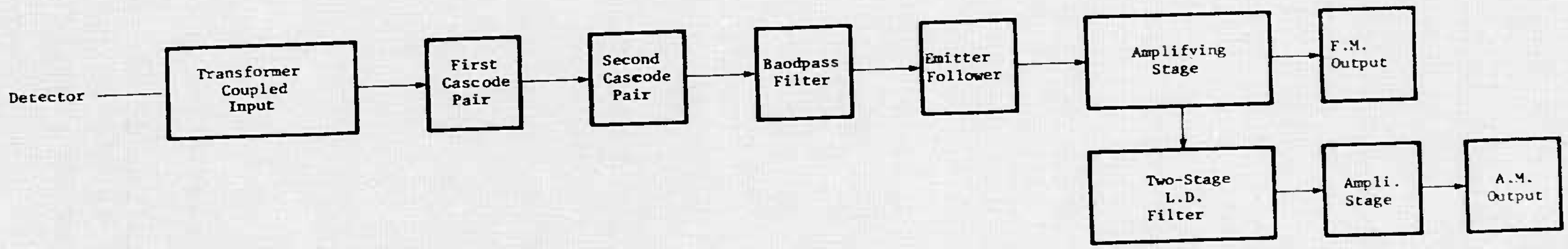

Figure 41 Preamplifier block design

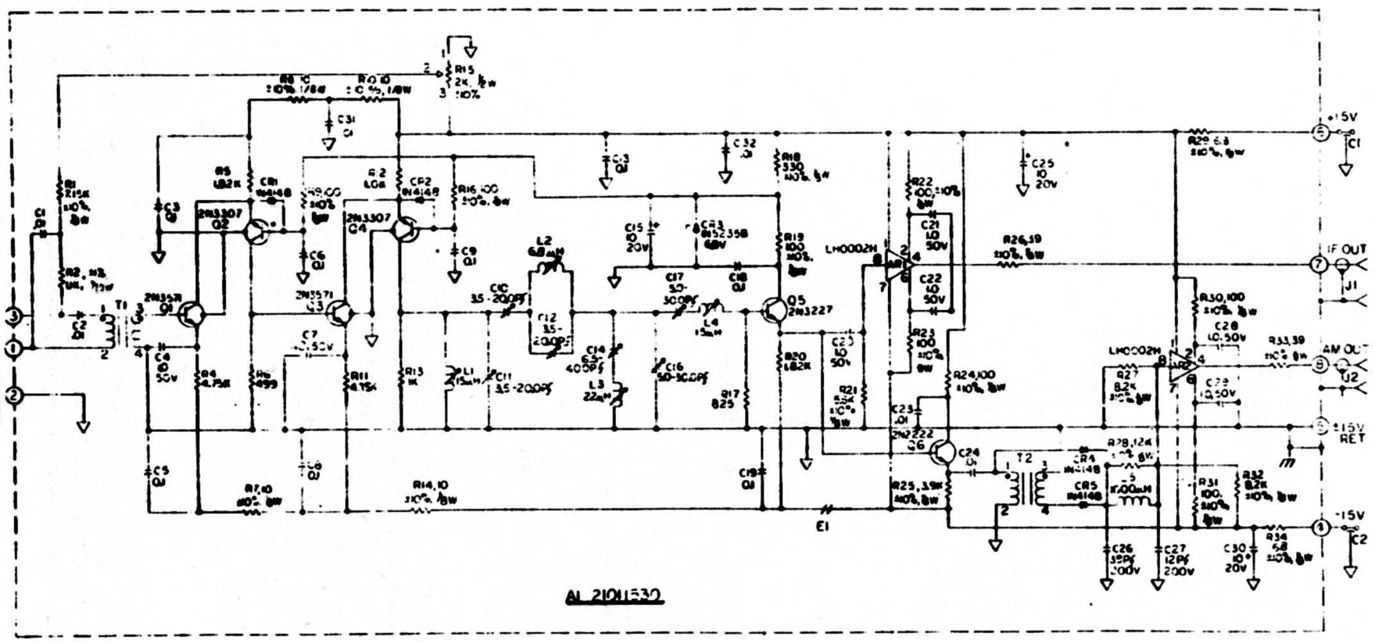

Figure 42 Preamplifier schematic

Dc conditions

As the base of Q_1 is referenced to ground, R in emitter of Q_1 establishes an emitter current

$$T_e = \frac{15 - V_{be}}{R}$$

Since Q_1 has a minimum beta of 10, then

$$I_c = I_e$$

The Q2 collector current is established by R_{LI}

$$I_c(\theta_2) = \frac{15V - (7.5V - V_{be})}{R_{LI}} - I_c\,(Q_1)$$

The signal gain of the complete cascode is to a first approximation

$$\frac{R_{L2}\, I_e\,(Q_1)}{26}$$

The cascaded cascodes comprising Q_1 through Q_4 provide a voltage gain of 60 dB.

The four-pole Cauer Bandpass Filter controls the overall frequency and phase response i-f channel of the preamplifier. Its passband is from 7 MHz to 13 MHz centered at 10 MHz.

The Emitter Follower Q5 and buffer amplifier ARI provide a unity voltage gain buffer with a low impedance output to drive a 70-ohm coaxial fm output.

a-m Channel

The i-f signals are obtained from the output of Emitter Follower Q5 and fed to current driver transistor Q6. T_2 operates as a broadband phase splitting transformer.[2]

The outputs of T_2 are full-wave rectified and filtered by the network comprising R28, L5, C32 and C33. Voltage divider R26 and R27 provide a forward bias to both detector diodes CR2 and

CR3. The low pass characteristics of the a-m channel are determined by the LP filter and provide a passband of dc to 1 MHz 3 dB cut-off with an approximately 40 dB/decade roll-off.

Unity gain buffer AR2 transforms the filter output impedance to the low impedance required to drive a 70-ohm coaxial output cable.

Preamplifier Test Results

The effect of input resistance on typical preamplifier noise figure is shown in Figure 45 while the dynamic ranges of all five pre-amplifiers are shown in Figure 46 through 50.

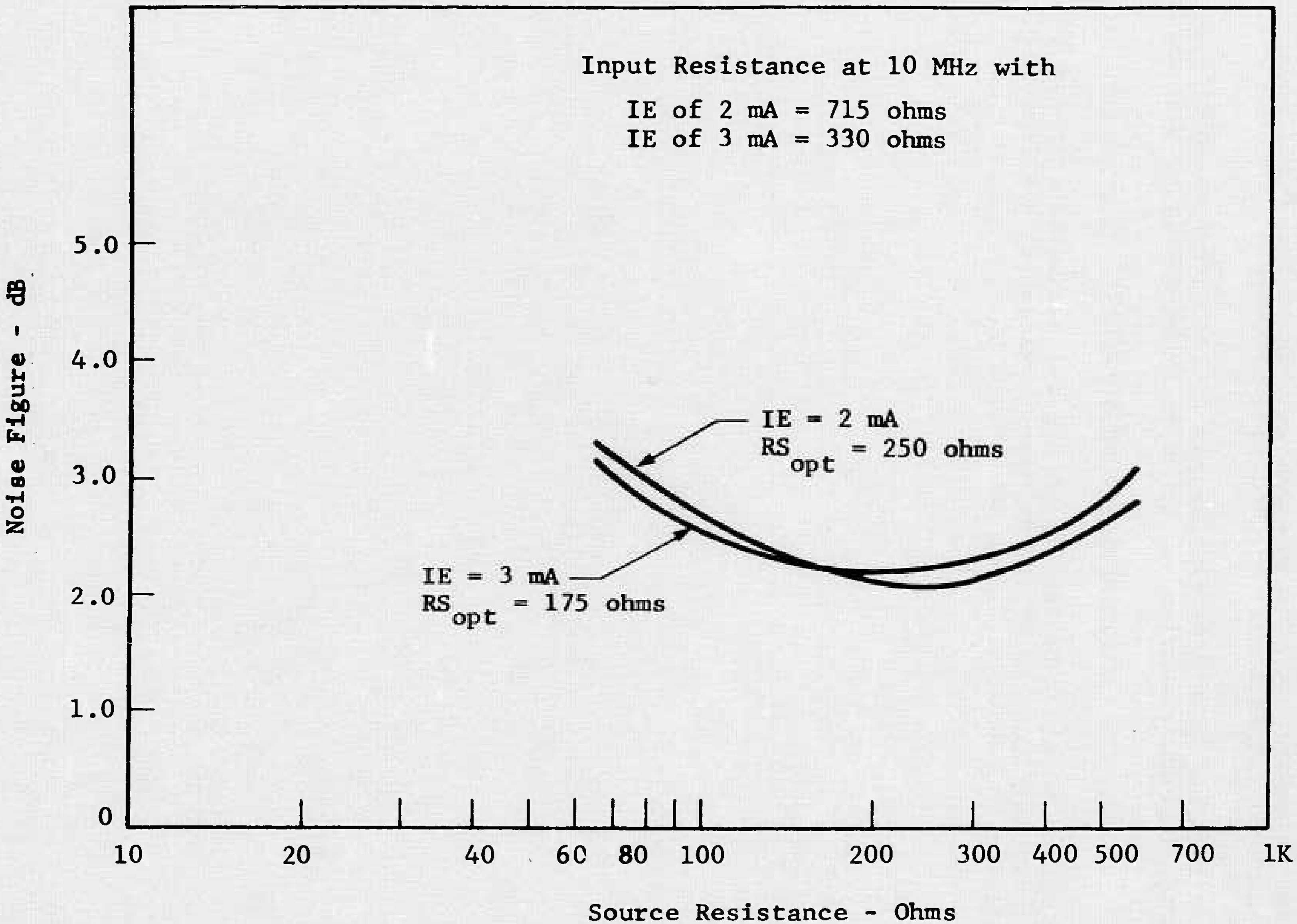

Figure 45 Typical LDA preamplifier noise figure versus source R

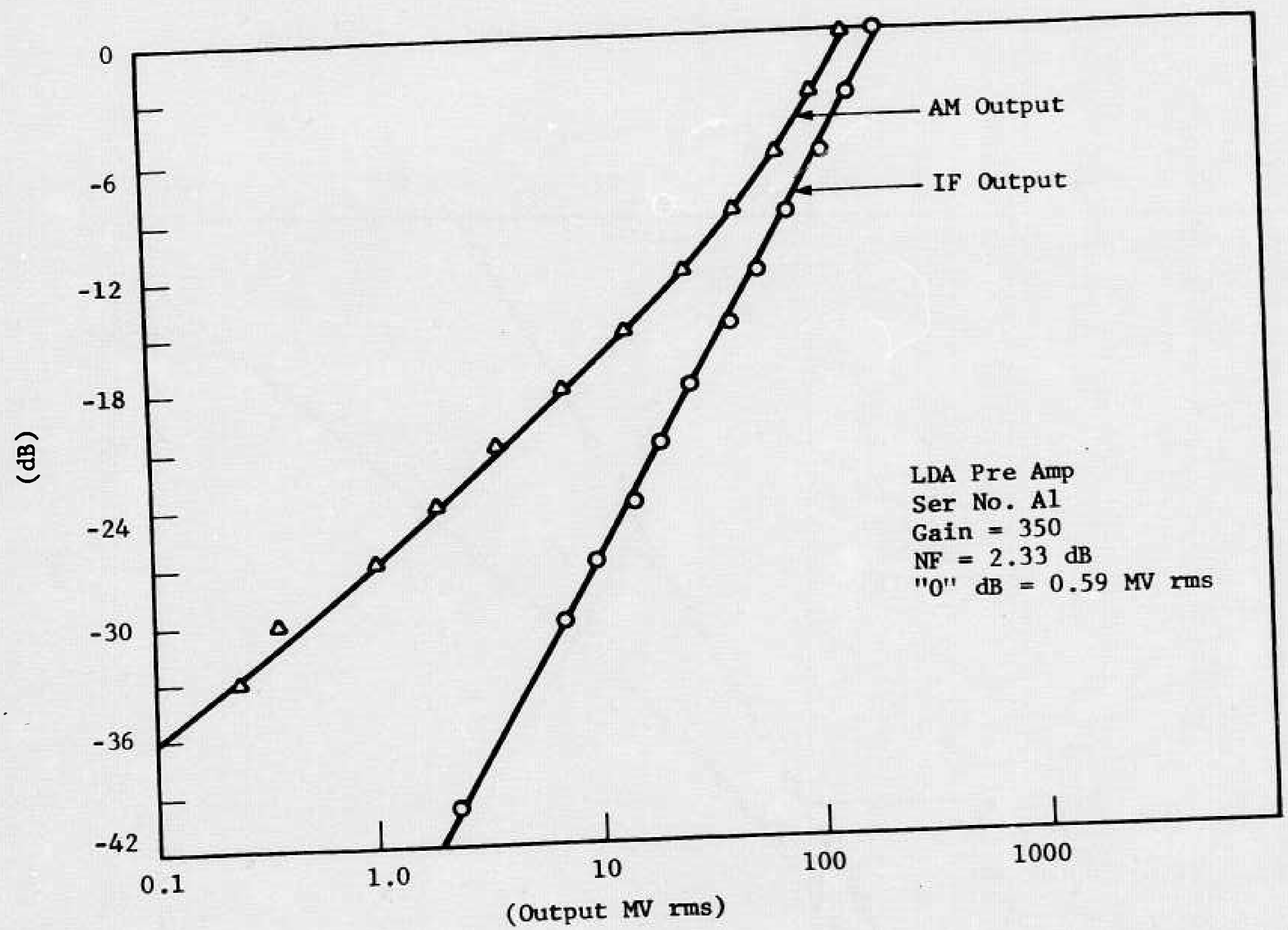

Figure 46 Dynamic range of preamplifier, ser. no. A1

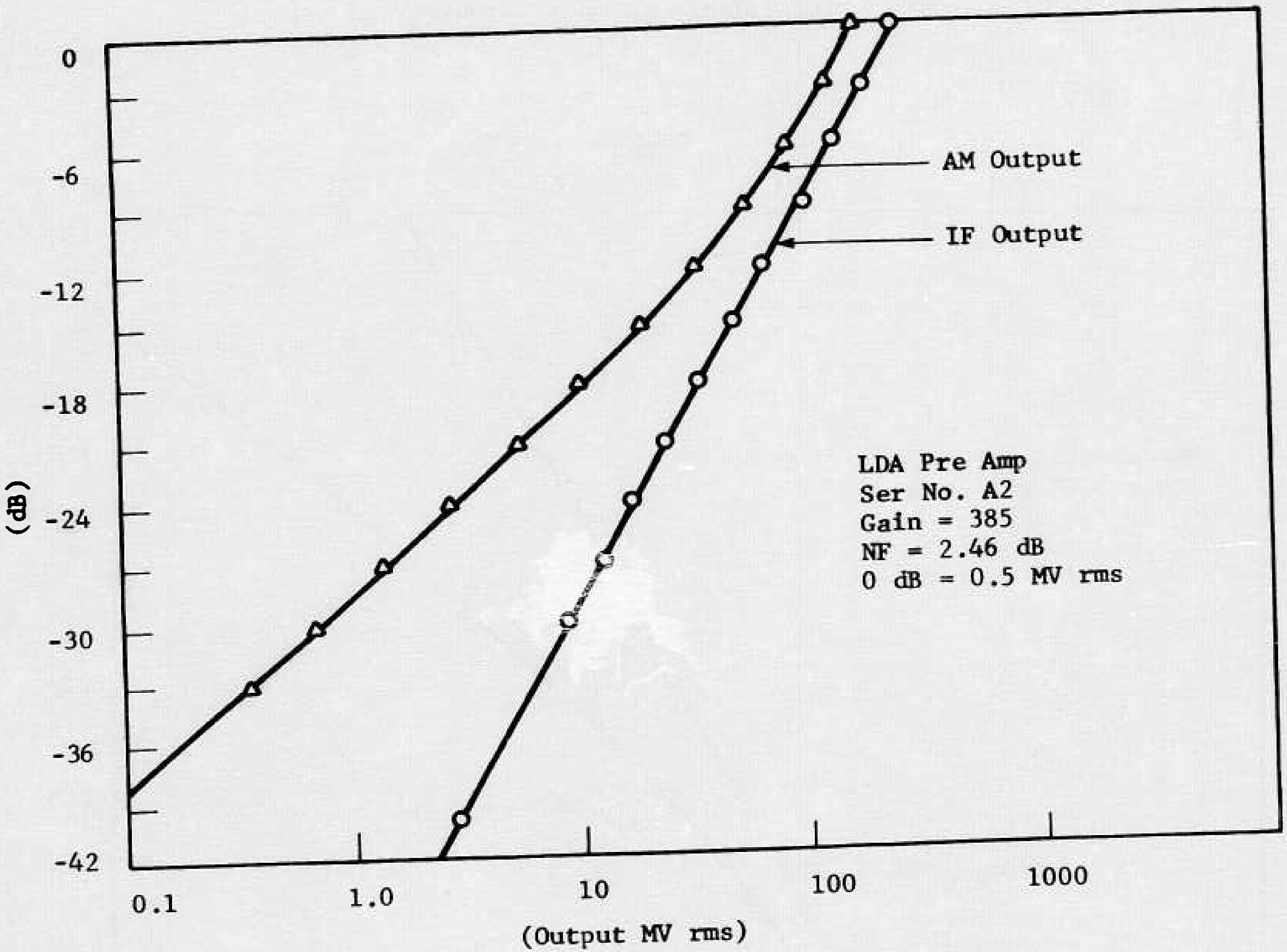

Figure 47 Dynamic range of preamplifier, ser. no. A2

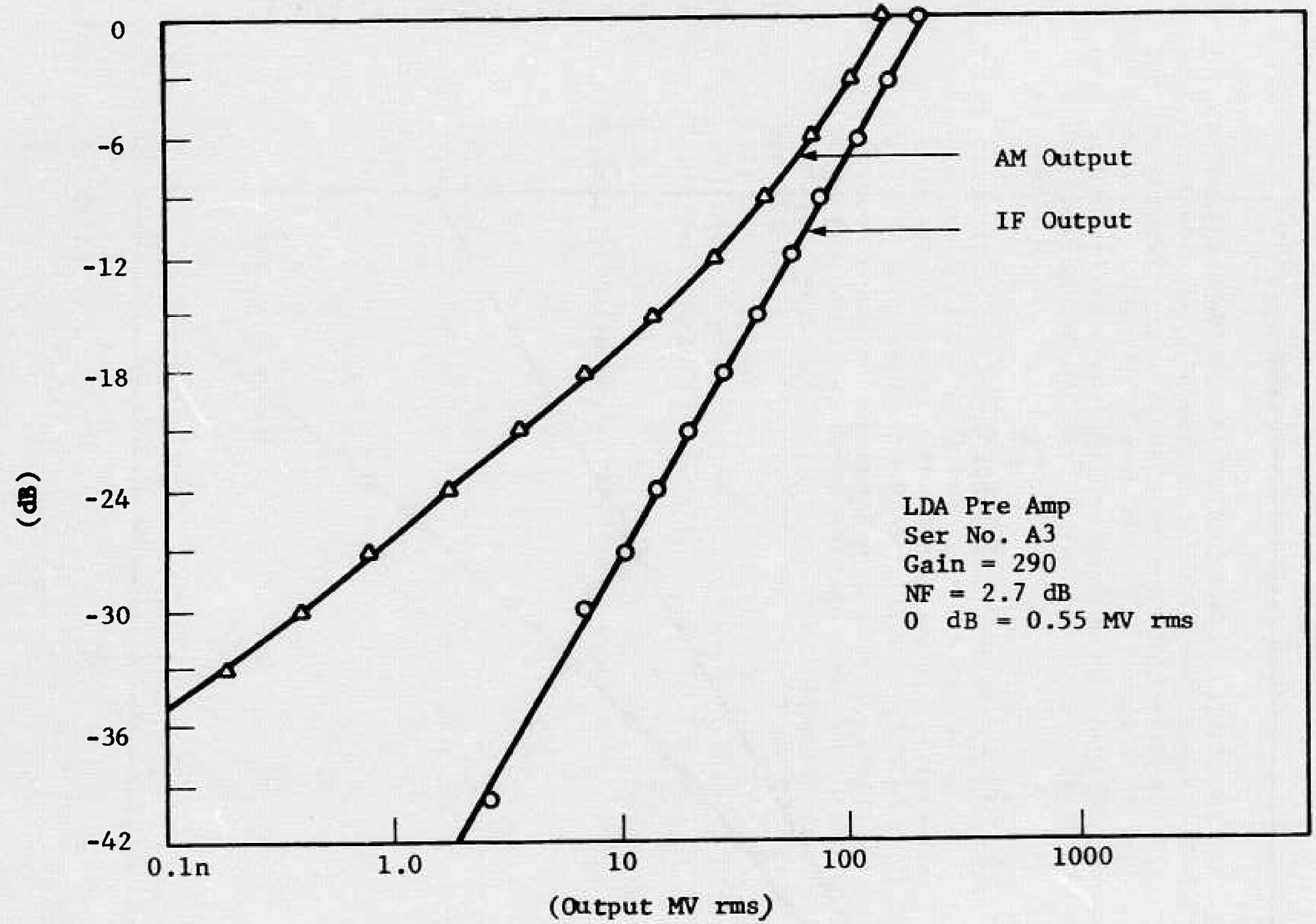

Figure 48 Dynamic range of preamplifier, ser. no. A3

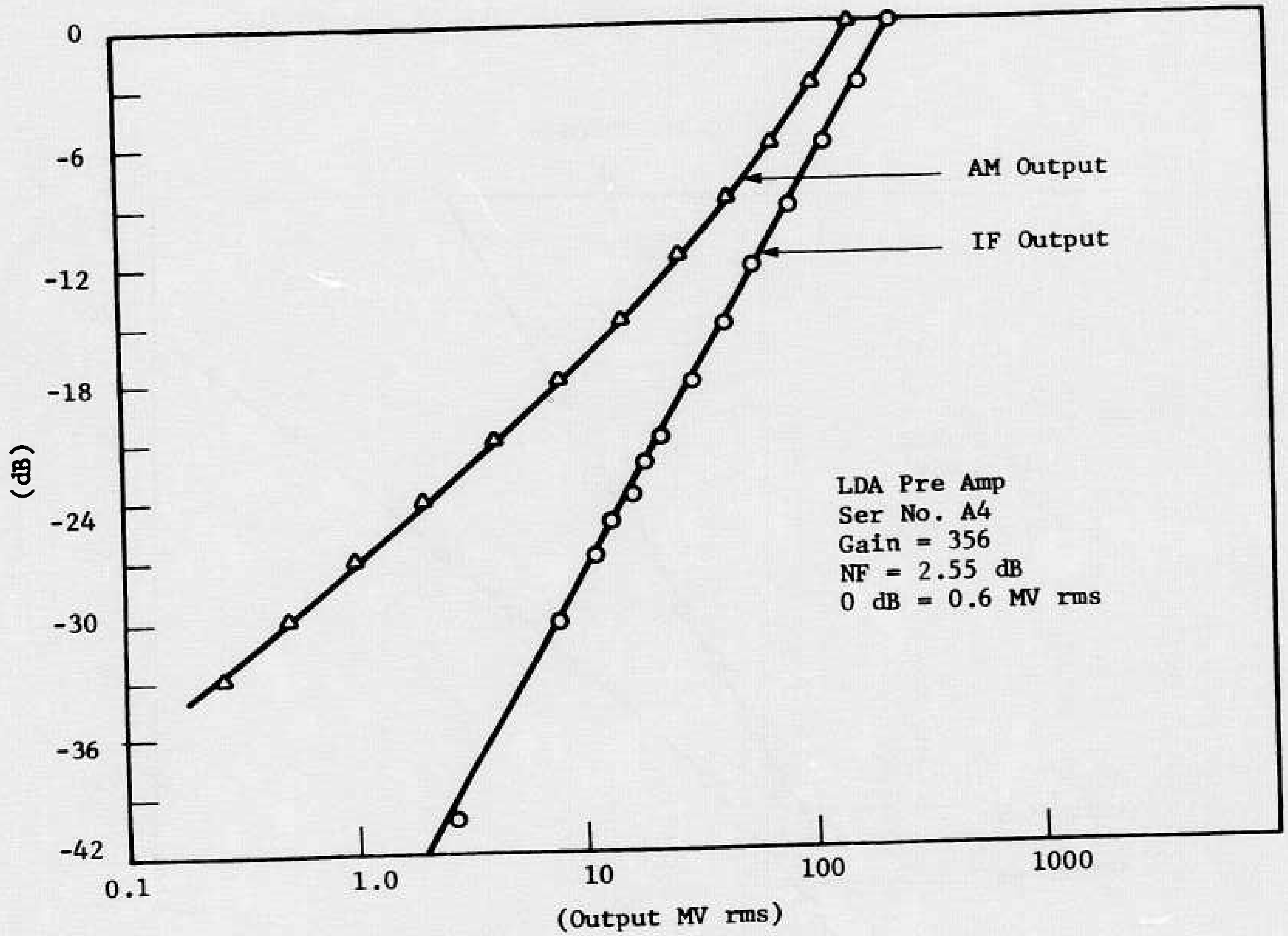

Figure 49 Dynamic range of preamplifier, ser. no. A4

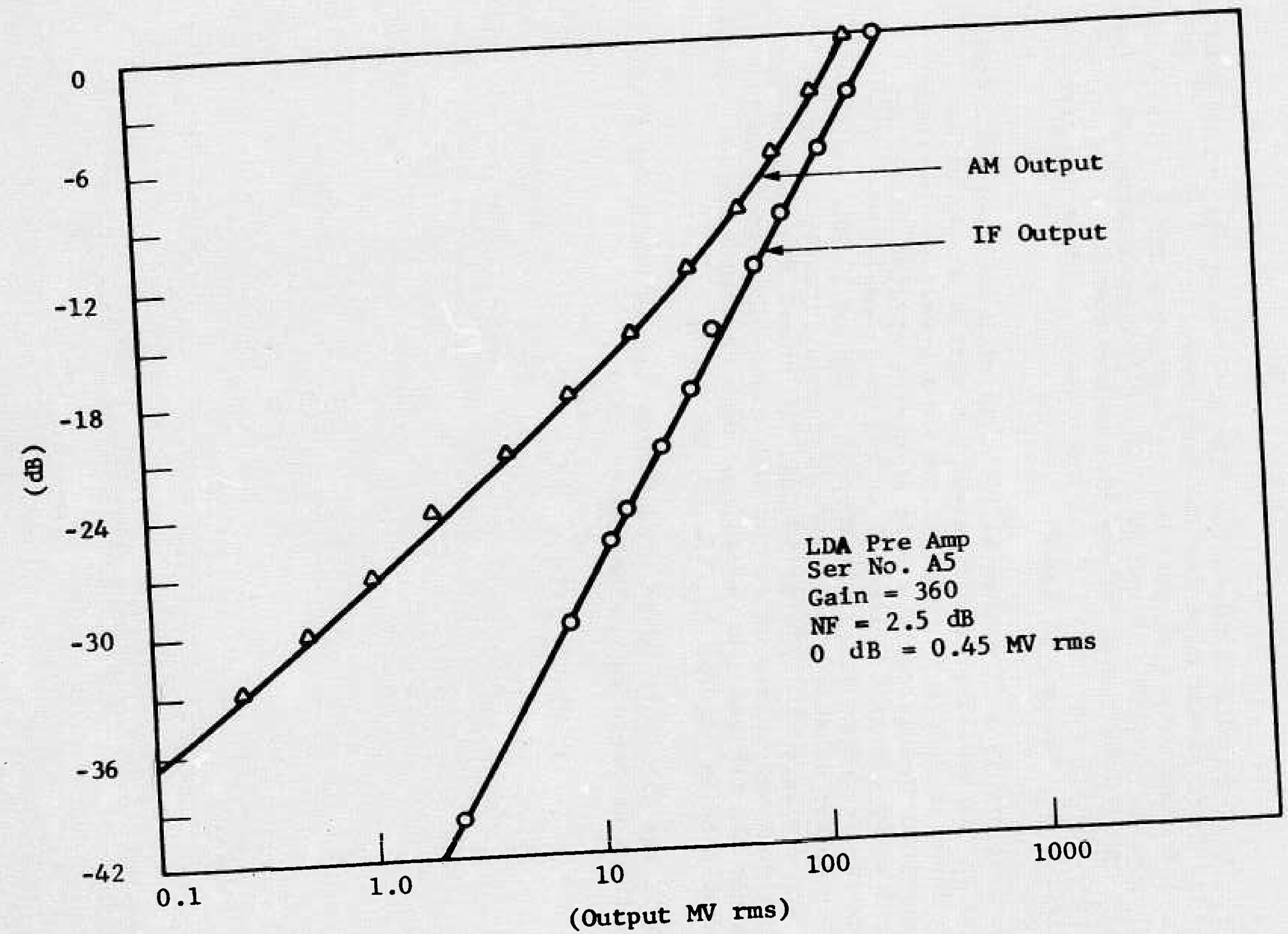

Figure 50 Dynamic range of preamplifier, ser. no. A5

FINAL RECEIVER RESULTS

Before final assembly each of the five amplifiers was tested with swept r-f input signal covering the frequency range 7 MHz to 13 MHz. The a-m channel output signals were photographed and are displayed in Figures 51, 53, 55, 57 and 59. The response of each amplifier to a 10-MHz pulsed signal of one microsecond nominal duration was recorded showing both the i-f and a-m outputs. These are displayed in Figures 52, 54, 56, 58 and 60.

After assembly as a five-channel receiver with each detector connected to its amplifier the receiver was tested on an optical bench shown in Figure 61. The output of a 3-watt cw CO_2 laser was amplitude modulated by a GaAs modulator crystal driven by the r-f sweep generator, through an ENI power amplifier. The modulation frequency was swept through 7 MHz to 13 MHz and the total receiver passband, both i-f and a-m outputs, recorded. They are displayed in Figures 62, 64, 66, 68 and 70. Then the optical input signal was pulsed at 10 MHz with a one-microsecond nominal pulse and the i-f and a-m response of each channel recorded. These are displayed in Figures 63, 65, 67, 69 and 71.

The unit was then shipped to the Avionics Lab at WPAFB for final measurement of Noise Equivalent Power (NEP).

AMPLIFIER NO. 1

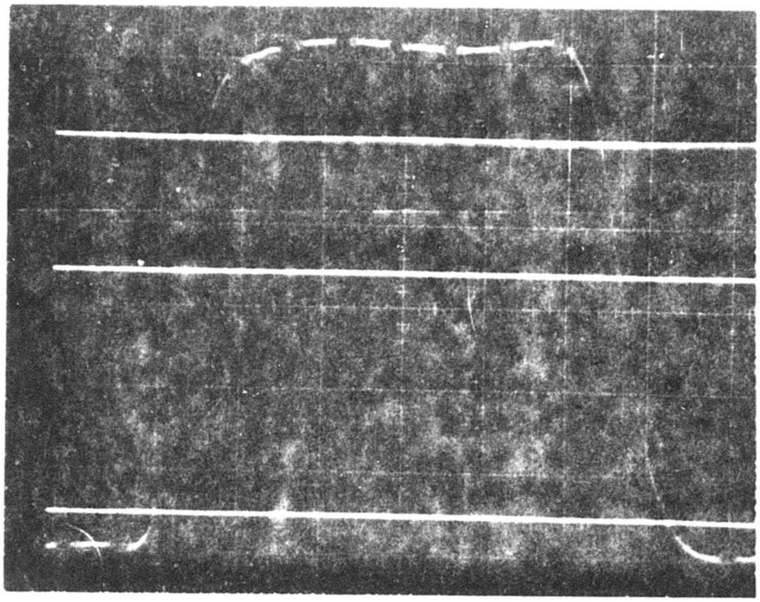

Figure 51 Amplifier output

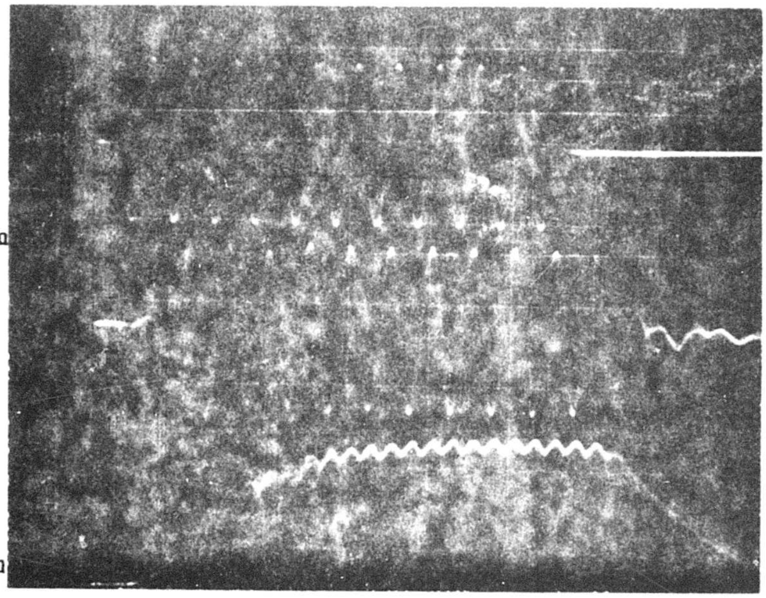

Figure 52 Amplifier output

AMPLIFIER NO. II

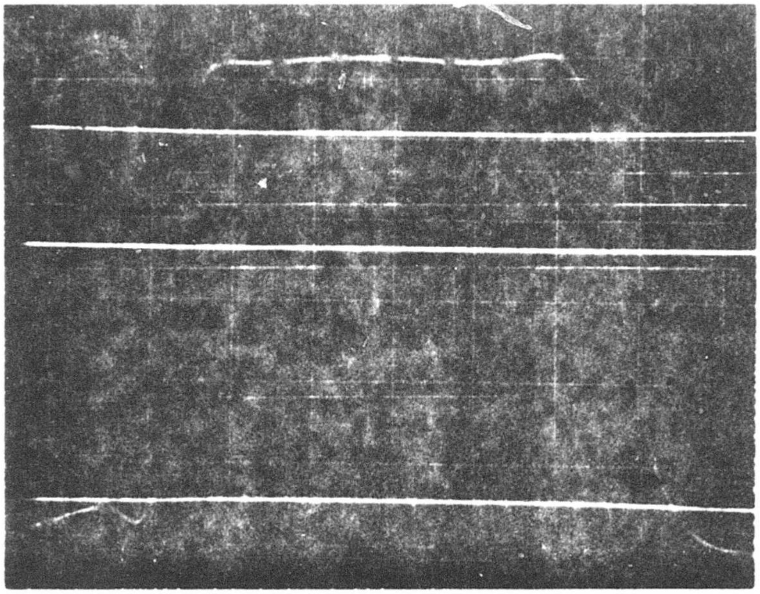

Figure 53 Amplifier output

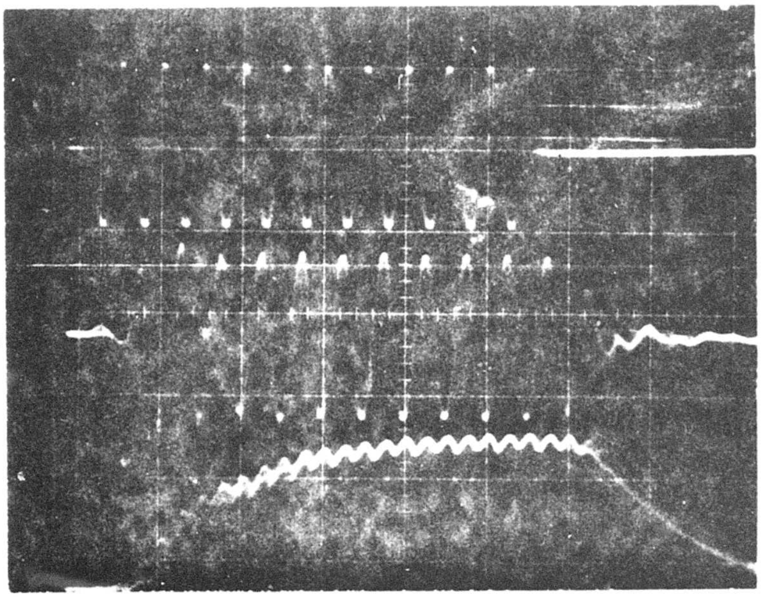

Figure 54 Amplifier output

AMPLIFIER NO. III

Center
10 MHz

1 MHz
Markers
-1 dB

-3 dB

-12 dB

A3
20 mV/cm

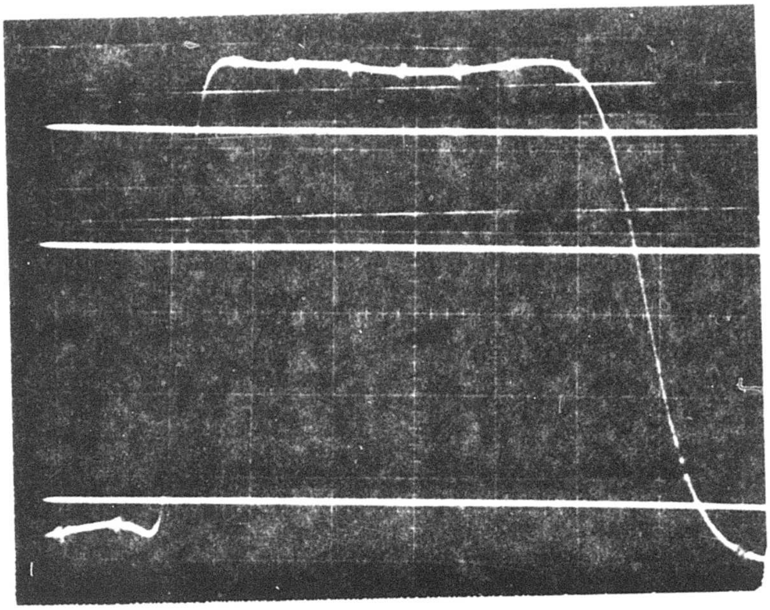

Response to
Swept Micro-
wave Input
Signal A.M.
Output

Figure 55 Amplifier output

Input
50 mV/cm

IF Out
200 mV/cm

A.M. Out
50 mV/cm

A3
0.2 μs/cm

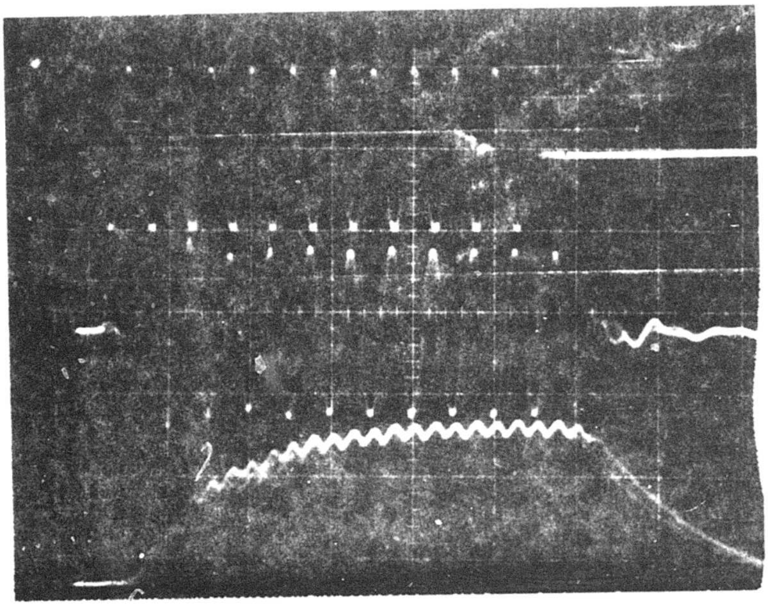

Input
10 MHz
Pulse
1 μs nom.

IF Output

A.M. Output

Figure 56 Amplifier output

AMPLIFIER NO. IV

Center
10 MHz

1 MHz
Markers

-1 dB

-3 dB

-12 dB

A4
20 mV/cm

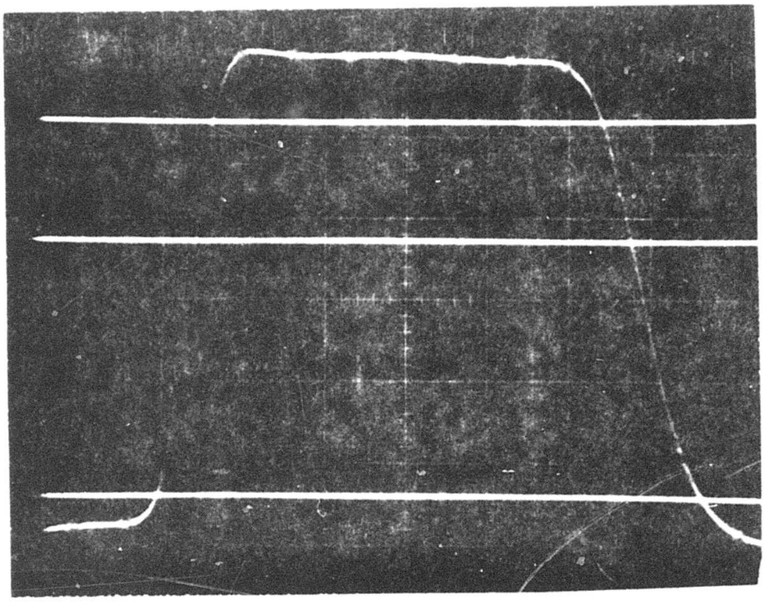

Response
to Swept
Microwave
Input
Signal
A.M. Output

Figure 57 Amplifier output

Input
50 mV/cm

IF Out
200 mV/cm

A.M. Out
50 mV/cm

A4
0.2 μs/cm

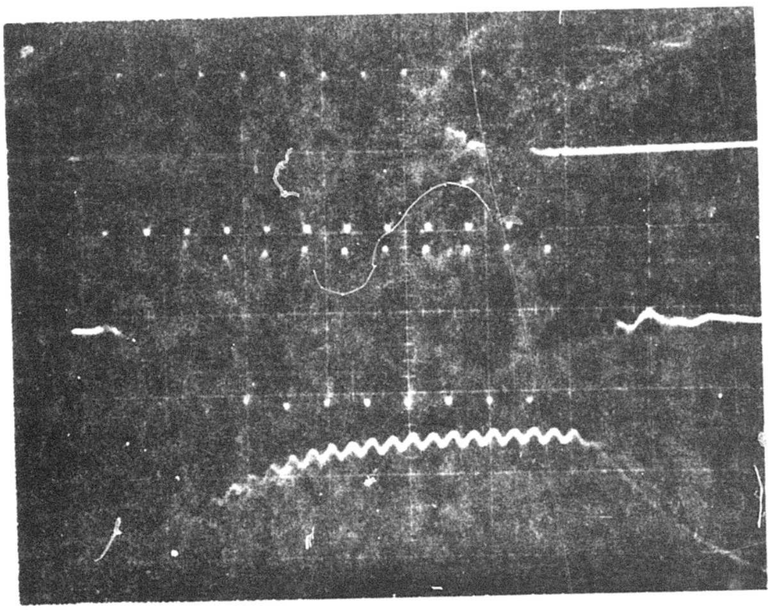

Input
10 MHz
Pulse
1 μs nom.

IF Output

A.M. Output

Figure 58 Amplifier output

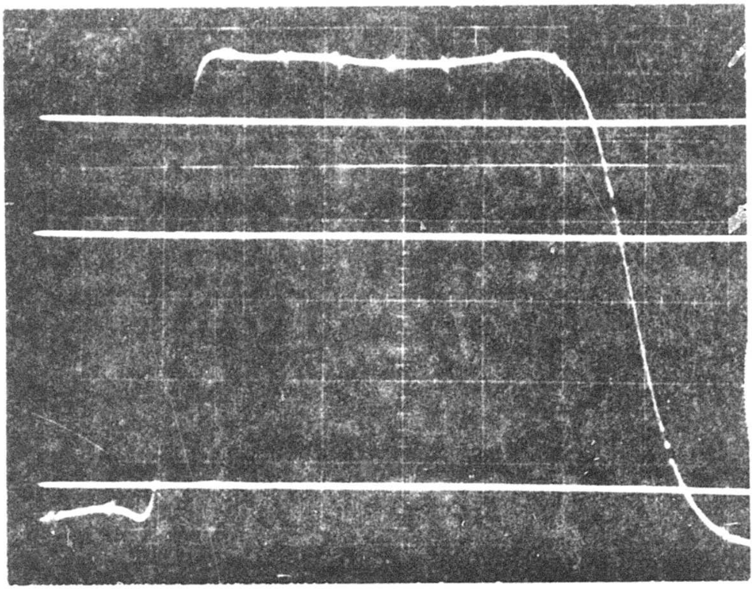

Figure 59 Amplifier output

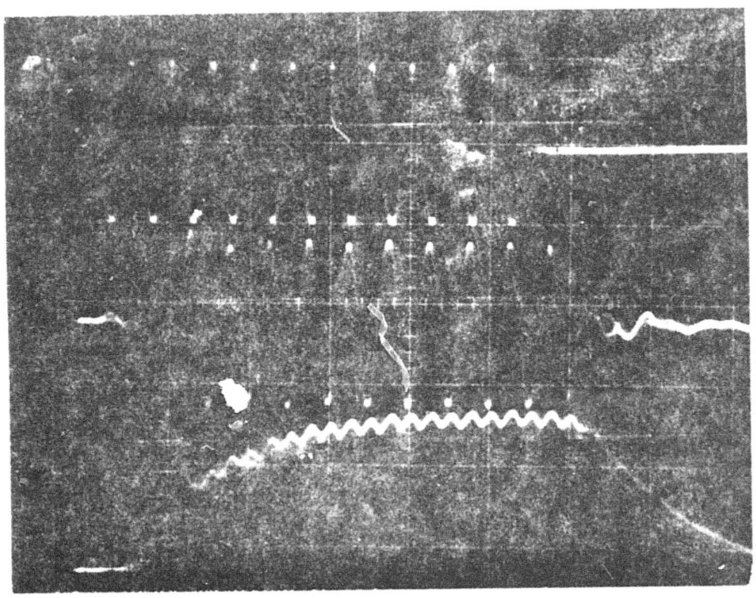

Figure 60 Amplifier output

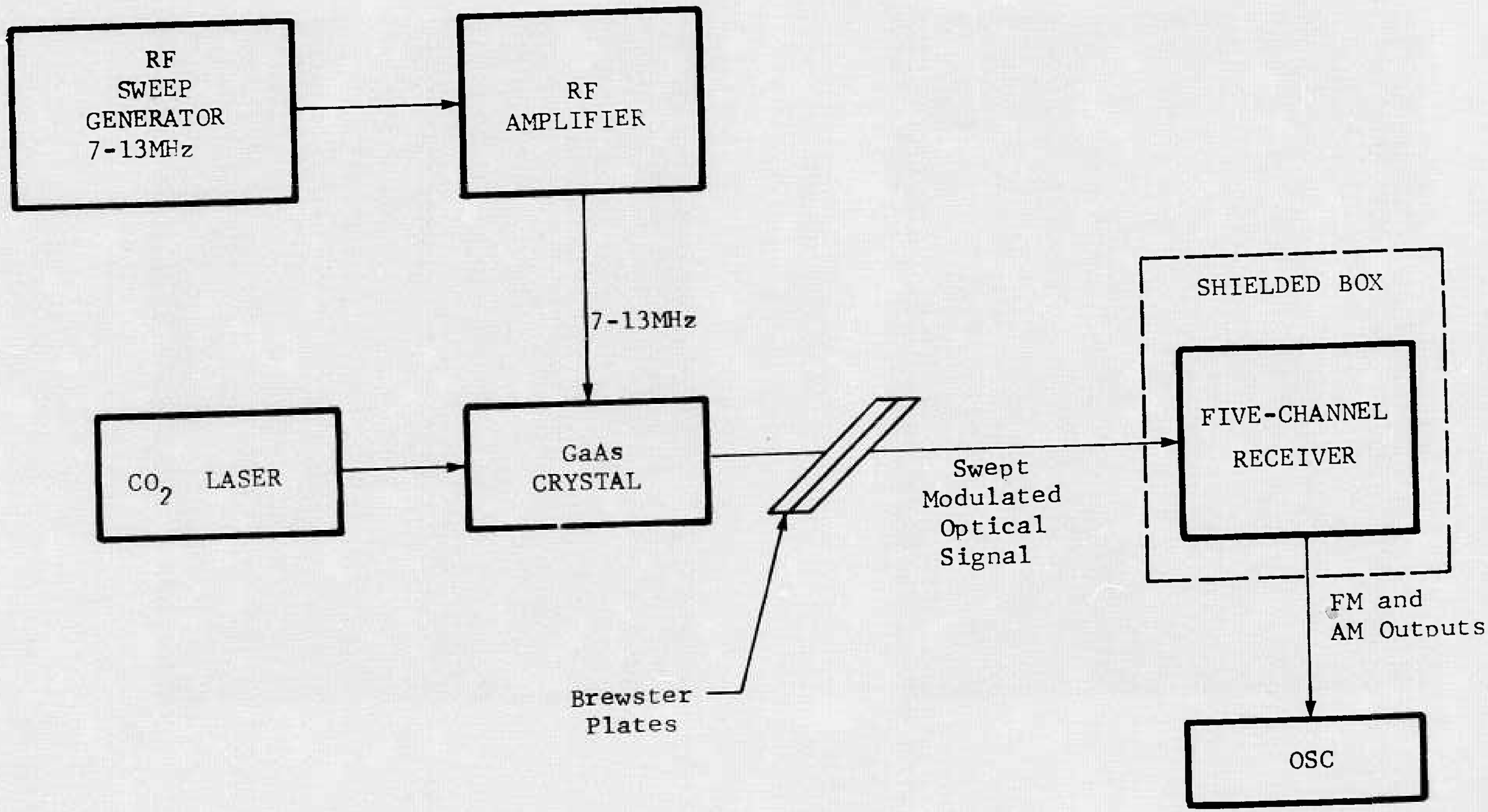

Figure 61 Test bench for five-channel receiver

RECEIVER CHANNEL I

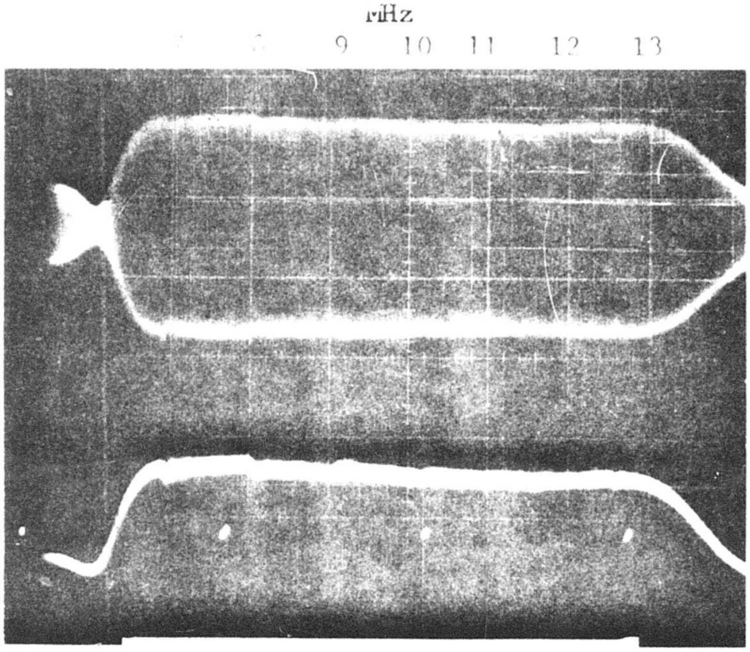

Swept Response to Modulated 10.6 μm Signal Output

IF Output

AM Output

Figure 62 Receiver output

RESPONSE TO 1 μs (NOM.) OPTICAL PULSE

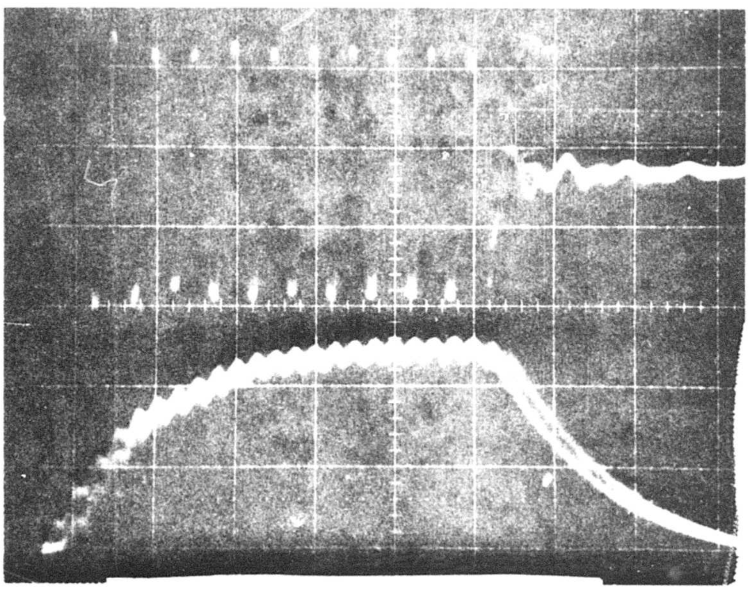

IF Output
10 MHz

AM Output

Figure 63 Receiver output

0.2 μs/cm

RECEIVER CHANNEL II

MHz

7 8 9 10 11 12 13

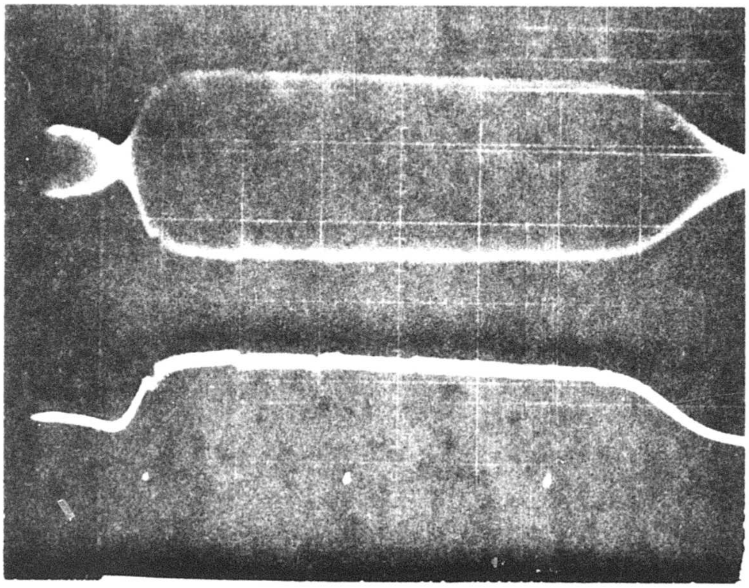

Swept
Response
to Modulated
10.6 μm Input
Signal
IF Input

AM Output

Figure 64 Receiver output

RESPONSE TO 1 μs (NOM.) OPTICAL PULSE

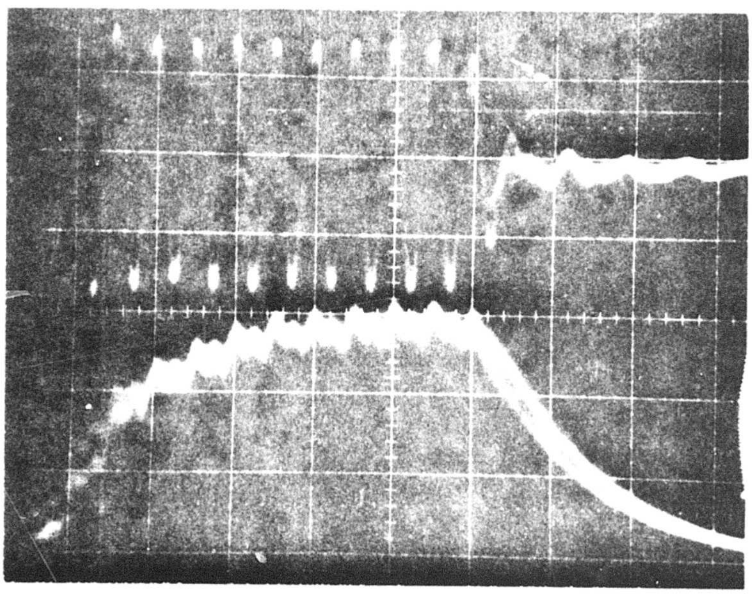

IF Output
10 MHz

AM Output

Figure 65 Receiver output

0.2 μs/cm

RECEIVER CHANNEL III

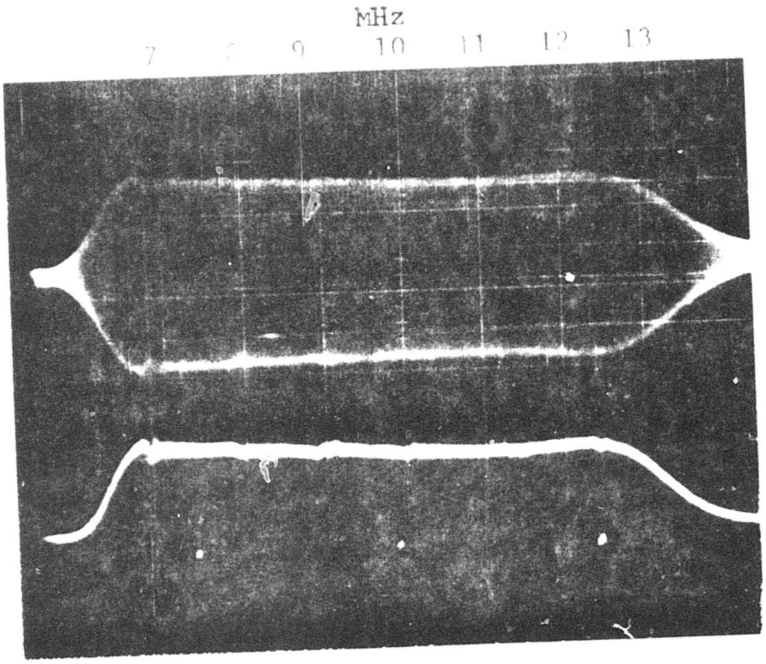

Swept Response to Modulated 10.6 μm Input Signal

IF Output

Figure 66 Receiver output

RESPONSE TO 1 μs (NOM.) OPTICAL PULSE

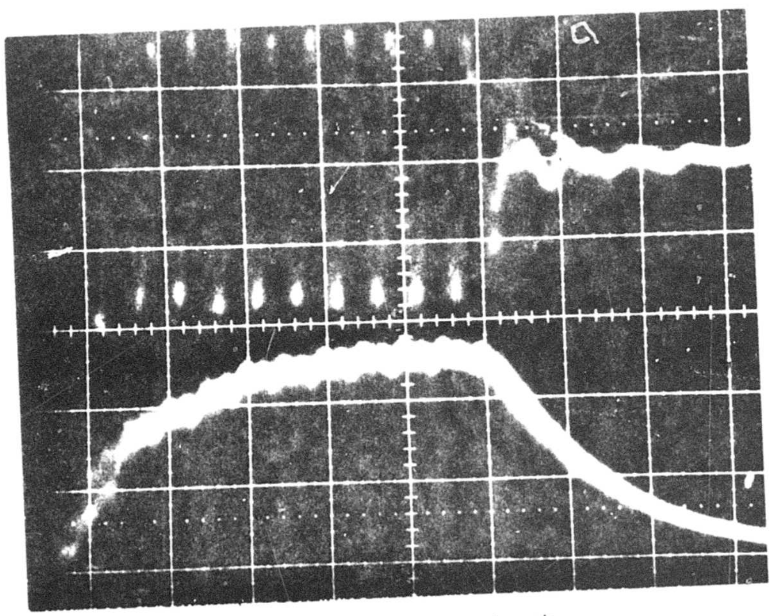

IF OUTPUT 10 MHz

AM OUTPUT

Figure 67 Receiver output

0.2 μs/cm

RECEIVER CHANNEL IV

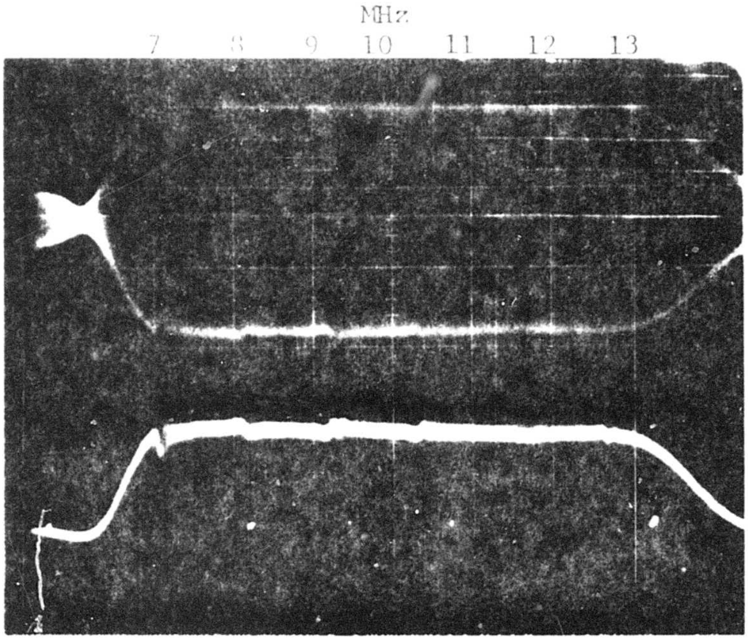

Figure 68 Receiver output

RESPONSE TO 1 μs (NOM.) OPTICAL PULSE

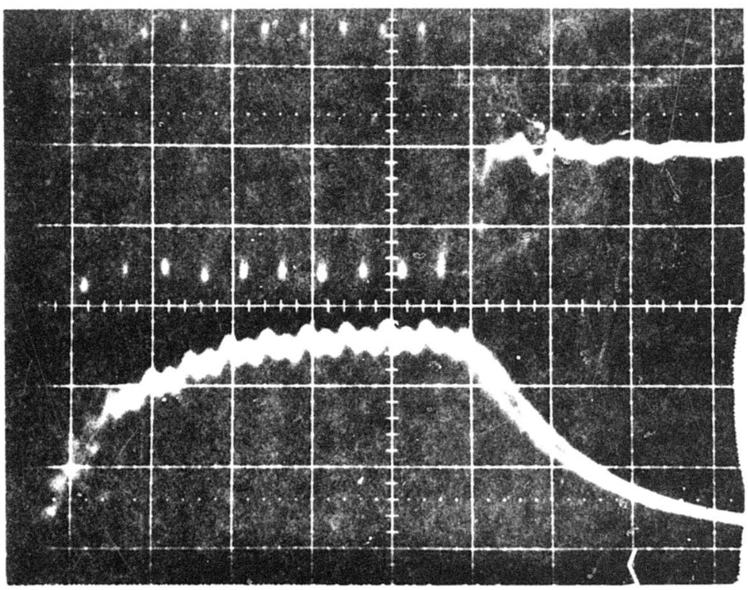

Figure 69 Receiver output

0.2 μs/cm

RECEIVER CHANNEL V

7 8 9 10 11 12 13

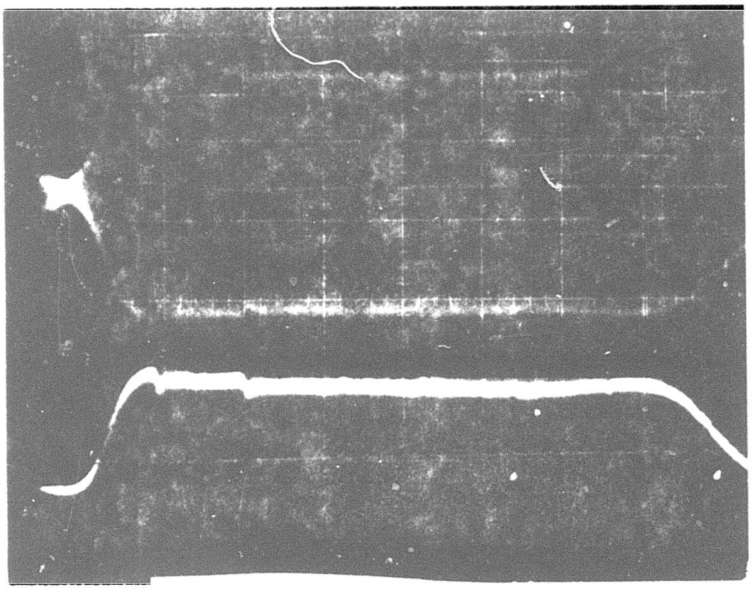

Swept Response to Modulated 10.6 μm Input Signal

IF Output

AM Output

Figure 70 Receiver output

RESPONSE TO 1 μs (NOM.) OPTICAL PULSE

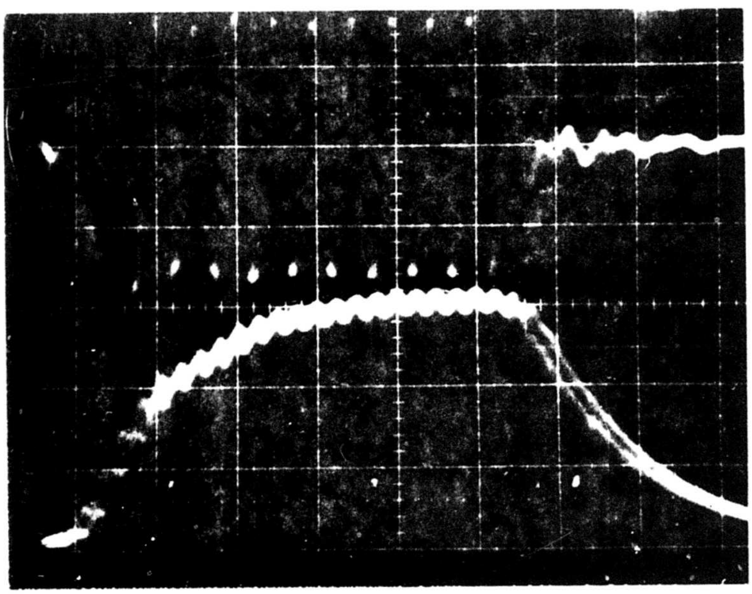

IF Output 10 MHz

AM Output

Figure 71 Receiver output

0.2 μs/cm

APPENDIX A

SCHEMATICS

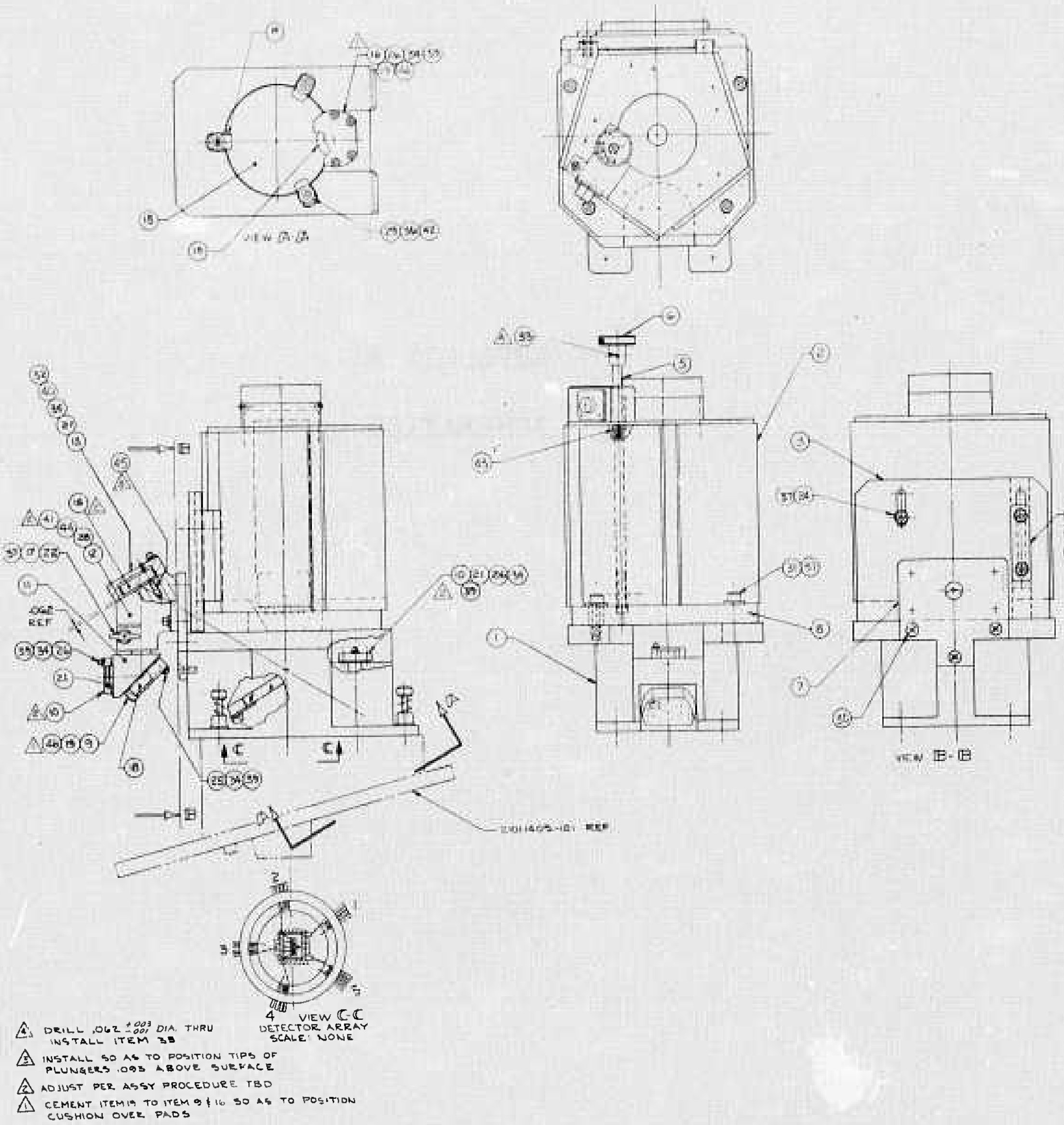

Figure A.1 Receiver assembly (21014645)

AD NUMBER

B007 291

CLASSIFICATION CHANGES

TO

FROM

AUTHORITY

Wright Lab/DODS Notice of Changes
dtd 13 NOV 91

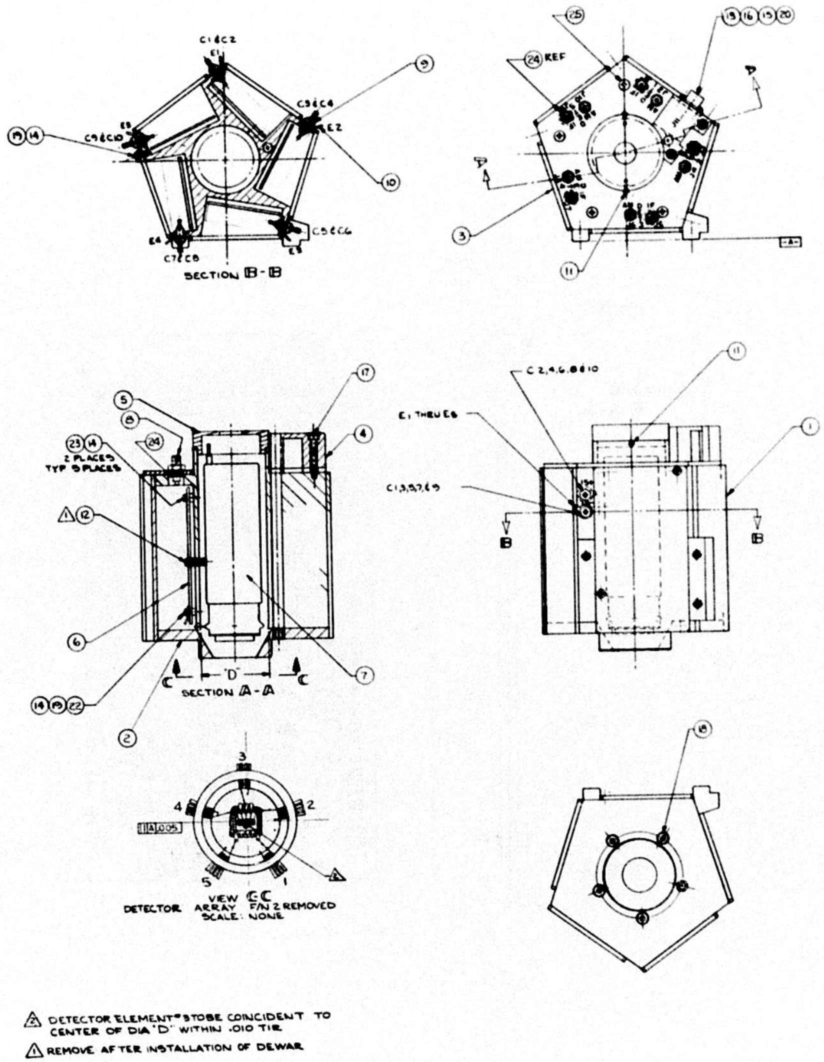

Figure A.2 Amplifier detector assembly (21014644)

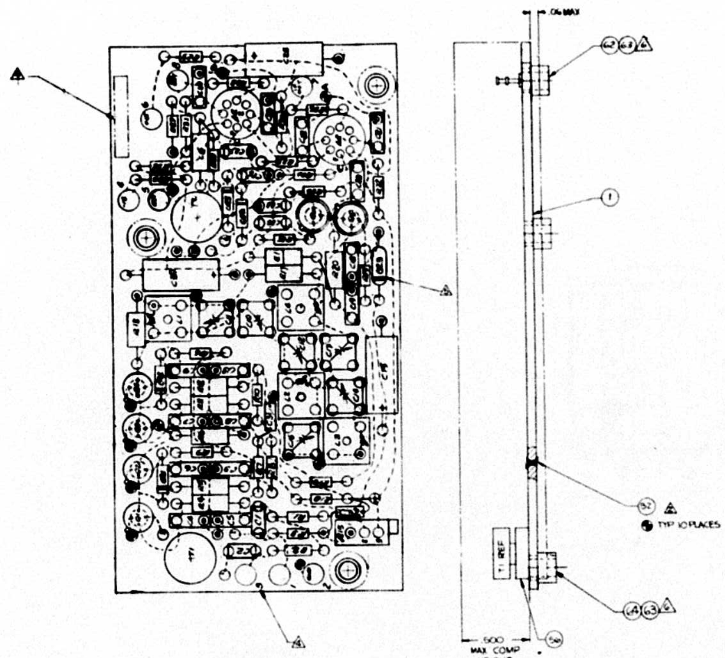

Figure A.3 Board assembly biased preamplifier (21011530)

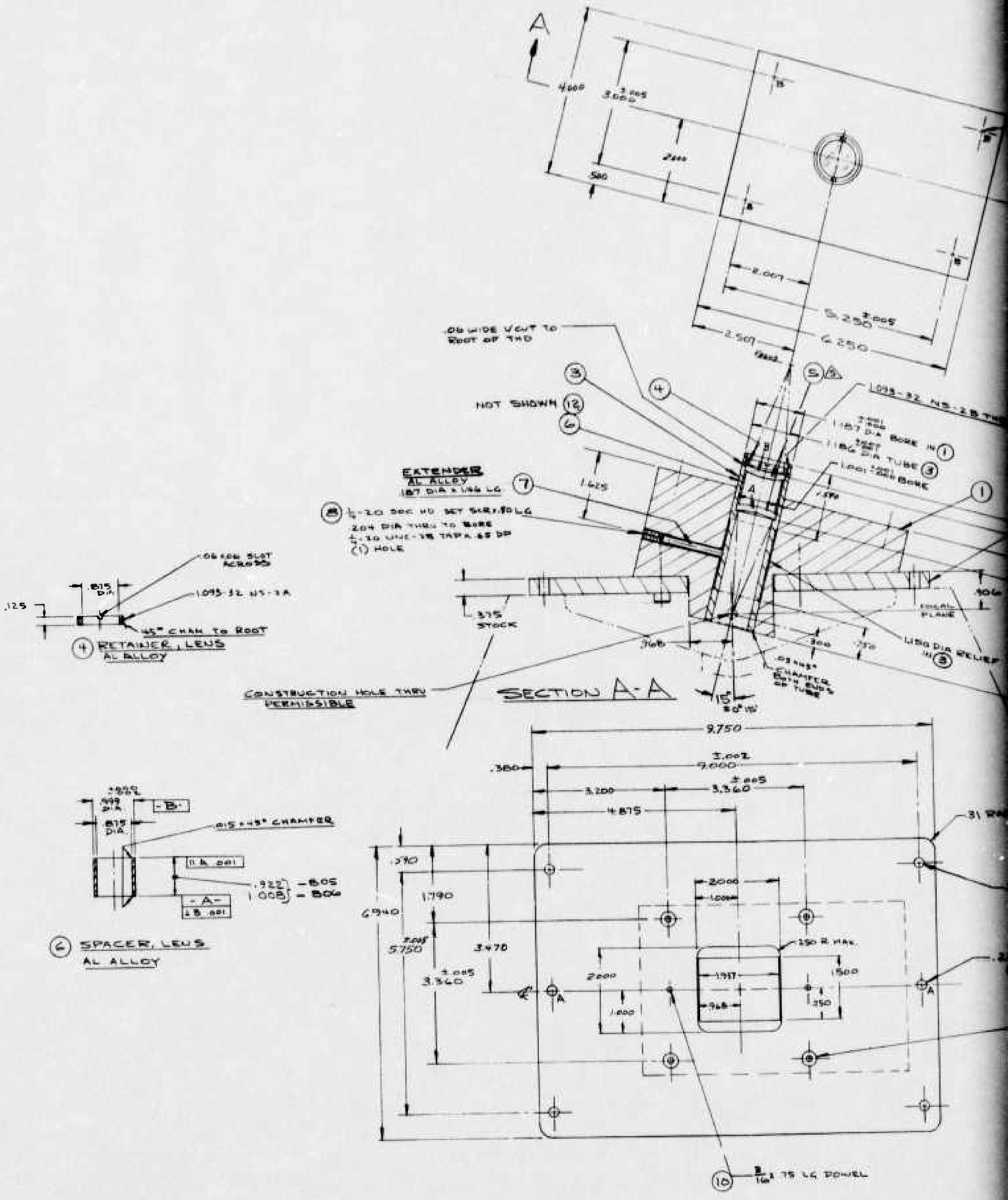

Figure A.4 Detector mount heterodyne

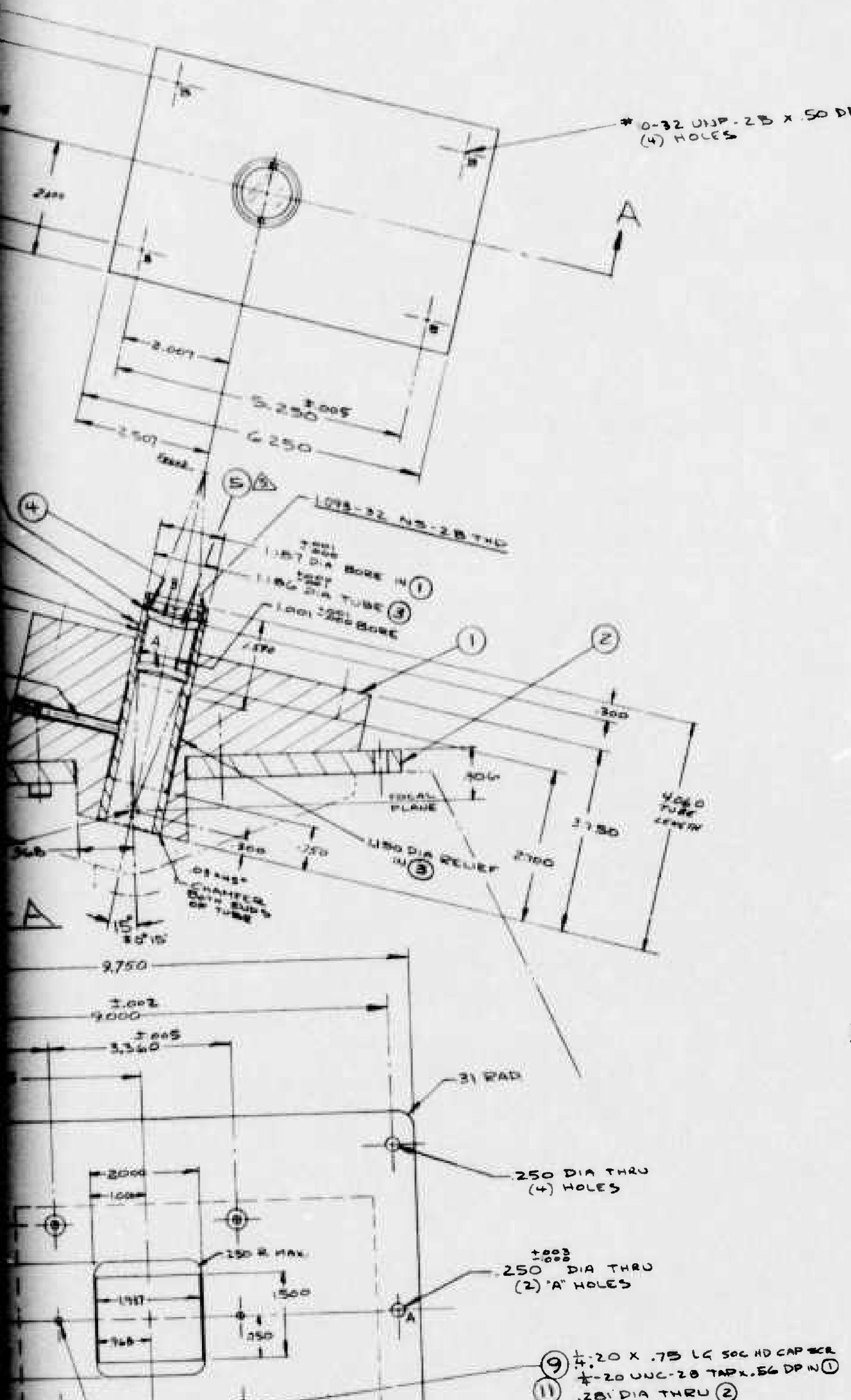

NOTE

1. AL ALLOY PARTS ARE TO BE BLACK ANODIZED
2. ALL DIMENSIONS ARE AFTER ANODIZING
3. BREAK SHARP CORNERS
4. FURNISHED BY HRC
5. FOR USE WITH COLLIMATED LIGHT, REMOVE LENS "A" AND REPLACE WITH SPACER FURNISHED

4 Detector mount heterodyne (21011405)

DISTRIBUTION LIST for Contract F33615-72-C-1556

	Copy No.
DDC Cameron Station Alexandria, VA 22314	1 & 2
HQ USAF/SAMID Wash, DC 20330	3
AFSC/INA Andrews AFB, MD 20334	4
Air University Library Maxwell AFB, AL 36112	5
2650 AF WG/SSL Wright-Patterson AFB, OH 45433	6
AFAL/TSR Wright-Patterson AFB, OH 45433	7 & 8
AFAL/RWI Attn: W. Schoonover Wright-Patterson AFB, Ohio 45433	9 - 15
AFAL/TEO Attn: S. Wagner Wright-Patterson AFB, Ohio 45433	16
ASD/ENAME Attn: R. Davis Wright-Patterson AFB, Ohio 45433	17
ASD/ENAMB Attn: R. Nichols Wright-Patterson AFB, Ohio 45433	18
U. S. Naval Air Development Center Attn: Mr. C. Haney Johnsville, NADC Warminster, PA 18974	19
USAECOM, CJ & TA LAB. Attn: AMSEL-CT-L Dr. R. G. Buser Fort Monmouth, New Jersey 07703	20

Distribution List for Contract F33615-72-C-1556 (Continued)

	Copy No.
Naval Electronics Laboratory Center Attn: Mr. D. Forbes, Code 2510 271 Catalina Blvd. San Diego, California 92152	21
Lincoln Laboratory, MIT Attn: Dr. R. H. Rediker Lexington, Mass. 02173	22
The Institute of Defense Analysis Attn: Dr. V. Corcoran 400 Army-Navy Drive Arlington, Virginia 22202	23
United Technology Corporation Research Center Attn: Dr. Carl Buczek 400 Main St. East Hartford, Conn. 06108	24
Rockwell International Autonetics Division Attn: Dr. R. Brandewie 3370 Miraloma Avenue Anaheim, California 92803	25
Raytheon Company Attn: R. McManus Equipment Division Sudbury, MA 01776	26
The RAND Corporation Attn: Dr. L. Mundie Santa Monica, California 90807	27
Xerox Corporation Electro-Optical Systems Division Attn: Mr. L. Dale Green 300 North Halstead Street Pasadena, California 91107	28
McDonnell Douglas Reconnaissance Laboratory Attn: L. G. Holmes St. Louis, MO 63116	29

Distribution List for Contract F33615-72-C-1556 (Continued)

	Copy No.
Philco-Ford Corporation Aeronutronic Division Attn: Mr. R. U. Pierotti Ford Road Newport Beach, California 92663	30
Westinghouse Defense and Space Center Aerospace Division Attn: Mr. Charles R. Kline Baltimore, Maryland 21202	31
Sperry Rand Gyroscope Division Electro-Optical Group Attn: Mr. I. Roth Great Neck, New York 11020	32
Sylvania Western Division Sylvania Electric Products, Incorporated Attn: Dr. T. S. Fehlen Mountain View, California 94040	33
Navy Underwater Sound Laboratory Attn: Mr. Milton Green New London, Connecticut 06320	34
Texas Instruments, Incorporated Equipment Group Attn: Mr. Hugh Harris P. O. Box 6015 3500 North Central Expressway Dallas, Texas 75222	35
Palisades Institute for Research Services, Incorporated Working Group D. 9th Floor 201 Varick Street New York, NY 10014	36 & 37
Perkin Elmer Corporation Electro-Optical Division Attn: Mr. W. Paige Main Avenue Norwal, Connecticut 06852	38

Distribution List for Contract F33615-72-C-1556 (Continued)

	Copy No.
Lincoln Laboratory Massachusetts Institute of Technology Attn: Library Lexington, MA 02173	39
General Electric Company AED MD904 Attn: Mr. A. P. Carpentier 901 Broad Street Utica, NY 13501	40
RCA/Government and Commercial Systems Aerospace Systems Division Attn: Mr. Larry S. O'Hara P. O. Box 588, MS No. 10 Burlington, MA 01801	41
Naval Weapon Center Code 4081 Attn: Mr. Steven Barber China Lake, CA 03555	42
The MITRE Corporation Attn: Library P. O. Box 208 Bedford, MA 01730	43
Strategic Systems Project Office Lockheed Missiles and Space Company P. O. Box 504 Sunnyvale, CA 94088	44
Actron Industries, Incorporated Attn: Mr. C. B. Bicknell 700 Royal Oaks Drive Monrovia, CA 91016	45
RCA Applied Physics Laboratory Government & Commercial Systems Attn: Dr. D. J. Woywood Camden, NJ 08102	46

Distribution List for Contract F33615-72-C-1556 (Continued)

	Copy No.
Environmental Research Institute of Michigan Attn: IRIA Library P. O. Box 618 Ann Arbor, MI 48107	47
Environmental Research Institute of Michigan Attn: Mr. Max Bair P. O. Box 618 Ann Arbor, MI 48107	48 & 49